A PDMS SAMPLE PRETREATMENT DEVICE FOR THE OPTIMIZATION OF ELECTROKINETIC MANIPULATIONS OF BLOOD SERUM

A Thesis

Presented to the Faculty of

California Polytechnic State University,

San Luis Obispo

In Partial Fulfillment of the Requirements for the Degree

Master of Science in Engineering, with Specializations in Biomedical Engineering

by

Timothy J. Abram

September 2009

COMMITTEE MEMBERSHIP

TITLE: A PDMS SAMPLE PRETREATMENT DEVICE FOR THE OPTIMIZATION OF ELECTROKINETIC MANIPULATIONS OF BLOOD SERUM

AUTHOR: Timothy J. Abram

DATE SUBMITTED: September 2009

COMMITTEE CHAIR: David Clague, Ph.D.
Assistant Professor, Biomedical and General Engineering
California Polytechnic State University, San Luis Obispo

COMMITTEE MEMBER: Scott Hazelwood, Ph.D.
Assistant Professor, Biomedical and General Engineering
California Polytechnic State University, San Luis Obispo

COMMITTEE MEMBER: Lanny Griffin, Ph.D.
Chair, Biomedical and General Engineering
California Polytechnic State University, San Luis Obispo

ABSTRACT

A PDMS SAMPLE PRETREATMENT DEVICE FOR THE OPTIMIZATION OF ELECTROKINETIC MANIPULATIONS OF BLOOD SERUM

Timothy J. Abram

This project encompasses the design of a pretreatment protocol for blood serum and adaption of that protocol to a microfluidic environment in order to optimize key sample characteristics, namely pH, conductivity, and viscosity, to enable on-chip electrokinetic separations. The two major parts of this project include (1) designing a pretreatment protocol to optimize key parameters of the sample solution within a target range and (2) designing /fabricating a microchip that will effectively combine the sample solution with the appropriate buffers to replicate the same bench-scale protocol on the micro-scale.

Biomarker detection in complex samples such as blood necessitates appropriate sample "pretreatment" in order for specific markers to be isolated through subsequent separations. This project, though using conventional mixing techniques and buffer solutions, is one of the first to observe the effects of the combination of micro-mixing and sample pretreatment in order to create an all-in-one "pretreatment chip".

Using previous literature related to capillary electrophoresis, a bench-scale pretreatment protocol was developed to tune these parameters to an optimal range. A PDMS device was fabricated and used to combine raw sample with specific buffer solutions. Off-chip electrodes were used to induce electrokinetic micro-mixing in the mixing chamber, where homogeneous analyte mixing was achieved in less than one second using an 800V DC pulse wave. Ultimately, we wish to incorporate this device with pre-fabricated electrokinetic devices to optimize certain bioseparations.

Keywords: Pretreatment, Microfluidic, Micro-mixing, Diagnostic, Electrokinetic, PDMS

ACKNOWLEDGMENTS

I would first like to thank Dr. David Clague for his guidance, insight, and endless support. Without his enthusiastic dedication to student research, this thesis would not be possible.

Additionally, I would like to thank my committee members, Dr. Hazelwood and Dr. Griffin, for their assistance in the writing and defense process and for all their encouragement throughout this project.

I'd like to thank all the members of the Cal Poly Biofluidics group for all of their help throughout this project especially with equipment setup and training, purchase orders, and general troubleshooting. Special thanks go out to Josh Fadriquela for his assistance in project planning, experimental setup, and for his microfab expertise.

Finally I'd like to thank my family for their endless love and support throughout my entire academic career and for being a constant source of motivation.

This work has been supported through DARPA grant #N66001-08-1-2071.

TABLE OF CONTENTS

LIST OF TABLES

LIST OF FIGURES

1 Introduction/Background

1.1 Point-of-Care Diagnostics

Since their inception in the early 1990's, Lab-on-a-chip (LOC) technologies, i.e. devices which miniaturize one or more laboratory functions on a single chip with features no larger than a few centimeters, have inspired the development of miniaturized clinical diagnostics in the modern world. However, LOC technologies have yet to access resource-poor, developing countries, which is one of the greatest perceived potentials for such technologies. Due to their small size and volume requirements, LOC technologies have the potential to establish portable, point-of-care (POC) diagnostics that could have a profound effect on global health. While POC testing is a concept that can benefit urban, modernized centers as well, the design requirements for devices utilized in developing countries are much more demanding.

The concept behind POC testing revolves around enabling diagnostic testing at the site of an outbreak or a rural center that is not located near a clinic or hospital. Additionally, remote diagnostic testing can aid in disease screening and diagnosis without exposing emergency room patients to highly contagious diseases. Low-cost POC testing promises the potential for higher throughput of patients without disrupting the already hectic operating conditions of a clinic or hospital, which would enhance treatment prioritization. Through such diagnostic tests, improved health outcomes are expected owing to early diagnosis. POC testing in other settings can be important in the case of an epidemiologic outbreak where a vast number of patients must be diagnosed in an isolated area. In developed countries, POC testing can lay the groundwork for

personalized medicine, while also enabling patients to become more closely involved in their own disease management [1].There are numerous advantages to POC testing, especially when combined with the diagnostic promise of LOC technologies. Though our lab is not directly designing devices intended to operate in resource-poor regions, the unique design criteria that these locations pose will be considered throughout our own design process. For an excellent review of these unique criteria and some of the most critical health conditions/diseases plaguing these areas, please refer to Chin and Sia's 2006 Lab on a Chip review article [2].

1.2 Modular design of diagnostics

A recent trend in bioanalytical diagnostic tool design has been the miniaturization of many traditional principles of analyte detection, such as the Enzyme-Linked Immunosorbent Assay (ELISA) format, into a microfluidic platform. Thus, as technology has progressed, diagnostic tools continue to decrease in size, becoming more portable, efficient, and economical as the volumes of samples and reagents decrease dramatically. Another benefit of microchip-based technologies is the short processing times involved, leading to quicker diagnoses. LOC bioanalytical devices differ from many bench-scale clinical diagnostics in that LOC systems must incorporate many combined micro-processes into an operational instrument. The complexity of integration remains an important hurdle in current research, as process integration has the potential to increase the portability and ease-of-use of such devices [3].

There are several fundamental steps present in most clinical diagnostic protocols. These include sample collection, sample pretreatment, sample preparation via bio-separations, detection, and post processing. The Biofluidics group at Cal Poly has adopted this modular paradigm, seen in Figure 1, which necessitates that a large-scale vision be applied to individual "modules" to improve their future integration.

Figure 1 – Conceptual, modular flowchart of main processes in a diagnostic test

The concept of the modular paradigm of LOC diagnostic device design is presented in a flow-chart, where each step is dependent on the preceding step. The module presented in red shows where the role of "sample pretreatment" lies. Sample pre-treatment is dependent on sample collection and is necessary for correct sample preparation and detection.

1.2.1 Sample Collection

It can be argued that sample collection is the most important procedure in a bioanalytical system since even the most evolved detection technique cannot compensate for bad sampling [4]. Since only nano- or micro-liter volumes may be used, the sample must be an accurate representation of the entire system, i.e. the blood sample reflects the overall patient. Procedures that prove to be simple, reproducible and provide little chance of contamination are best suited for bioanalytical sample collection. The two most common sources of sampling errors include external contamination, which is usually a result of contaminated sampling equipment, and the use of the wrong sampling technique [4], which can render the sample useless. Different biological samples have unique characteristics which require specialized sampling procedures. For example, the most common biological samples used are blood serum and blood plasma [5], both of which pose unique challenges when compared to the collection of other samples, such as sweat or saliva. If whole blood or plasma is collected, anticoagulants must be used to prevent blood clot formation, even though the use of anticoagulants may potentially interfere with result interpretation [5]. Whole blood is less commonly used since the formed elements present in whole blood contribute to its complexity and are more difficult to incorporate into a microfluidic platform due to the possibility of cell adherence to micro-channels, channel clogging, and other contaminating

effects. Blood plasma is the yellowish fluid separated from whole blood when processed in a centrifuge and is devoid of the formed elements found in whole blood. Blood serum is the fluid component of blood plasma without clotting factors. Therefore, serum is an ideal biological fluid to use in a microfluidic system since it is free of formed elements and clotting factors and can essentially be treated as a Newtonian fluid, which allows for easier modeling and more idealized flow behavior. One advantage of using blood plasma over blood serum is that protein fractions in plasma are more reproducible since none of the clotting factors have precipitated [4]. Another advantage of using plasma is that blood viscosity can be a good, nonspecific indicator of disease progress and has significant pathophysiological relevance due to its dependency on the expression of clotting factors [6], which are not present in serum.

Since there is usually a delay between sample collection and analysis in bench-scale diagnostics, there can be a sample preservation step before sample pretreatment [7]. Though common in bench-scale detections, this step is undesirable and unnecessary in point-of-care diagnostic tools since the fundamental steps are integrated together with relatively short delays.

1.2.2 Sample Pretreatment

Sample pretreatment, also known as sample conditioning, involves the "conditioning" of a raw sample in order to adjust key parameters with the intention of yielding a usable aliquot for microfluidic platforms. The key parameters that we have identified in this project are fluid viscosity, pH, and electrical conductivity. Highly viscous samples such as sputum or whole blood can significantly increase processing time and power requirements, clog microchannels, and interfere with flow, ultimately rendering a device useless. In the case of electrophoretic micro-chips, sample parameters such as pH, conductivity, and ionic strength have a major influence on the intended effects of the chips, namely electrolysis and Joule heating. Therefore, this pretreatment step will prove essential for subsequent chips that depend on similar electrophoretic

manipulations. More generically, sample pretreatment may include the addition of buffers, treatment with specific enzymes, dilutions, and other adjustments of the initial sample.

1.2.3 Sample preparation

Also referred to as sample pre-concentration, target isolation, or signal amplification, this step aims to adjust the concentration of analyte in a sample so that it falls in the limit of detection range for the specific analytical technique used. Since there is often background "noise" in a raw sample, such as high levels of protein or DNA expression, the sample concentration step usually involves the separation of the sample noise from the analyte of interest. This essentially "purifies" the sample, making it easier to detect the target analyte. One should note, however, that the amount of analyte in the sample does not change; rather, the apparent concentration of analyte increases, which is based on the amount of exogenous analytes.

An area of increasing interest in microfluidics involves electrochemical microfluidic chips that perform separations of fluid samples. Most of these techniques utilize differences in the electrophoretic mobilities of different components of a sample to their advantage, by separating particles based on their size or charge. Through their use, it is possible to filter out background components without the use of a mechanical filter, which have been known to clog or fail. On-chip or off-chip electrodes function to create the electrical field that is felt by the sample fluid. Therefore, pretreatment procedures that involve the refining of a sample's pH or conductivity are of great importance since most raw samples exhibit values of these parameters outside a given accepted range and will not allow for productive separations. Pre-concentration is not always necessary with a sample but can greatly enhance the detection capabilities of the analytical technique.

1.2.4 Detection/ Post processing

The most identifiable step in the entire bioanalysis cascade is the detection step. It is here that a specific analyte from an initial sample is either recovered or overlooked. Traditional immunodetection theory has been applied to many different detection techniques by functionalizing micro-surfaces with antibodies specific to a target analyte. Once the analyte binds with its specific antibody, a change occurs in some physical property (electrical, optical, mechanical, etc.) which is then converted to an electrical signal that can be processed. After the signal is generated, a user can interpret collected data to determine whether a target analyte is found, and in what quantity. Post-processing is usually required before data can be effectively interpreted since there is generally a significant amount of background noise that can obscure the signal of interest, such as non-specific binding. If qualitative results are preferred, a simpler approach may include user inspection as a detection technique, as seen with fluorescent or colorimetric strips, found in many OTC pregnancy tests. Due to the large amounts of raw data collected, post processing is usually desired to alleviate some of the interpretational responsibilities of the user.

1.3 Pretreatment Introduction

1.3.1 Why pretreatment is necessary

The term “sample pretreatment” encompasses a wide range of procedures and can have a variety of meanings. For the purposes of this project, we will continue to refer to “sample pretreatment” as described earlier, namely the step in between sample collection and sample preparation where samples undergo primary conditioning so they can become more optimized for subsequent steps. Pretreatment procedures can include buffer addition, mixing, enzymatic digestion, centrifugation, dilutions, heating, cooling, condensing, or any other action that prepares the sample for its utilization in the detection device. Traditionally these procedures are performed off-chip, in a

laboratory setting using bench-scale instrumentation. Trained users are required to carry out these actions which involve significant sample handling and the use of additional laboratory equipment before the sample is optimized for its next step. If the intended use of the diagnostic instrument is in a clinical setting where trained staff members have access to this necessary equipment, then on-chip pretreatment procedures may not be necessary. However, the ultimate objective of POC diagnostic devices is to target remote locations that could be hundreds of miles from a medical center. In order for devices to operate in such extreme conditions, sample pretreatment procedures should be self-contained within the device.

Off-chip sample pretreatment raises a number of concerns. First, user-handling becomes an issue if the end user is required to perform pretreatment procedures themselves, necessitating user training. There are also concerns about sample contamination, as increasing the number of contacting surfaces increases the risk of contamination. Lastly, if the device requires laboratory procedures to pre-treat samples, the portability of the device is severely limited.

In order to address these concerns, we have proposed to develop a self-contained pretreatment chip to incorporate with the fluidic network of a detection device. The proposed pretreatment chip will allow for complete incorporation of multiple fluids via previously established micro-mixing techniques. Eventually the chip will be incorporated with other microfluidic devices, so it will be designed and fabricated using common polymeric micro-fabrication techniques. Since the device requires experimental validation, it will be designed and fabricated to functionally operate independently of any subsequent microchip.

1.3.2 Current Pretreatment Strategies

There is no universal preparatory technique for biological samples since sample preparation is highly dependent on not only the location or type of sample, but also the identity of the target analyte and constituents of the sample. Consider testing for the presence of glucose in whole

blood and in pancreatic tissue extracts; even though the target analytes are the same, the compositions of both samples are vastly different. Currently, sample preparation and pretreatment techniques are conducted on the bench-scale, in clinical laboratories after raw samples have been received. Even the bench-scale instrumentation that is currently used has not evolved to the point where a raw sample can be completely analyzed without an intermediate step [7].

Bench-scale pretreatment methods include the solubilization of tissues, partial/complete sample decomposition, sample dissolution, and analyte extraction from complex matrices, all of which result in aqueous solutions [8]. Furthermore, processes such as sample filtration, centrifugation, distillation, dilution, target amplification, and extraction are also considered to fall under the realm of bench-scale clinical pretreatment techniques [9]. Clinical pretreatment protocols often involve the depletion of a raw sample from commonly occurring background analytes, such as removing albumin from blood serum [10], or proteins from urine [11]. The primary goal of bench-scale sample pretreatment is to arrive at a solution where the resulting analyte is present in a form that is compatible with the detection technique.

On-chip sample pretreatment has made progress in areas of liquid manipulations associated with bench-scale techniques, such as aliquoting, adding reagents, and mixing, though manipulations involving variable raw samples have yet to be realized [3]. Besides the complexity of certain raw samples used, the very small volumes incorporated on-chip makes certain manipulations, such as sample dilutions, much more difficult than their bench-scale equivalents. One major concern about the use of biological samples in microchips remains the possibility of surface adhesion and clogging, especially if the initial raw sample inlet becomes clogged. Parameters such as viscosity must therefore carefully be selected on-chip or off-chip.

Another area of sample pretreatment is concerned with the method of flow injection techniques, which involves the automation of sample and reagent handling with strict control of reaction

conditions [12]. Some of these methods include filtration, dialysis, gas diffusion and column sorption [12] which are primarily concerned with chemical samples and overlap into the category of sample preparation. Progress has been made in this field as on-line sample digestion is becoming incorporated with flow injection.

Most literature reviews of on-chip sample pretreatment and preparation primarily focus on separations, which function to isolate the target from the background matrix or pre-concentrate the specific analyte by filtering out exogenous analytes. However, most of these publications fail to account for methods of optimizing the initial sample for these preparation steps, especially if electrical phenomena are involved. This idea of pretreating raw samples to optimize them for immediately following separations has become the primary motivation for this project.

1.3.3 Project goals

Sample pretreatment is often an overlooked area of LOC diagnostic devices. Most bioseparation and detection research is performed with pre-conditioned samples instead of raw samples, which are the intended clinical targets. This project also aims at developing awareness of the importance of on-chip raw sample pretreatment.

The Cal Poly Biofluidics lab has several on-going projects that deal with electrophoretic manipulations on polydimethyl siloxane (PDMS) chips, such as dielectrophoresis (DEP), isotachophoresis (ITP), isoelectric focusing (IEF), and free flow electrophoresis (FFE). Therefore, the device originating from this project is intended to ultimately serve as a preliminary chip that could interface with one of these developed devices. The optimization of electrophoretic separation chips usually involves minor changes in the electroosmotic mobilities of target analytes and background molecules. Therefore, the pretreatment regimen proposed for this device was designed to adjust the pH and conductivity of the raw sample, two properties that can highly

influence a particle's electroosmotic mobility. In addition, the sample viscosity will also be adjusted in order to make the sample more compatible with microchannel flow.

The goals of this project include (1) demonstrating knowledge of current pretreatment techniques, (2) scaling down a bench scale pretreatment protocol to incorporate with a microfluidic device, (3) designing, manufacturing and testing a microfluidic chip, (4) modeling fluid interactions with COMSOL™, (5) verifying sample/buffer incorporation on chip by experimentally observing a homogeneous distribution of sample through the exit channel, and (6) producing these effects rapidly on-chip, within several seconds . Our project will be deemed successful if these goals are met.

1.4 Electrophoresis Background

1.4.1 History and Background of Serum Fractions

The diagnostic promise of serum protein analyses is by no means a novel, recent development. Serum fractions have been analyzed clinically since the early 1940's [13]. At that time, researchers were concerned with fractionating different serum proteins for therapeutic usage during World War II, but diagnostic interest grew as correlations were made between the expression of certain proteins and patient disease stages [13]. For more than 20 years [14], agarose gel electrophoresis has been one of the most widely used methods of protein fractionalization in clinical biochemistry. Information related to the operation of agarose gel electrophoresis can be found in Appendix A. Operating on the same principle as agarose electrophoresis, capillary electrophoresis (CE) gained widespread popularity as another method for protein separation. Advantages of clinical-based CE over agarose gel electrophoresis include decreased separation time, decreased reagent usage, decreased sample consumption, and higher resolution [15]. The advent of CE in the mid 1980's [16] propelled research into micro-scale devices that can separate and analyze serum proteins faster and more accurately.

1.4.2 Capillary Electrophoresis

Capillary electrophoresis (CE) operates on very similar principles as gel electrophoresis except that there is usually no stationary phase. Most CE methods employ free solution approaches, which can be used to analyze a wide variety of charged and uncharged species of different sizes [16]. The most common method of CE, and most similar to the Biofluidics Group free flow electrophoresis microdevices, is capillary zone electrophoresis (CZE). In this method, a very small capillary is filled with an electrolyte buffer solution and connected to an anode at the sample entrance and a cathode at the detection region, as seen in Figure 2.

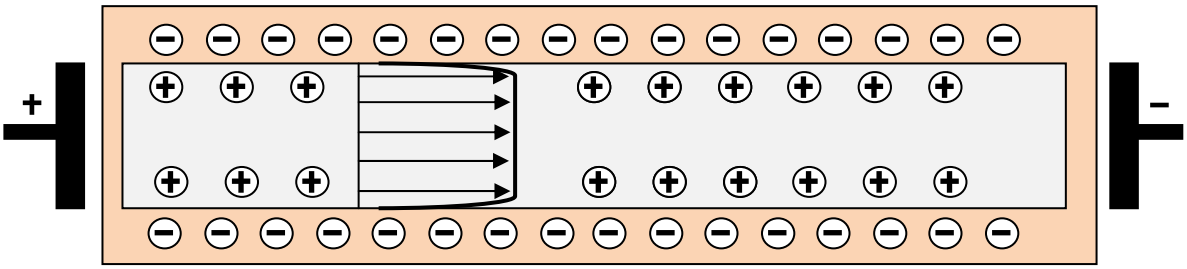

Figure 2 - Conceptual drawing of CE system

This figure represents a cross-section of a typical capillary electrophoresis system, viewed conceptually. As the voltage is applied through the electrodes at the ends of the capillary, a layer of positively charged ions migrate to the negatively charged glass walls, shown in beige. The electroosmotic flow through the system drives the solutes through with a flat velocity profile, shown by the directional arrows. Since the positive electrode is on the left of the above system, the solutes will elute out the right end of the capillary.

A small volume of sample is then injected into the inlet which fractionates into distinct “zones” in the capillary and elutes from the detection end in a predictable order [17]. Since the zones are separated, this method allows for reliable quantification and further isolation of sample fractions [16]. Instead of being pressure-driven, the buffer solution along with the injected sample undergo electroosmotic flow (EO flow), the term used to describe the movement of fluid under an applied electric field as ions in the fluid migrate towards the electrode of opposite charge.

The basis of almost all electrophoretic separation techniques is the innate migration of charged solute particles in an applied electric field. Subtle differences in the migration speed can effectively separate two otherwise similar solutes. This separation technique has been successfully applied to solutes ranging from single ions to whole cells [16]. The migratory velocity is known as the electrophoretic mobility, μ_E, and is defined as the average velocity with which an ion moves under influence of an applied electric field [16] and is expressed relative to the fluid domain. Another commonly used term to describe particle movement under the influence of an applied electric field is the electroosmotic mobility (EOM), which describes the

movement of a particle relative to a fixed, stationary phase such as a wall. CE separations commonly employ the term EOM when describing solute fraction selection. For more on the underlying theory of electrokinetic separations, refer to Appendix A.

1.4.3 Buffer influences on EO Flow and EPH Mobility

Not surprisingly, changes in buffer parameters such as pH and conductivity can have a considerable impact on the resolution of solutes in electrophoretic separations by influencing both EO flow and individual electrophoretic mobilities. Buffer pH has a significant effect on EO flow since it directly influences the amount of surface ionization of the capillary wall, which can alter the wall potential, known as the zeta potential. To see how the zeta potential influences the bulk movement of fluid, refer to equation 7 in Appendix A. High pH values have been shown to increase the EO flow by increasing the amount of surface ionization where low pH values have the reverse effect [18]. High EO flow rates are usually desired in CE since they result in faster separation times; however, there is a trade-off between rapid separation times and better resolution, with the latter ultimately preferred. Likewise, the pH of the buffer also influences the degree of ionization of the solutes themselves, which affects their electrophoretic mobilities, as seen in section 3 of Appendix A. Alternatively, when the ionic strength, or conductivity, of the buffer increases, the EO flow decreases due to a lowered zeta potential [18]. This has been shown in some cases where increases in ionic strength through the addition of NaCl resulted in a reduction of electric double layer thickness, which in turn decreased the EO flow [16].

Ionic strength, i.e. ionic concentration, is a property very closely related to the conductivity of the buffering solution since both deal with the amount of free charged species present in the fluid. Solution conductivity has a major influence on the electrophoretic mobilities of solutes since it can determine the amount of surface charge of particles and affect their degree of ionization.

The viscosity of the buffer solution is also important to select for since viscous buffers hinder electrophoretic mobilities and EO flow.

The influence of buffer pH on protein ionization affects bulk properties of the sample since serum fractions consist primarily of proteins. It is important to understand this effect, as it is the basis for much of our pretreatment process. Additional information regarding protein ionization can be found in section 3 of Appendix A.

In summary, buffer solutions must be selected carefully to optimize the differences in electrophoretic mobilities of solutes as well as the working conditions of the separation devices, such as the EO flow, which determines processing speed. Buffer pH, conductivity, ionic strength, and viscosity are highly influential in regards to solute separation resolution. Even though buffer selection depends on the target solutes to be separated, high pH values are generally preferred over low pH values and lower conductivities are more desired than high conductivities. The reasons for these selections will be discussed later.

1.4.4 Serum protein fractions using CE

Since capillary electrophoresis has been a well-developed model of clinical importance regarding serum protein fractions, most of the pretreatment work of this project is based on past success in the literature. While we will not be performing the clinical-based separation of serum proteins, the performance of CE is similar to what might be emulated in a microfluidic separation chip. Therefore, close attention is paid to the influence of the buffering solutions on the final resolution of the protein fractions in these works.

1.4.4.1 Serum protein fraction background

Typically, serum proteins are separated into five fractions: albumin, α1 – globulin, α2 – globulin, β-globulin, and γ-globulin [14]. Each fraction is separated based on their differing EOMs, which is greatly influenced by the pH and the composition of the solution buffer. Clinical-based serum separations in CE have traditionally used veronal buffer (5, 5' – diethylbarbiturate) [14], which replaced some of the use of borate buffer [19] due to its improved resolution capabilities; however, since veronal buffer is a controlled drug, other alternatives have been investigated. The replacement of the veronal buffer with Tricine (Tris-Tricine buffer) has had some success; however, it was noted that the α1 fraction co-migrated with the albumin fraction, causing a decrease in fraction resolution since the two EOMs were too similar to discern between [14]. Increasing the ionic strength of the buffer by adding NaCl was shown to help separate the two fractions, most likely by altering a binding site or promoting their disassembly. This is another example of the importance of carefully selecting a working range of solution conductivity and pH values since each can affect surface charge and solute mobility.

1.4.4.2 Case study I: Dolnik, 1995

In 1995, Dolnik's research group determined the effect of pH alterations in capillary electrophoresis fractions of serum proteins [14]. One of the primary trends that they observed was that the mobilities of the serum protein fractions increased with increasing pKa of the buffer, which corresponds to the pH of the solution. Also, at these higher pH ranges (~8-11) they noted a larger difference in the EOMs of albumin and the α1 fraction, thus providing better resolution. However, when the pH of the solution was too high, they started observing smaller differences between the EOMs of the β and γ fractions. Therefore, an ideal solution pH at which all fractions have maximized differences in their EOMs must exist. Dolnik's group reported the best

separation resolutions with MGA-EACA (pH 10.62) and MGA-GABA (pH 10.26) buffers, shown below.

MGA-EACA: [0.1M N-methyl-D-glucamine with 0.1M ε-amino-caproic-acid]
MGA-GABA: [0.1M N-methyl-D-glucamine with 0.1M γ-amino-butyric acid]

In order to prevent viscous clogging of capillary lumen and control the ionic strength of the solution, 4-fold dilutions were prepared for the serum samples before each run.

1.4.4.3 Case study II: Colyer, 1997

A similar analysis of buffer properties was performed by Colyer et al in 1997 on a microchip-based CE system [15]. The biggest difference in working with a microchip-based CE system as opposed to a conventional CE system is that microchips typically use lower voltages. Since lower voltages are associated with longer analysis times, it is crucial to find buffers that allow sufficient voltages to be implemented while simultaneously providing high resolutions. Dolnik's research team found that lower buffer ionic strength enables a higher operation voltage to be used [14]. Dolnik's standard CE system used applied voltages of 11kV for most of their buffers, while Colyer's micro-CE system used applied voltages around 8kV. The pH of the borate buffer used by Colyer was around 10, similar to the buffers used in Dolnik's research.
Colyer found that the high pH value of the buffer carried several benefits. First, the high pH corresponded with negatively charged serum proteins which were repelled from the negatively-charged walls of the glass capillaries. This led to fewer issues of fouling and quicker analysis times since the protein fractions experienced less hydro-dynamic interactions with the capillary walls. High pH values also yielded faster EOMs for the protein fractions which meant faster analysis times. However, there is a delicate balance between analysis time and separation

resolution. Extremely high pH values can result in unstable electropherogram baselines and less reproducible EOMs during experimentation [15]. When pH values are too high, the differences between the EOMs of the fractions start to decrease since they start to reach their maximum flow rates, which results in poorer resolution.

Colyer's group also found that increasing the concentration of the buffer solution caused decreases in EOMs of the fractions. Therefore, in addition to buffer pH, buffer concentrations must also be considered to idealize the separation effects. Another difference between the micro-CE and standard CE systems was that Colyer's team observed serum adsorption problems inside the micro-capillaries. In order to adjust for this issue, 10-fold dilutions were prepared from serum samples before their use. Since this is a common issue with micro-scale devices, care should also be taken to adjust the solution viscosity within an appropriate range.

1.4.5 Adaptation of literature to Cal Poly Biofluidics lab

Since we will not be dealing with actual protein analyses and electropherogram interpretations, the identity of our "idealized" buffer is not of the upmost concern; however, since work in this area has already been completed, we plan to use the two buffer solutions recommended in Dolnik's paper, namely MGA-EACA and MGA-GABA. Previous work with CE buffers [14, 15],[20] has shown that the electrophoretic mobilities of serum protein fractions rely heavily on the pH of the buffer solution, since pH determines the extent of the ionization of serum proteins. Sanz-Nebot [20], along with many others, has shown that for neutral pH values where most serum proteins exist at their isoelectric point, electrophoretic mobilities reach their minimum and almost no movement is observed. In comparison, the maximum electrophoretic mobility of a species is observed when it is fully ionized [20]. This condition exists at either end of the possible pH spectrum since proteins will either accept protons or donate protons in the acidic region or basic region, respectively (refer to the Henderson-Hasselbalch equation in Appendix A, Equation

9). Even though Sanz-Nebot's research team proposed the use of acidic buffers with a pH range around 2.5, similar separations are found in the basic range around a pH of 9-10 with a negative electroosmotic mobility (EOM) [20]. The sign convention of the electroosmotic mobility is of no real concern since it is dependent upon how the system is driven, determined by the location of the positive electrode. The basic pH range is also considered ideal for our application since it should be less abrasive on our PDMS microchannel walls than the acidic buffers presented in Sanz-Nebot's work. The additional benefit of choosing a basic range for separation buffers is that most serum proteins are negatively charged at a high pH, creating an electrostatic repulsion force with the negatively charged PDMS and glass walls [15]. To some degree, this can ameliorate issues of protein adhesion to microchannel walls and prevent biofouling. Also, the basic pH range is likely to result in a more universal surface charge of most proteins, which facilitates separations that are based on solute size.

After our literature survey of pretreatment protocols and optimal electrophoretic manipulation operating conditions, we arrived at a target range for our pretreatment values, shown below in Table 1. Raw serum values were measured for bovine calf serum (BCS) in-house and agree with standard literature values for human serum.

Table 1 - Initial and target pretreatment parameter ranges

Sample	**pH**	**Conductivity (µS/cm)**	**Viscosity (cP)**
Raw Serum	6.924 – 7.144	10,540 – 10,880	1.21 - 1.32
Target Values	10.26 - 10.62 [14]	< 500 - 1000 [21]	1.0 - 1.1cP [22],[23]

1.4.6 Nonspecific Biofouling and Albumin Biofouling

Even though much of the pretreatment protocols presented in this work are based on experimental data from capillary electrophoretic separations of the 5 major serum protein fractions, these broad protein separations can also be applied to electrophoretic-based microfluidic chips. Ideally, electrophoretic separations are utilized to isolate small concentrations of target analyte from a dense population of other biomolecules in a complex matrix. Therefore, separations of this nature are much more specific, targeting a single biomolecule instead of a "fraction" of biomolecules like the five aforementioned serum protein fractions; however, coarse-separation chips can operate on the same scale as the broad CE serum separations by isolating a single protein fraction for further purification. These chips are often used in preliminary separations that can isolate a target range of biomolecules from the complex matrix of the clinical sample.

One of the most important issues in maintaining the integrity of microfluidic chips is the prevention of biofouling. This phenomenon concerns the adhesion of biological substrates such as proteins, bacteria, and viruses to the walls of microchannels. While developments have been made in surface treatments of microchannel walls that prevent this adhesion, care can also be taken to ensure that common fouling agents are removed from these samples. This concern is evident when working with concentrated matrix-solutions, such as blood samples.

Even though whole blood presents clotting and adhesion issues, it is still one of the most commonly used biological samples due to its clinical importance [5]. In order to avoid problems with clotting, we are using blood serum, which is the liquid portion of blood that remains after formed elements and clotting factors are removed. In reality, we are simplifying the ideal end-goal of directly using whole blood removed from a patient as the sample, as the use of whole blood is beyond the scope of this project. There is much ongoing research into the development of on-chip whole blood separations that separate erythrocytes from the liquid portion of blood, which could ultimately incorporate into the present blood serum pretreatment chip.

Though easier to work with, blood serum is not completely void of biofouling concern. Albumin, the most abundant plasma protein [13], is notorious for adhering to surfaces and clogging microchannels. Therefore, by using a pretreatment protocol that is based on the optimized differences in electrophoretic mobilities of the 5 main protein fractions, a preliminary separation chip combined with our pretreatment chip could exploit the buffer's capacity for filtering out the albumin fraction. The resulting "treated" sample would still likely contain the analyte of interest but would be more suitable for transport through microchannels in subsequent microfluidic devices.

1.5 MICRO-MIXING BACKGROUND

This project encompasses both the development of a pretreatment protocol and the incorporation of that protocol onto a microfluidic platform. Since a key requirement for the microfluidic chip is to establish a homogeneous mixture of the initial sample with the pretreatment buffers, it is important to understand common micro-scale mixing schemes and the issues that they face.

1.5.1 Issues with Mixing at the Microscale

The physics that govern phenomena of the macroscale world give rise to numerous effects that are not inherently present at the microscale. For example, turbulent mixing of two liquid streams is extremely difficult, if not impossible, to create in channels on the order of tens to hundreds of microns. Through these microchannels, liquid flow is invariably laminar flow due to the dominant viscous forces generated at the walls [24]. In fact, turbulence all but ceases in microchannel flow. This implies that the primary mode of transverse solute transport in a microchannel is diffusion. An experimental image of fluid segregation in microchannel flow is shown below in Figure 3.

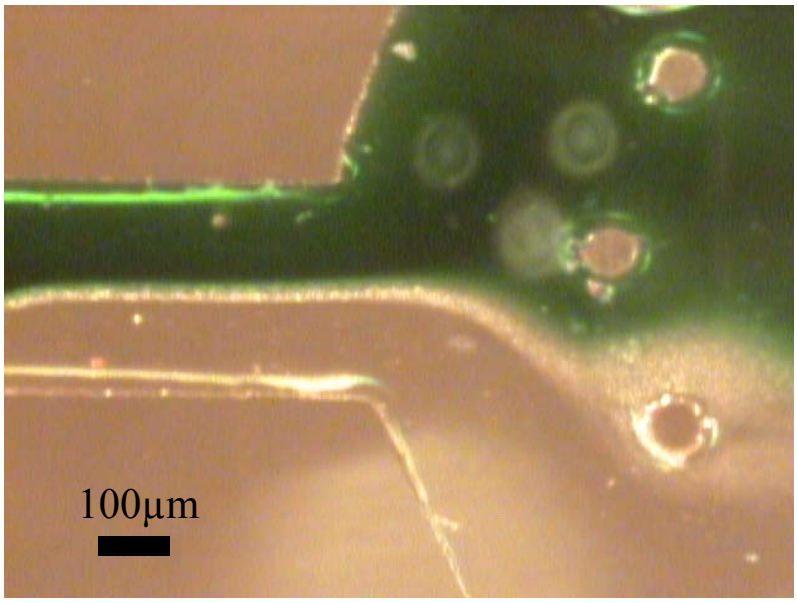

Figure 3 - Experimental image of parallel fluids that stay segregated through microchannel

This image, taken from the LabSmith® inverted microscope, shows the segregation of the sample and buffer inlet streams passing into the mixing chamber. Green food dye was used as the sample solution and DI water was used as the buffer. This inherent segregation of parallel fluid streams is seen in geometries on the micro-scale and is the primary motivation behind the use of micro-mixers when homogenous fluid mixing is desired.

Diffusion can be exploited in many microfluidic designs, but is not sufficient when rapid mixing is desired, due to the long time scale necessary for diffusive mixing. At higher flow velocities, convection becomes dominant over diffusion, creating a highly idealized flow environment in which two parallel fluid stream lines have very little interaction, and thus do not mix. This is an example of how the dimensionless Peclet number can be utilized, as it relates the relative contributions of convection and diffusion. The Peclet number, shown below in equation 1, can elucidate optimal experimental and device parameters to achieve desired effects.

$$Pe \equiv \frac{U_0 w}{D} \qquad (1)$$

In this equation, Pe is the Peclet number, U_0 is the inlet velocity in µm/s, w is the channel width in µm, and D is the diffusion coefficient in $\mu m^2/s$. If we assume a inlet velocity of 100 µm/s

(roughly 1.7 μm/min), a width of 300 μm and a diffusion coefficient of 40 $\mu m^2/s$, which is similar to that of small proteins [25], we obtain a Peclet number of 750. Since our Peclet number is much greater than 1, we can assume that convective phenomena dominate over diffusive phenomena given our experimental conditions. In other words, diffusive mixing would not be expected in our device, since the time-scale necessary for diffusion is much greater than that for convection. In order to enhance this diffusive mixing, we can design narrower channels and use lower flow rates, both of which would decrease the Peclet number. However, there is some trade-off since narrow channels experience higher fluidic resistance and can lead to plugged flow, and lower flow rates may take too long to process.

Since our system is primarily concerned with low Reynold's numbers and high Peclet numbers, we must add either a passive or active mixing component into our system to facilitate the mixing of our two fluids.

1.5.2 Dimensionless numbers

Design in microfluidics revolves around scaling laws, where ideas conceived on the macro-scale must be miniaturized for chip fabrication; however, since the governing laws of physics behave uniquely on the micro-scale in terms of fluidic transport, the same analysis performed on the macro-scale must also be re-examined to verify the intended phenomena throughout the designed system. For this reason, dimensionless numbers are used extensively in microfluidics since they represent the ratio of two competing phenomena which can be easily scaled up or down. Transport properties such as the diffusion coefficient (D), kinematic viscosity (ν), and thermal diffusivity (α) all have the same units of m^2/s and can be combined as nondimensional ratios to estimate which processes dominate [24]. For example, the Reynolds number relates inertial forces to viscous forces and can be used to determine if flow is laminar or turbulent. Even though the Reynolds number is utilized in microfluidics, it is almost irrelevant since most flow on the micro-

scale operates at very low Reynolds numbers and is thus primarily laminar, which contrasts the high Reynolds number intuition most are used to operating with on the macro-scale [25]. Another useful dimensionless number, previously described, is the Peclet number, which relates solute convection with diffusion. This number is relevant to our design because it can determine processing rates of the micro-mixing based on criteria for diffusive mixing.

1.5.3 Types of micromixers

In order to promote mixing at the micro-scale, numerous strategies and designs have been attempted. The broadest distinction between these mixers involves the fields of passive and active mixing. Active micromixers involve the use of an applied external stimulus (mechanical, electrical, etc.) while passive micromixers rely on channel geometries that act as flow barriers [25].

1.5.3.1 Passive micromixers

Most passive micromixers rely solely on the principle of molecular diffusion to combine two streams of fluid. However, this approach is limited since generally long channel lengths are required [26] to reach a critical distance where the two fluids are fully incorporated in each other. In order to improve the capabilities of passive micromixers, research has been done to decrease the diffusion distance between the two fluid streams and induce lateral flow by creating geometric obstacles in channel walls. Decreasing the diffusion distance (channel width) can increase the amount of diffusion that occurs, but can also create more fluidic resistance, which can lead to undesirable consequences such as clogging or pressure build-up. Therefore, many passive micromixers make use of periodic geometric barriers throughout microchannels in order to encourage mixing.

One example of this is the incorporation of grooved microchannel bottom surfaces. In this case, the fluids experience unbalanced flow resistances under pressure-driven flow due to the low resistance felt when flowing along the ridges and the higher resistance felt flowing perpendicular to the ridges [26]. This introduces a rotational element which can result in chaotic stirring of the two separate fluids.

Another popular passive design, known as laminating mixing, splits the inlet channel into an array of smaller channels where the diffusion distances are reduced, and then joins the channels back at a single outlet [24]. The benefit of this design is that it produces the same diffusive mixing one would see in a single narrowed microchannel without the accompanying high fluidic resistance. Though both of these ideas warrant consideration, they also present more demands on microfabrication techniques to achieve their three-dimensional attributes and still require long processing times.

1.5.3.2 Active micromixers

Active micromixers utilize external forces such as electric fields or rotating parts to enhance micro-mixing. The primary benefit of active micromixers is that they provide accelerated incorporation of separate fluids into each other. This is not always the case with passive micromixers, which rely solely on diffusive phenomena; however, the requirements for externally applied stimuli, such as voltage sequencers, must be balanced with issues of device portability and ease of use.

Examples of different “disturbances” that can be externally applied to fluid flow include pressure driven, electrokinetic, magnetohydrodynamic, acoustic, and thermal disturbances [24]. Pressure-driven disturbances and micromachined moving parts were present in some of the earliest active micromixers due to their common use in macroscopic mixers. The major setbacks to moving parts in micromixers include difficulty in manufacturing, fragility, and consistency in operation.

Electrically assisted micro-mixing methods are generally popular alternatives to pressure-driven methods primarily because they can be designed to localize the mixing field in order to yield rapid, complete mixing. Unlike passive micromixers, however, active micromixers that use electric fields are very dependent on fluid properties, such as conductivity. Depending on such properties, an applied electric field may not have much effect on mixing. The applied electric field may also result in undesired consequences of analyte compromising, such as cellular lysis, ionization, or protein denaturing.

For this project, active micro-mixing was desired primarily due its superiority over passive micro-mixing regarding mixing rates. Since portability is an ultimate goal, we will focus on using simpler, reduced electrohydrodynamic disturbances through the application of off-chip electrodes.

1.6 Restatement of Project Goals

After reviewing the principle steps in diagnostic tests along with some of the theory behind electrophoretic separations and micro-mixing, it is evident that an on-chip sample pretreatment chip is of critical importance to the success of POC diagnostic chips. In this project, a PDMS micromixer chip was designed, fabricated, and incorporated with specific buffering solutions so that raw blood serum may be conditioned. The major goal of this project was to rapidly condition at least one of the three target parameters of raw serum, i.e. viscosity, pH, and conductivity, within our target range on-chip.

2 Materials and Methods

2.1 Chip Design

Though the term "sample pretreatment" can include a wide variety of sample manipulations ranging from simple dilutions to enzymatic digestion, this project is focused on the mixing of two or more solutions, which is the technique commonly used in adjusting certain parameters of a sample fluid. Preliminary pretreatment chip design concepts were inspired by a range of active and passive micromixers found in the literature [21, 24, 26, 27]. Since a successful mixing process can be characterized by its speed, active micromixers were an attractive option due to their superiority over passive micromixers with regards to this aspect.

2.1.1 Conceptual Designs

The initial conceptual design included three separate mixing chambers where three key fluid parameters would be modified in a serial fashion. Fluidic ports were connected between all three chambers so that the sample would progress from the first to the last. Ports were also connected to each chamber independently so that separate buffers could be added to their respective chambers. Outlets were also added to each chamber in addition to the main outlet on the last chamber enabling sampling and quantification of desired results at each of the three-stages, shown below in Figure 4.

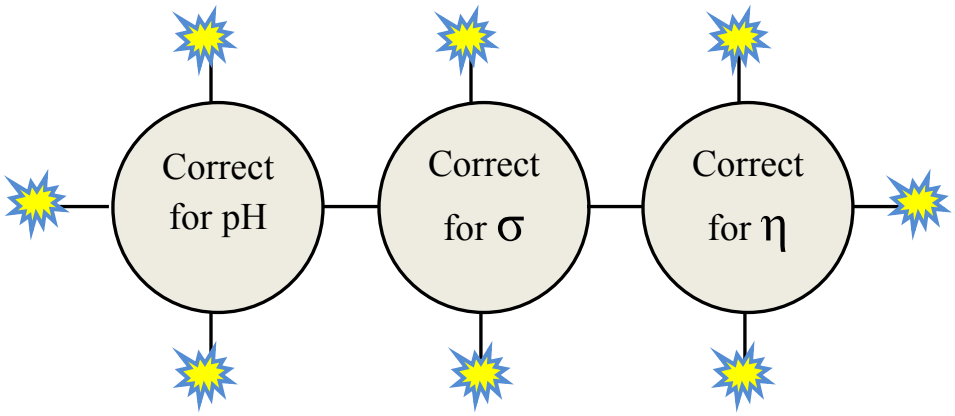

Figure 4 - Conceptual drawing of three chamber mixer

This conceptual drawing shows the three separate locations for serial fluid parameter modification. The yellow stars at the inlets/outlets represent possible sampling locations or inlets for additional buffers.

In the above concept, mixing would have been induced via on-chip electrodes plated onto the surface of the glass substrate underneath four arc lengths of each chamber. However, as pretreatment buffering solutions were investigated, it was apparent that the addition of a single buffer can possible adjust all three parameters simultaneously, thus requiring the use of only a single mixing chamber. The interdependencies of pH, conductivity, and ionic strength provide evidence for this observation.

2.1.2 Single chamber mixer with On-chip electrodes

The second preliminary design dealt with a modified version of the three-chamber mixer in which only a single chamber would be used. The fluidic ports remained in place, allowing for either multiple inlets or multiple outlets, seen in Figure 5.

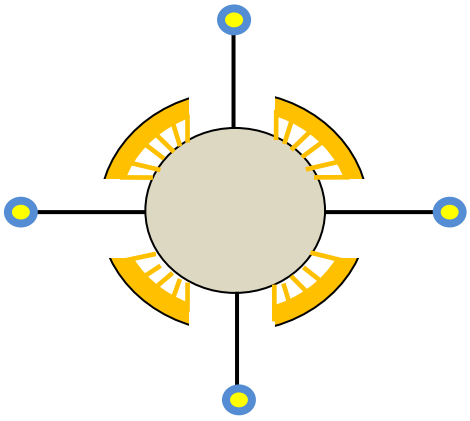

Figure 5 - Concept drawing of single chamber mixer with on-chip electrodes

This conceptual drawing of a single micro-mixer well incorporates on-chip electrodes, shown as the gold arc lengths, with small protrusions towards the fluid interface in the central mixing chamber. Inlet and outlet locations are represented by yellow circles.

This design also incorporated on-chip electrodes, which was ultimately modified in the final chip design to allow for off-chip electrodes. Off-chip electrodes allow for some minor adjustments in positioning, which was helpful in generating experimental data on optimal electrode placement. Ultimately, if our fabricated chip were to be incorporated into a lab-on-chip platform, on-chip electrodes would be desired in order to minimize bulk instrumentation.

2.1.3 Single chamber mixer with Off-chip electrodes

The primary inspiration for AC field-induced electroosmotic micro-mixing came from Michael Oddy's and Juan Santiago's micro-mixing chip from Stanford's microfluidics lab [21]. Through experimentation, they observed an effect they termed "electrokinetic instability", which is the driving force behind their electroosmotic micro-mixing. Two micromixer designs were fabricated in their work: one PDMS chip designed to produce AC-electrokinetic mixing through a channel, and one glass device that contained much smaller channels and a localized mixing region. Their glass chip was fabricated by common photolithographic techniques to etch microchannels into the borosilicate glass. Key geometric features included 300 μm wide by 100 μm deep microchannels

and a 1mm x 1mm x 100μm square mixing chamber that housed a net volume of 0.1μL. However, right angles found in such rectangular chambers are notorious for resulting "dead space" – areas where fluid flux is insufficient to prevent collection of solutes or debris. The main similarity between our design and Oddy and Santiago's is the off-chip electrode placement in two electrolyte reservoirs that are connected to the mixing chamber. Two important modifications to this existing design incorporated into this project include replacing the glass chip with PDMS and fabricating a circular mixing chamber to eliminate "dead" space. In order to justify the selection of PDMS as our platform material, we have included a short overview of PDMS and its properties that make it a suitable material for POC diagnostic platforms in Appendix B.

Our design also included a series of angled obstacles to create flow barriers, ensuring that appropriate mixing is maintained after the sample exits the mixing chamber. The role of the obstacles is to divert flow sufficiently to cause analytes to cross adjacent stream lines. This passive mixing element was inspired by the periodic geometric posts used by Chanh-Hsien Tai [27]. Tai's lab incorporated passive and active components into their design to create an effective micromixer but also used glass as their working material. Since our mixing obstacles would be fabricated out of PDMS, a common elastomeric MEMS material, a computer model was created in COMSOL™ to ensure that the obstacles would not experience sufficient shearing under typical fluid velocities to cause obstacle buckling.

2.1.4 Design requirements

Additional design requirements were imposed by fabrication limitations. Chip designs were sent to the Stanford Microfluidic Foundry for fabrication of a mask and several PDMS chips. The foundry had several different design criteria that had to be met in order to ensure that the fabrication limitations were not exceeded. One important restriction was that no feature could be designed or fabricated having an aspect ratio lower than 1:10, height to width. Since PDMS is an

elastomeric material, it is prone to collapse in structures with higher aspect ratios and could cause unfortunate blockages in fluidic channels. Features can be created with aspect ratios larger than 1:10 as long as they provide support posts in the design where the spacing between the posts is lower than the limiting 1:10 aspect ratio. Support posts were necessary in the design of the pretreatment chip since the mixing chamber had an aspect ratio greater than 1:10 (calculated at 1:37.5). After some simple geometric analysis, it was determined that the best post locations would be one at the center of the mixing chamber and 8 equally spaced apart lying on a inscribed circle with half the radius of the mixing chamber. Another design criterion was that alignment tolerances had to be designed for at least 30 microns, which meant that features should be designed to function properly despite alignment errors of 30 microns in all directions. Other geometric parameter limits included the following, seen in Table 2:

Table 2 – Important design limitations for PDMS chips, Stanford Microfluidics Foundry

Parameter	**Value**
Minimum overall chip thickness	3 mm
Maximum overall chip thickness	7 mm
Minimum possible feature size	5 μm
Maximum possible feature size (rectangular profile)	150 μm
Minimum center-to-center spacing between punch holes (20 gauge)	1500 μm

2.1.5 Mask Design

Mask designs were made using AutoCAD™ [28], as specified by the Stanford foundry due to its high resolution, which is essential when dealing with micron-sized features, and compatibility with the foundry's design protocols. The final mask design is shown below, in Figure 6.

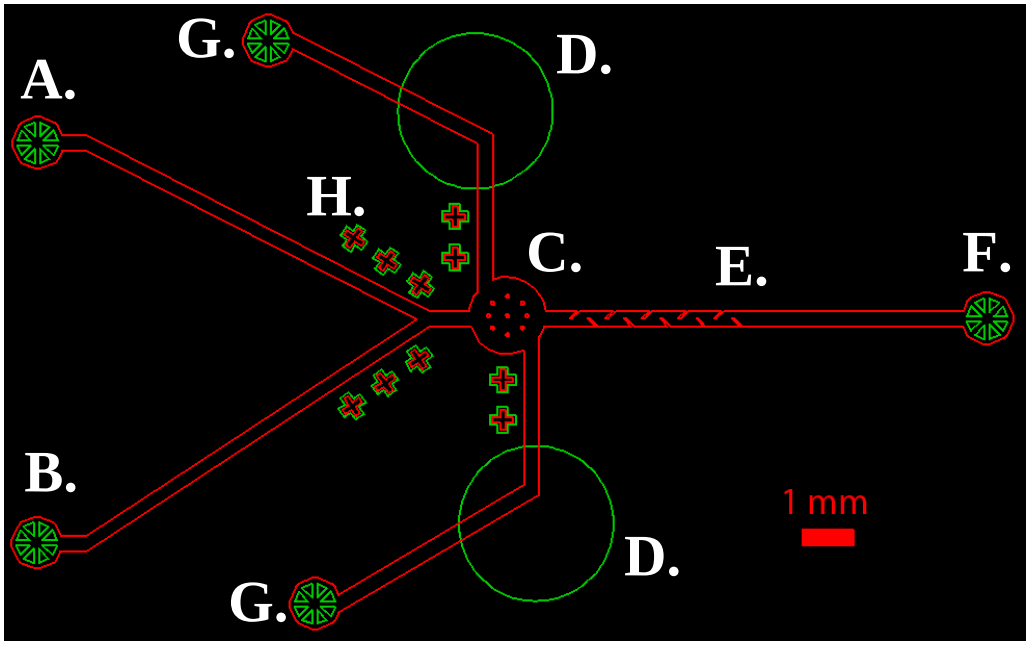

Figure 6 – AutoCAD™ mask design

This figure is a screen shot of the AutoCAD™ mask that was sent to the Stanford Microfluidics Foundry. Geometries created on the first layer are highlighted in red, while geometries created on the second layer are highlighted in green. Overlap of the two layers, as seen where the green electrolyte reservoirs overlap the red fluidic network, ensures that all geometries drawn will be connected once the PDMS is pored over the resultant mold. Key features in the mask to note include: A) Sample inlet, B) Buffer inlet, C) Mixing chamber, D) Electrolyte reservoirs, E) Outlet channel with mixing obstacles, F) Outlet port, G) Electrolyte inlet ports, H) Alignment markers.

The electrolyte reservoirs were desired to be slightly deeper than the rest of the channels. As a consequence, it was necessary to produce a multilayer mask design. In order to create the mask template, a fluidic network was drawn onto the first layer containing the mixing chamber outline, post outlines, and mixing obstacle outlines with the electrolyte reservoirs drawn onto the second, raised layer, shown in green in Figure 6. Alignment markers, shown above as (H) in Figure 6, were included around geometry features to minimize error with aligning the mask for the second layer. Also, all geometries that were connected, such as the fluidic network, were drawn so that the geometries slightly overlapped, preventing any possible gap between them. Punch marks were added at the intended fluidic inlets and outlets to allow for easy alignment with the foundry's hole

puncher. Three copies of the same design were drawn onto the same mask template in order to be more cost efficient. A Solidworks™ rendering of the final, assembled chip can be seen below in Figure 7.

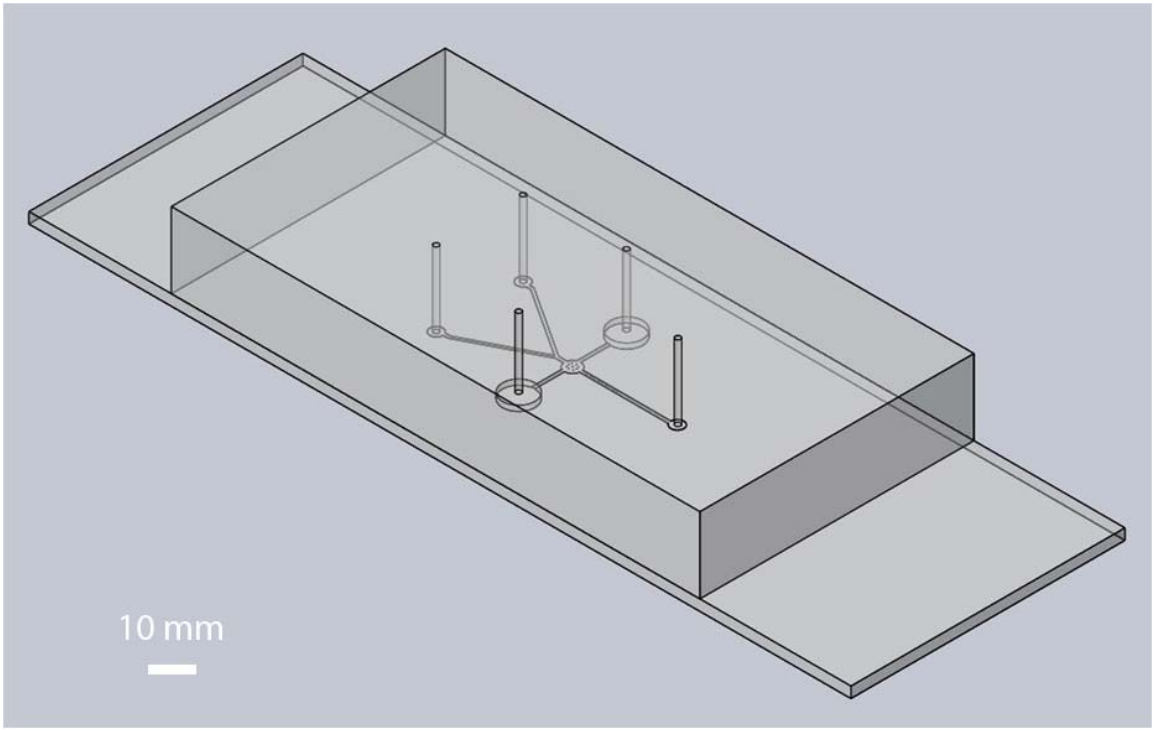

Figure 7 – Solidworks™ rendering of final PDMS chip bound to a glass substrate

The same geometry created in AutoCAD™ was drawn in Solidworks™ to present a 3D rendering of the final device. PDMS is shown as the top rectangular prism with the mask geometries embedded in the bottom surface. The PDMS is then bound to a glass substrate, in our case, a 1”x3” microscope slide. Punch holes are also represented in the above figure as cylindrical holes spanning the length of the PDMS block.

2.1.6 Computer Modeling

During the design process, computer modeling was employed to optimize important characteristics of the microchip design using the multiphysics finite element analysis program, COMSOL™ [29]. This software allowed for simultaneous combinations of fluid flow, convection and diffusion, and electrokinetic analyses. As mentioned earlier, COMSOL™ was also used to

perform fluid-structure interaction analyses with the PDMS mixing obstacles. Initial chip designs were drawn by hand before being drawn in AutoCAD™. From AutoCAD™, the geometry files were imported into COMSOL™ in order to analyze the design.

2.2 COMSOL Modeling

During the design process, computer-based modeling simulations were employed to aid in the optimization of mixing effects as a function of microchip geometries. COMSOL™ Multiphysics, a finite element analysis package used extensively in fluid mechanics studies, was used as a key mask design tool and also as an experimental design tool for optimizing certain parameters. The basic process behind simulations in COMSOL™ includes defining a working geometry, specifying certain subdomain and boundary conditions, creating a mesh over that geometry, and solving the selected equations to yield any desired results. Since the main geometrical difference between our proposed design and Oddy's was the passive mixing obstacles present in the exit channel, we ran a COMSOL™ analysis on the inclusion of the obstacles to observe the effects they had on the degree of mixing.

2.2.1 Obstacle Validation

In order to study the effects of the mixing obstacles, a simple geometry was created in COMSOL™ that included a mixing chamber, an inlet channel, and an outlet channel. The dimensions of the geometry were not of any concern as long as the comparison of the two scenarios was conservative. Support posts were added to the mixing chamber geometry to add to the authenticity of the model. The COMSOL™ model was made in 2D since the height : width aspect ratio of the geometry was small enough to warrant the assumption; therefore, posts and obstacles added to the model were simply voids where the fluidic network must flow around. The physics models selected for this simulation were the Navier-Stokes equations, Convection and

Diffusion equations, and Conductive Media equations. Using these modules, a simulation of an electrokinetic mixing chip was created where two sets of positive and negative electrodes were implemented around the mixing chamber to stir two separated fluid streams. Two separate geometry models were analyzed: one with the passive mixing obstacles present in the exit channel and one with the obstacles absent. Each of these models was simulated for conditions when the electric field was turned on and when the field was off. After a 0.5 second simulation, surface plots of concentration for each of the geometries were displayed, seen in Figure 8.

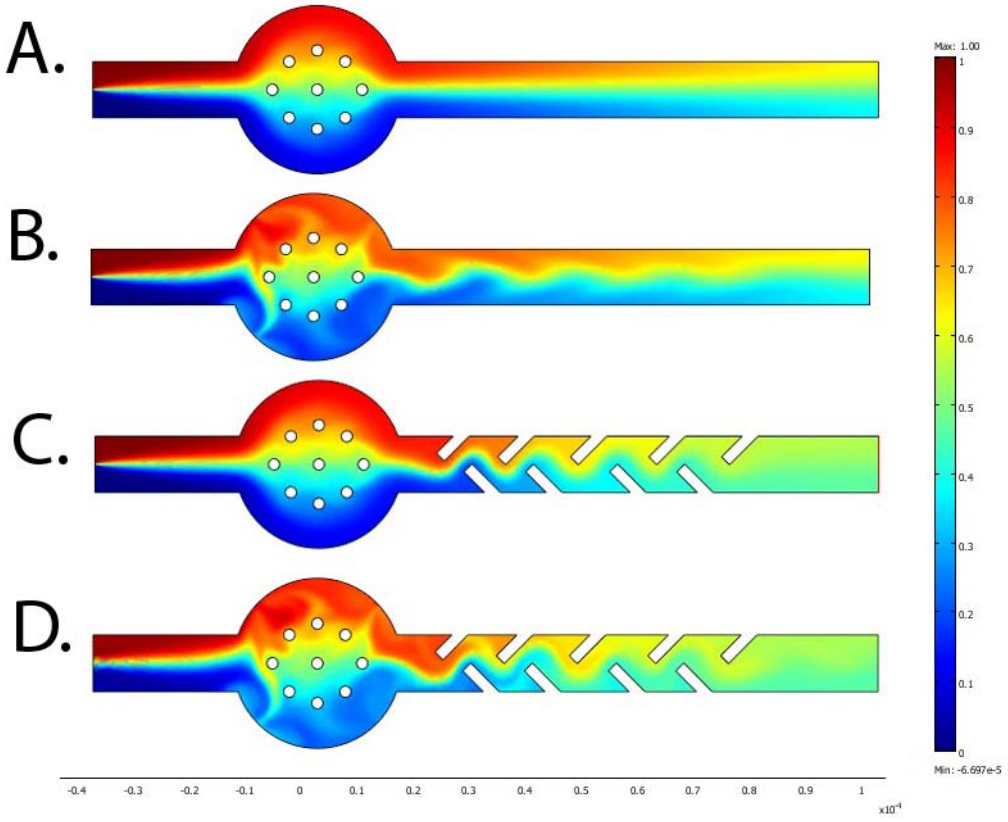

Figure 8 – COMSOL™ surface plots of concentration for obstacle analysis

The colorbar on the right is scaled between 0 and 1, represented as blue and red, respectively. A value of 1 corresponds with 100%, concentration i.e. the raw sample, while a value of 0 equals 0% concentration, i.e. the buffer solution. Analyses were performed for the following cases: A) No obstacles present, no E field, B) No obstacles present, E field on, C) Obstacles present, no E field, D) Obstacles present, E field on. From these analyses, it was apparent that outlet concentrations were more homogeneous in the two cases with obstacles present, C and D.

The four scenarios were visually inspected to detect any major differences and also used to collect a cross-sectional plot of concentration in the outlet stream. This data was compiled into SigmaPlot™ for analysis. The concentration surface plot was displayed as a color map image on a scale from zero to one where one represented “100% concentration” (i.e. the sample inlet concentration), and zero represented “0% concentration” (i.e. the buffer inlet concentration). This data can also be viewed as an estimate of fluorescence intensity if the sample solution was a fluorescent dye.

Inspection of the combined outlet concentration cross-section plots for all four cases yielded some interesting results. Since the data displays the concentration profile of the end of the outlet channel, a horizontal line at 50% (concentration = 0.5) would be indicative of homogeneous mixing, where the sample fluid is completely incorporated in the buffer fluid. A case where mixing is not optimized would yield a more vertical plot where the width of the exit channel contains two extreme concentrations: closer to one and zero, respectively. The plot is shown below, in Figure 9.

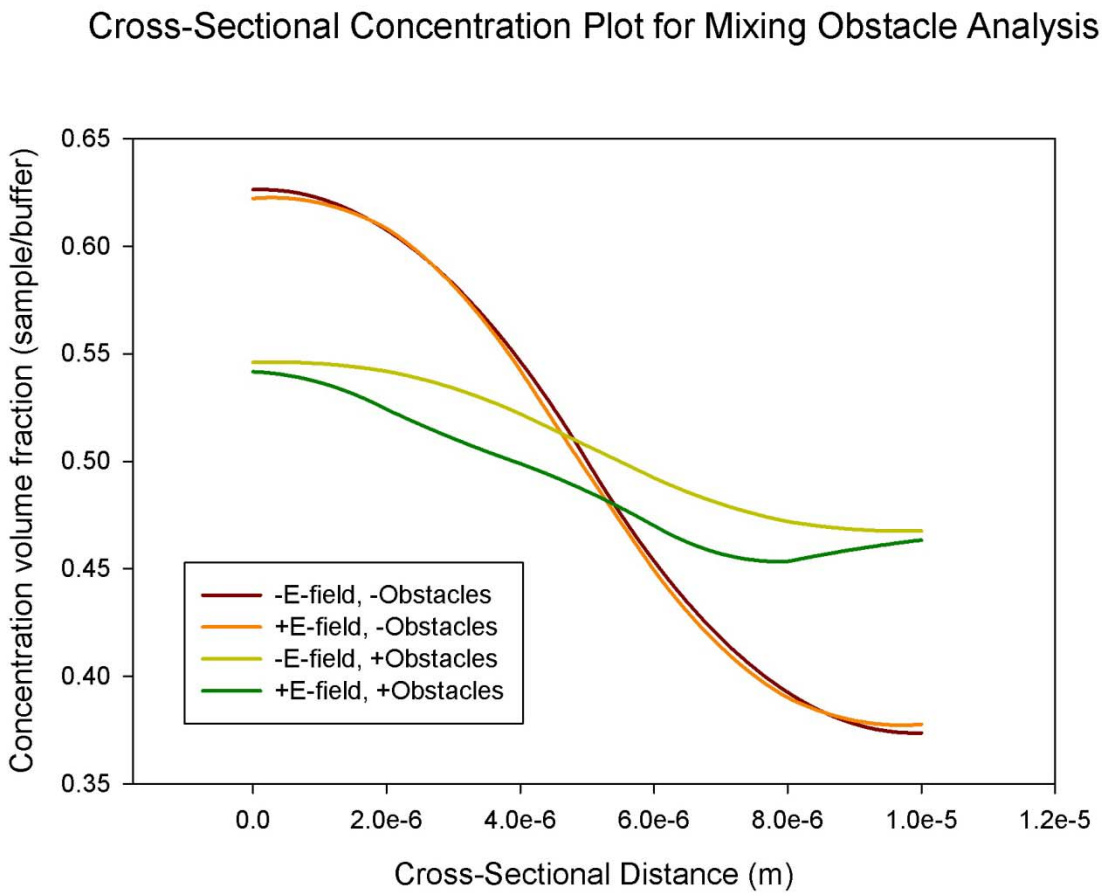

Figure 9 - Outlet concentration plots for COMSOL™ obstacle analysis

Concentration data from Figure 11 were extracted at the end of the exit channel and plotted in SigmaPlot™. Homogeneous outlet concentration was expected to have a horizontal concentration curve indicating that similar concentrations were observed across the total exit channel width. The curves in the above plot correspond with the legend, indicating the experimental conditions for each study. From this plot it was abundantly clear that the presence of the obstacles contributed significantly to homogeneous mixing.

After inspecting the first two cases where the geometry did not include obstacles, it appeared that there was little difference in the concentration profiles between the cases where the electric field was on and off. In both cases there was still significant separation of the two fluids in the exit channel, though the case where the electric field was on did seem to produce a slightly more horizontal curve, which could have become more apparent after a longer simulation time. Comparing the last two cases resulted in a similar phenomenon where there was not a major

difference for the electric field case of the same geometry; however, it appeared that the electric field had a small impact on the concentration profile in the outlet stream, possibly showing a synergistic effect. The most obvious difference in the four cases was between the two geometry models. The model with the mixing obstacles present clearly resulted in a more normalized outlet concentration profile closer to 50%. Even using the obstacles model without any electrokinetic mixing appeared to yield better mixed outlet streams than the active mixing model without obstacles. Results from this analysis indicated the importance of these passive mixing obstacles for ensuring that a well-mixed sample reaches the outlet.

2.2.2 Obstacle Shearing Analysis

Before we decided to include the obstacles into the final design, we ran a fluid-structure interaction simulation in COMSOL™ to determine if the obstacle geometry would hold up to repetitive flow introduction. Since the geometry model used for this simulation clearly influences the results, we imported the same AutoCAD™ geometry used to fabricate the mask into COMSOL™ for analysis. Conditions were assigned such that the two main variables of the analysis included the inlet flow rate and the elastic modulus of the obstacles. This analysis was also run in two dimensions which meant that the obstacle geometry was a planar trapezoidal figure. At first, all ten obstacles were run in the same simulation. However, it was noted that the first two obstacles experience the greatest fluid velocity, and thus the most mechanical stimulus. Therefore, the analysis was simplified to studying a single obstacle at the start of the exit channel. Since PDMS is a polymer that is prepared by adding a crosslinking agent to a base, its mechanical properties are highly dependent on the ratio of these two components. The elastic modulus of PDMS is said to vary anywhere between 100kPa and 3MPa [30]. We ran two different modulus cases, one at a “worst case scenario” 100kPa, and one at a conservative 1MPa. For each case, six different inlet velocities were analyzed (only three shown), including 100μm/s, 500μm/s,

1000μm/s, 5000μm/s, 1cm/s, and 5cm/s. After each computational study, an image was recorded that contained a surface plot of the displacement (microns), a contour plot of the Von Mises stresses (Pa), and a streamline plot of the fluid velocity field, shown below in Figure 10.

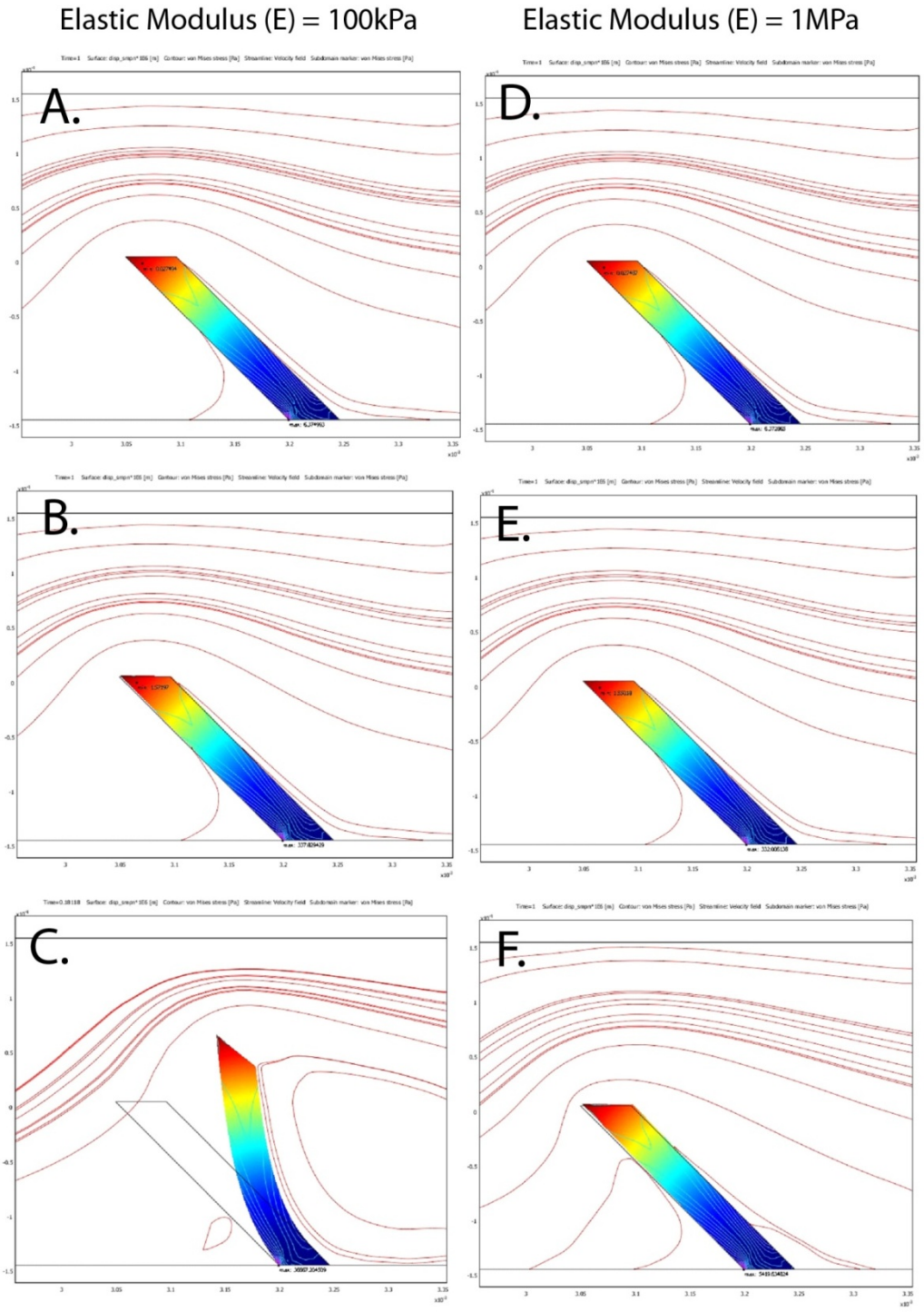

Figure 10 - COMSOL obstacle shearing analysis results

This figure demonstrates the range of obstacle shearing that was generated under different test scenarios. Images A, B, and C represent tests where a PDMS elastic modulus of 100kPa was assumed and images D, E, and F represent tests where a modulus of 1MPa was assumed. Flow rates were adjusted for each case as well and are shown in Table 3.

Table 3 - Modeling parameters for obstacle shearing analysis (Figure 10)

Figure Letter	Inlet flow rate (μm/s)	Maximum stress (Pa)
A	100	6.37
B	5000	337
C	50,000	36,700
D	100	6.37
E	5000	332
F	50,000	5,420

Comparisons between the two moduli appeared similar, though as predicted, the study with the lower modulus experienced higher stresses and greater displacements. Even though we did notice obstacle failure in the 100kPa-5cm/s scenario, these conditions are extremes that we would likely never see in our application. Possible flow rates in our chip were on the order of a few hundred microns per second with the possibility of a few thousand microns per second when the chip would be flushed out by hand. Still, this model neglected the influence of the three dimensional geometry where the top and bottom surfaces were strongly anchored, as the top was embedded in PDMS and the bottom was plasma bonded to glass. Even though we would not likely observe the same stresses in our chip, it was important to note that the highest stress in each case occurred in the same critical location. The stress was concentrated at the bottom left corner of the obstacle, where it made contact with the exit channel. This effect was expected due to the sharp edges drawn into the mask geometry, yielding a stress concentration. A fillet geometry could have been used to alleviate this condition, but would also create fabrication challenges. As long as inlet velocities remain around our workable range, the mixing obstacles pose no functional problems.

2.2.3 Velocity / Flow Rate Model

After chip fabrication but prior to experimental observations, a COMSOL™ model was created in order to optimize the inlet and outlet flow conditions so that the sample fluid would be directed towards the outlet and not towards the electrolyte reservoirs. The AutoCAD™ file that was used to create the mask was imported into COMSOL™ so that all of the channel geometries would be accounted for. No other module besides the Navier-Stokes equations was necessary since all that was being observed was fluid velocity profiles. The sample and buffer inlets were set at the same flow rate while the two electrolyte reservoir ports were set as open boundaries. All volumetric flow rates had to be converted to velocities by dividing by the cross sectional area of the inlet tubing, which was 300 microns in diameter. The inlet flow rates were held to a constant 1μL/s (= 235.78μm/s), while the outlet flow rate was adjusted to account for different ratios of inflow to outflow. Two-dimensional finite element analyses were performed where the outlet flow rate equaled 0%, 50%, 100%, 175%, 200%, and 300% of the inlet flow rate. Surface plots of the velocity field were generated for visual inspection, as seen below in Figure 11.

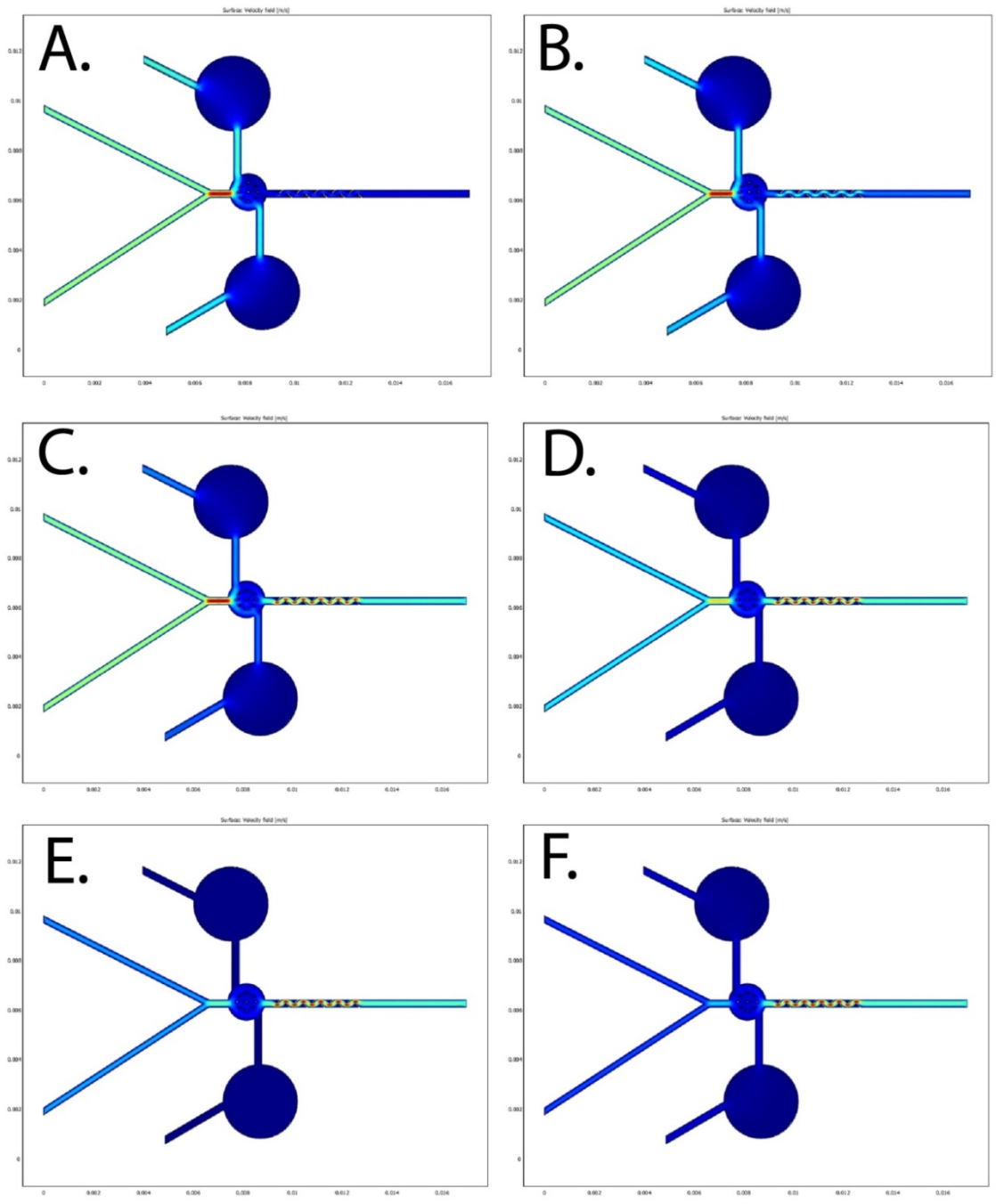

Figure 11 - COMSOL results for flow rate analysis

Surface plots are shown for various inlet: outlet flow rate ratios, where light blue to red regions depict higher velocities indicative of convection regions while dark blue regions depict lower velocities, where flow becomes stagnant. In COMSOL™ the following conditions were used: A) Q_{out} = 0% Q_{in} (open boundary), B) Q_{out} = 50% Q_{in}, C) Q_{out} = 100% Q_{in}, D) Q_{out} = 175% Q_{in}. E) Q_{out} = 200% Q_{in}, and F) Q_{out} = 300% Q_{in}. From this analysis we determined that an outlet flow rate equal to at least 200% of the inlet flow rate was necessary to divert flow from the electrolyte reservoirs.

Table 4 - Modeling parameters for flow rate analysis (Figure 11)

Figure Letter	Outlet flow rate
A	Q_{out} = 0% Q_{in} (open boundary)
B	Q_{out} = 50% Q_{in}
C	Q_{out} = 100% Q_{in}
D	Q_{out} = 175% Q_{in}
E	Q_{out} = 200% Q_{in}
F	Q_{out} = 300% Q_{in}

At the 0% initial case, the outlet was set as an open boundary which appeared to direct almost no flow towards the outlet. As the outlet flow rate increased, the flow rates to the electrolyte reservoirs decreased, directing the flow towards the outlet. Once the outlet flow rate surpassed 200% of the inlet flow rate, flow was sufficiently diverted from the electrolyte reservoirs to the exit channel; therefore, we determined that an inlet to outlet ratio of 1:2 would be the optimal operating condition. Of course this model cannot account for any air present inside the geometry which has a great effect on how flow is directed and was present throughout our experimentation.

2.3 Pretreatment Methods

As mentioned earlier, the buffering solutions chosen for this project resulted primarily from the work of Dolnik (1995) [14] in which a review of how solution variables affected capillary zone electrophoresis (CZE) was conducted. Since most of the pertinent electrophoretic separation technologies to be used in conjunction with this pretreatment device are based heavily on the underlying theory of CZE, we feel that the same buffering solutions should present similar phenomena in a micro-separation device. Figure 12 shows how these buffers were optimized in previous literature work.

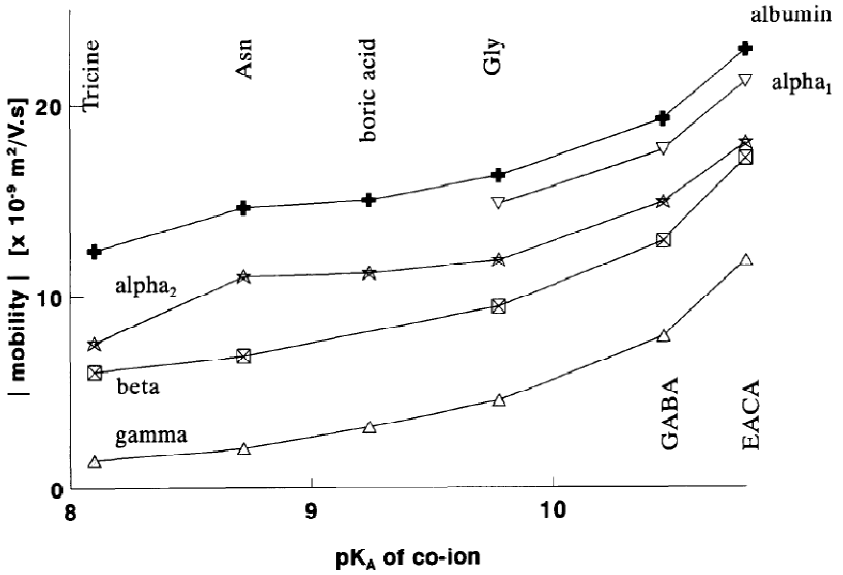

Fig. 4. Effect of pK_A of co-ion on the mobility of serum proteins with methylglucamine as counter ion. Operational electrolyte: 0.1 *M* methylglucamine–0.1 *M* co-ion. Other experimental conditions as in Fig. 1.

Figure 12 – Electrophoretic mobility comparison between serum fractions for different buffer solutions (Dolnik, 1995[14])

Capillary electrophoresis separations of the 5 main serum protein fractions are shown as a measure of electrophoretic mobility for different buffering conditions [14]. An operational electrolyte of 0.1M MGA was used for all cases, though different co-ion solutions were added, as indicated by the vertical text for each of the 6 measurement groups. Since the highest resolutions obtained in CE occur when there is a significant difference between the electrophoretic mobilities of the target solutes, this plot is useful in determining the correct buffering solutions that yield the greatest differences in electrophoretic mobility. For this reason, we chose EACA and GABA as our operational electrolytes, as was done in this original work [14].

After reviewing the separations of protein fractions using different operational buffers performed in this work, it was noted that the optimal buffering solutions presented were 0.1 M MGA-0.1M EACA and 0.1M MGA-0.1M GABA. The plot shown above (Figure 12) indicates how these two buffering solutions achieved the greatest differences in the electrophoretic mobilities of the five protein fractions, which lead to the highest resolutions recorded. It is also important to point out from the plot that the α1-fraction was not even resolved as a separate fraction until the pH almost reached 10, providing more validation for our basic range of buffers.

2.3.1 Buffer and Serum Preparation

The three solutions (meglumine, ε-aminocaproic acid, and γ-butyric acid) were purchased in powdered form from Sigma Aldrich (St. Louis, MO, USA) and stored in a dry environment. Molar solutions were prepared by constituting the separate dry buffers with deionized water. Using the molecular weights of each buffer, specific molarities were produced by adding the correct amount of deionized (DI) water. For example, to create 45 milliliters of 0.1 M solution of MGA, the following calculation was performed, shown in Figure 13:

$$0.1M = \frac{0.1\ mol}{L} \times \frac{195.21\ g}{mol} \times \frac{1\ L}{1000\ ml} \times 45\ ml = 0.878$$

Figure 13 – Sample calculation for buffer preparation

In this case, 0.878 grams of MGA was weighed on a digital scale and added to 45 ml's of DI water in an Erlenmeyer flask. Normally, solutions are corrected to a total desired volume by adding enough solvent, but our method of measuring solute and solvent separately was more consistent and should only deviate slightly from the expected molarities due to the small volumes used. If we had prepared large volumes of buffer, the prior method would have been utilized. The flask was then swirled until all of the dry MGA was dissolved. Once solutions were swirled by

hand, they were transferred to 15 ml centrifuge tubes and vortexed for several seconds. Buffer solutions were normally used within the same day they were prepared, otherwise the solutions were kept at room conditions in tube racks until use. All glassware used to prepare the solutions were thoroughly rinsed with tap water and left to air dry on a rack.

Bovine calf serum was used as a substitute for human blood serum and was purchased in 100ml vials from Sigma. The serum arrived frozen in dry ice and was thawed in a 25°C water bath for one hour. When the serum was not in use it was left in a 2°C refrigerator including all accompanying aliquots. The serum aliquots were removed from the fridge and placed in a tube rack for about 30 minutes prior to use to bring the serum up to ambient conditions. Aliquots of the 100ml sample were kept in 15 ml centrifuge tubes and were vortexed for about 10 seconds before use.

A serum analysis was performed to assess the robustness of each parameter. These included serial dilutions to observe the influence of solution volume on pH and conductivity and linear dilutions to observe the influence of solution volume on viscosity. Buffer solutions were optimized after collecting pH and conductivity measurements for differing concentrations and volume mixtures of each buffer. Since we desired a buffer solution with high pH values and low conductivity values, regression analyses were performed on collected data in order to determine if there were any positive or negative correlations between our measured values and the concentration and volume of buffer solutions. After buffers were optimized, mixtures of raw serum and buffer were prepared and measured to observe the conditioning of solution pH and conductivity, as described below.

2.3.2 Equipment

2.3.2.1 Accumet

Solution pH and conductivity were measured using the Accumet XL60 meter (Fisher Scientific) fitted with the respective probes. The multi-port function of the XL60 allowed for simultaneous measurement of pH, conductivity, and temperature. However, since most of the glassware used during measurements were low volume, it was not possible to sample the solution with both probes at the same time. Both pH and conductivity probes were left in a beaker of tap water to soak for about 20 minutes prior to measuring. The pH meter required just enough sample to fill past the electrode tip, a volume of about 5 milliliters. After preliminary testing, it was discovered that the conductivity probe was highly dependent on the amount of solution in contact with the probe. In order to regulate this, a 10ml graduated cylinder was filled with 6ml of solution, which coated the entire conductivity probe when it was placed inside. The 10ml graduated cylinder was thus used for both pH and conductivity measurements and thoroughly rinsed between each sample measurement. Since pH is dependent on solution temperature, initial measurements of pH also included temperature measurements to account for any differences in external conditions. Values for pH and conductivity were recorded after they each had ample time to stabilize. Conductivity values stabilized within several seconds, whereas pH values were more variable and required several minutes to stabilize, most likely due to the high sensitivity of the pH electrode. Between measurements, the probes were rinsed with DI water, blotted dry with Kimwipes, and held on the electrode arm mount of the Accumet meter.

2.3.2.2 Vilastic

Solution viscosity was measured using the Vilastic-3 system (Vilastic Scientific), which consisted of an external measuring device and data collection software on a linked computer. The Vilastic system required about 30 minutes to warm up prior to measuring. Given the option of using 1.5ml

or 0.5ml sample caps, we opted for the 0.5ml caps due to the lower volume requirements. Samples were pipetted into the caps on the bench and then carefully transferred to the holding cup base of the external device via tweezers. A one milliliter syringe (BD) was screwed to the top of the measurement tube using the Luer-Lok™ attachments. Once the sample was secured to the device the syringe was pulled up to create suction and pulled about 200-250 microliters (0.2-0.25 ml) of the sample into the measurement chamber. The three-way valve that the syringe was attached to was then turned to the "off" position to close the measurement chamber. Using the accompanying Vmax software, viscosity values were measured by evoking the "stretch" protocol within the menu options. Parameters selected based on standard operating procedures are shown in Table 5.

Table 5 - Vilastic-3 operating parameters

Vmax "Stretch" Parameter	Value
Frequency	2 Hz
Integration time	5 seconds
Low drive	10 %
High drive	30 %

After the viscosity values were recorded, the measurement chamber was rinsed with about 30ml of DI water by replacing the 1ml syringe with a 10 ml syringe (BD) and forcing the water into a waste collection beaker. Air bubbles in the measurement chamber can result in invalid results and were avoided by adjusting a three-way valve such that the path of the syringe fluid would flow into a waste reservoir when first connected to purge any air bubbles present at the tip. The valve was then positioned to connect the syringe with the measurement chamber in order to flush out

any remaining sample. Once the chamber was thoroughly washed, a new sample cap could be added.

2.3.2.3 Osmette

Solution osmolality was measured using the micro-Osmette (Precision Systems). The Osmette only required 50 microliters of sample for analysis which were pipetted into 1.5ml microcentrifuge tubes provided with the machine. Prior to analysis, the Osmette was allowed to warm up for approximately 20 minutes. The tubes were then loaded one at a time into the sample chamber on the device, where the liquid sample underwent a freezing point depression analysis to get an estimate of the amount of solute particles in the sample. After the temperature cycle was complete, the osmolality was displayed on the machine and the centrifuge tube was freed from the sample holder. The used tube was discarded and the temperature probe was wiped carefully with a Kimwipe.

Solution osmolality and osmolarity have a notorious reputation for causing confusion and even improper substitution of one term for the other. Both of these values express the osmotic concentration of a solution, but with respect to different terms. The use of either term usually depends on the method behind the instrumentation's measurement. Since the Osmette instrument measures concentration by freezing point depression, its values are expressed in terms of the solvent, in our case water, which depicts the usage of osmola**L**ity. Instruments that measure in terms of the solute are expressed in osmola**R**ity. There is a simple correlation between the two in case one term is preferred over the other,

$$\text{OsmolaRity} = \text{OsmolaLity} \times (\rho_{solution} - c_a) \qquad (2)$$

where $\rho_{solution}$ = the density of the solution and c_a = the anhydrous solute concentration in grams per milliliter.

2.4 Chip Testing – Experimental Methods

2.4.1 Chip Set-up

After the AutoCAD™ drawings had been sent to the Stanford Microfluidics Foundry, our PDMS chips were received soon after. Prior to fluid introduction, the chips were carefully inspected under a microscope and over the LabSmith™ inverted fluorescence microscope to verify correct geometries and layer bonding following the soft lithography process. The channels appeared free from any debris and were well bonded to the glass substrate. If the chips were intended for continuous use within a system, the first fluid that came in contact with the chips would have been carefully selected to ensure proper microchannel wetting and charge distribution. Since the chips were only intended for experimental testing and not integration with other test station components, this condition was not a concern. Initially, DI water was used to flush out the channels, followed by a saline solution rinse. Capillary tubing was connected directly to the sample inlet port and attached to a 1ml syringe filled with the rinse solution via a Luer-Lok™ tip attachment. After the chip had been thoroughly rinsed by hand, it was allowed to air dry while chip packaging components (LabSmith™ kit) were prepared. Capillary tubing ports were bonded to the surface of the PDMS by an epoxy compound. After all ports had adapters connected, the epoxy was allowed to dry overnight. Meanwhile, a microfluidic breadboard was prepared using a dremel to cut out a section for the glass slide to rest in, and several fluid valves were attached to its surface by the supplied screws, seen in Figure 14.

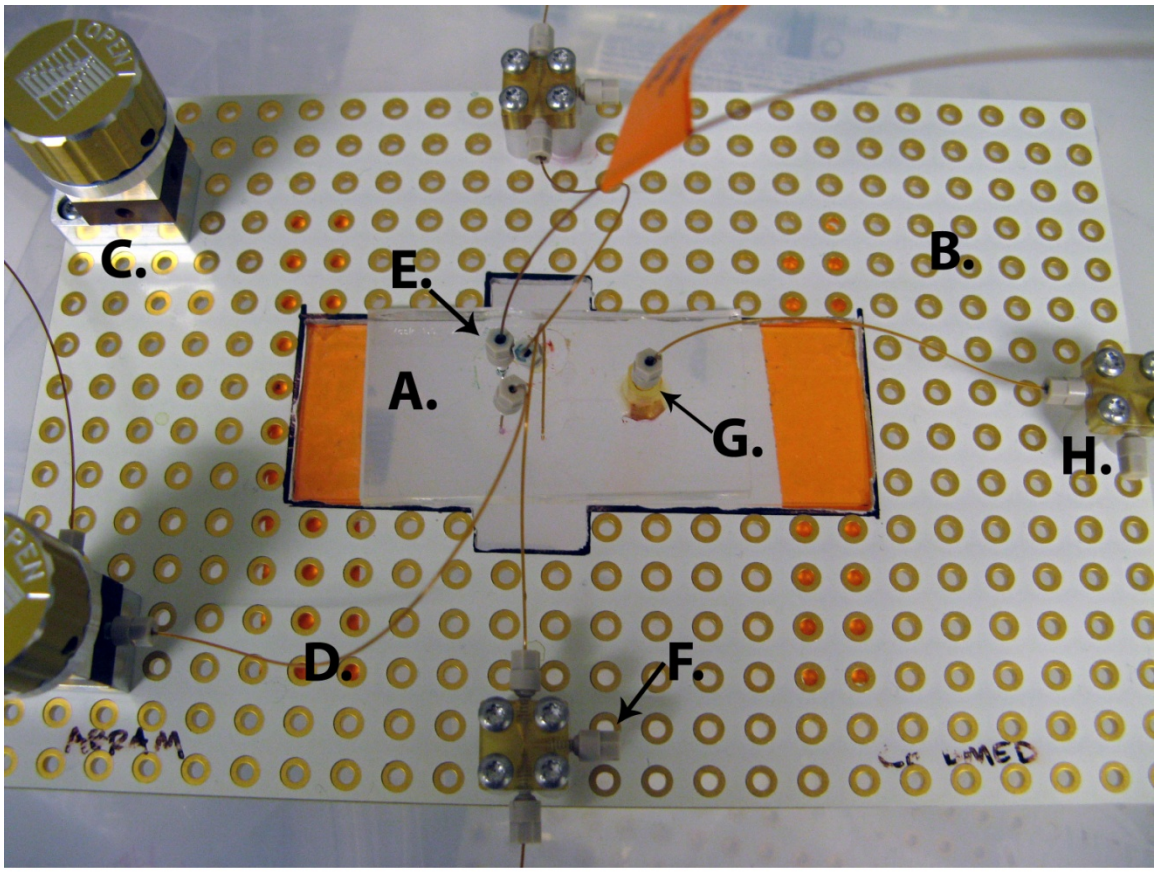

Off-Chip Packaging

A. PDMS/glass micromixer chip
B. LabSmith microfluidic breadboard
C. Inlet flow valves (3-port)
D. Capillary tubing
E. One-piece fittings
F. One-piece plugs
G. Epoxy-bonded port connector
H. T-interconnects

Figure 14 - Labeled image of off-chip packaging via LabSmith™ breadboard

Once the epoxy connections had dried sufficiently, the chip was connected to the microfluidic breadboard and placed on the inverted microscope. Capillary tubing was connected from three 1ml syringes to the sample inlet port, sample buffer port, and outlet port, respectively, in order to control the flow rate through the microchannels and mixing chamber. Originally, the electrolyte reservoirs were designed to store several microliters of an electrolyte solution in order to ensure connectivity of the electric field from the off-chip electrodes to the mixing chamber through the connecting microchannel. However, after initial fluidic filling of the chip, it became apparent that

there was too much surface tension for a fluid sample to fill the entire electrolyte reservoir without the presence of air. The entire function of these reservoirs was not lost as fluid was still present in the microchannels and electrically connected the reservoir to the mixing chamber, meaning that excitation could still occur as long as the off-chip electrodes were placed near the fluid connection site. Since the intended function of the electrolyte reservoirs had changed, the reservoir filling ports were "plugged" by attaching the connected capillary tubing to a plug attachment. The main focus from thereon out was the manipulation of the sample inlet, buffer inlet, and outlet ports to achieve the optimal throughput of the sample.

2.4.2 Flow set-up

The three syringes connected to the chip were coupled to three syringe pumps (Harvard Apparatus Plus11 Infuse/Withdraw), shown with the entire experimental setup in Figure 15, in order to control the rate of volumetric flow. As described earlier, COMSOL™ analysis had determined that the optimal ratio of inlet to outlet flow rates was between 1:2 and 1:3. Sample and buffer inlet flow rates were set at 1μL/min in the "infuse" state and the outlet flow rate was set at 2μL/min in the "withdraw" state. Green food dye was used in the sample inlet port in order to visualize the segregation of sample and buffer throughout the chip. DI water was used for buffer solution and was also used to flush out the microchannels before the chip was attached to the syringes. All syringe pumps were started at the same initial time value and allowed to run for about 20 minutes. Throughout this time, air bubbles were trapped in the channels and the mixing chamber, preventing a clean separation between the two fluid streams. Flow was also observed to direct towards the electrolyte reservoirs instead of to the outlet port. The outlet flow rate was then increased to 3μL/min (a 1:3 in: out ratio) in order to correct this anomaly.

Experimental Set-up List

A. Syringe Pump (Harvard Apparatus)
A1. Sample Inlet Syringe (BD)
A2. Buffer Inlet Syringe (BD)
A3. Outlet Suction Syringe (BD)
B. Inverted Fluorescence Microscope (LabSmith uScope)
C. High Voltage Sequencer (LabSmith HVS)
D. Tygon(R) Tubing
E. Electrolyte Reservoir Baths (15 ml Centrifuge tube)
F. High Voltage Cables (LabSmith)
G. PDMS uMixer Chip
H. Computer (connected to HVS and uScope) - Left of syringe pumps

Figure 15 – Experimental set-up during pretreatment process

2.4.2.1 Packaging changes

After several more attempts with varying success, it was determined that the capillary tubing should be exchanged with Tygon® tubing for several reasons; namely, the capillary tubing used in this project was very stiff, resulting in a very large bend radius that required long lengths of the tubing to attach from the syringe pumps to the microscope work station. These long lengths of tubing took longer to fill and thus slowed down the experiments. Tygon® tubing, on the other

hand, was much more elastic in nature and had a very tight bend radius that allowed much shorter lengths of tubing to be used. Another advantage of the Tygon® tubing was that, since it is mostly transparent, fluid and air bubbles could be visualized externally, which was extremely useful in preparing the lines before connecting them to the microchip. The Tygon® tubing was also much easier to cut to length since a razor blade would suffice, whereas the capillary tubing required a special cutting device. Because PDMS is difficult to bond to, the epoxy connections on the PDMS failed rapidly. Capillary tubing was still used after the epoxy failed by placing the ends directly into the fluid ports. Another advantage of the Tygon® tubing was that non-epoxy based port connections could be made by fitting to syringe tips.

In order to connect the Tygon® tubing to the PDMS chip, 20 gauge stainless steel syringe tips were prepped and inserted into each of the fluid ports. Each stainless steel tip was removed from its plastic Luer-Lok™ body with pliers and soaked in acetone to remove any residual adhesive. After being rinsed and dried, the tips were slightly bent to better direct the attached tubing and were carefully inserted into the fluid ports until a tight seal was achieved. The chip was connected to the different syringe pumps just as before only now with Tygon® tubing, seen in Figure16.

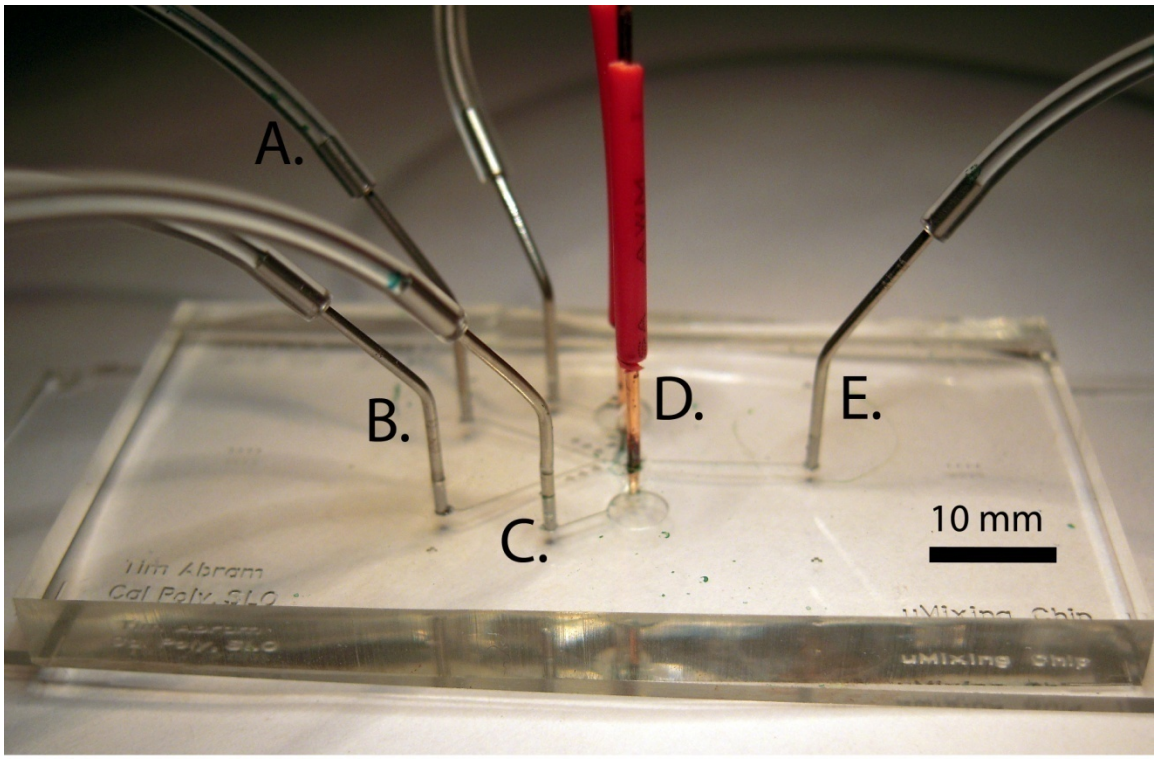

A. Sample inlet port
B. Buffer inlet port
C. Electrolyte reservoir filling port
D. Off-chip electrodes
E. Outlet port

Figure 16 - Photograph of PDMS chip with fluidic connections and electrodes

The lengths of Tygon® tubing were cut so that the two inlet ports and two electrolyte reservoir ports received equal lengths, respectively. This helped ensure that both sample and buffer would reach the chip at approximately the same time if the syringe pumps were activated simultaneously.

2.4.2.2 Air purging

Since air buildup inside of the chip was highly undesired, a new approach was adopted to purge the system of any residual air. Before any syringe pumps were activated but after all ports were connected to their tubing, the entire chip was submerged in a petri dish filled with DI water. The

electrolyte reservoir inlets were connected to tubing that was submersed in two separate 15ml centrifuge tubes filled with DI water. Through this approach, the entire chip was analogous to a closed system and could only be exposed to air that remained in the syringes. The outlet syringe pump was activated first, at a flow rate of 3μL/min in the "withdraw" direction. Negative pressure was established in the microchannels as the outlet syringe continued to pull for 5 minutes in order to "prep" the system prior to inlet flow. All air in the mixing chamber was removed through the outlet as water was transported from each of the reservoirs through the chamber. While the chip was still submerged, the inlet pumps were activated, with green food dye in the sample syringe and more DI water in the buffer syringe. After the newly introduced inlet fluids reached the mixing chamber in the absence of any air bubbles, the chip was removed from the bath, quickly blotted dry, and placed on the inverted microscope. Fluid stream separation was clearly visualized and recorded using the uScope's video recording capabilities. The system remained purged of air bubbles for several minutes, though eventually a few air bubbles would appear and become lodged in the mixing chamber. While the pumps were still running, the buffer pump was used to inject a few microliters by hand into the chip, which was effective at clearing any remaining air bubbles with sudden, relatively high volume influx. Subsequent flow tests also used a 50%/50% (v/v) solution of DI water and 95% ethanol as an operational buffer after group members had discovered that the solution was effective at purging air from within a microfluidic system.

2.4.3 Electrode Testing

The active mixing component in our chip was an oscillating DC-voltage source that would be confined within the mixing chamber and minimally penetrate the inlet channels. We based our electrode placement on Santiago and Oddy's design [21] where the positive electrode was placed

in the upper electrolyte reservoir and the negative, or grounded, electrode in the lower electrolyte reservoir. Unlike their experimental design, we hoped to reduce operational costs by disregarding the deposited gold/chrome layers on the glass substrate and the platinum off-chip electrodes. Instead, we used two pieces of 22 gauge connection wire cut to length and inserted carefully by hand into the PDMS at the ends of the two connecting channels. Voltage was sourced using the LabSmith™ High Voltage Sequencer (HVS), which was capable of issuing up to 3000 volts DC. The two leads from the back of the HSV were connected to a multimeter to validate the accuracy of the displayed voltage output before being inserted into the two electrode wire segments.

In order to assess the mixing of sample and buffer within the mixing chamber, a fluorescently-dyed sample distribution was experimentally observed in the exit channel for various applied voltages. When no electric field was applied, the sample solution was isolated to the top half width of the exit channel. We defined adequate micro-mixing by the homogeneous distribution of sample throughout the entire width of the exit channel, following electrical excitation. Continuous DC voltages, periodic AC voltages, and pulse DC voltages were each tested. Sample distribution was quantified by measuring the propagation distance of sample in the exit channel. Repeatability was assessed by measuring propagation distances for different voltages for 6 separate periods.

3 Results

3.1 Pretreatment Results

3.1.1 Serum Analysis

Before experimentation with serum and buffer mixtures, several tests were performed on raw serum alone in order to quantify its own properties. These tests included serial dilutions to measure changes in pH and conductivity and linear dilutions to measure changes in viscosity. For each dilution, serum was combined with DI water and thoroughly vortexed to incorporate the two fluids.

Serial dilutions are commonly used throughout biology and chemistry in order to estimate orders of magnitude for certain parameters. A typical 1:10 dilution may be achieved by combining 1ml of sample to 9ml of solvent (DI water) for a total of 10ml, of which the sample volume makes up one-tenth. The next dilution would follow as a 1:100 dilution where 1ml of the previous 1:10 solution is combined again with 9ml of solvent. The result is a 1:100 dilution where the volume of sample makes up one-hundredth of the total volume. This technique can be repeated until the desired numbers of dilutions are made. For this analysis, four dilutions were made for a total of five solutions (1:1, 1:10, 1:100, 1:1000, 1:10 000) as seen in Table 6.

Table 6 – pH and conductivity values for serial dilutions of bovine calf serum

Serum Serial Dilutions (with DI Water)		
Dilution amount (1:x)	pH	Conductivity (µS/cm)
1	6.967	10880
10	7.408	1327
100	7.292	178.3
1000	7.090	48.32
10000	7.196	40.13

Solution pH values remained relatively stable throughout the serial dilutions, shown below in Figure 17, indicating that pH is relatively independent of dilution volume, especially since the initial pH values for serum and DI water are relatively similar.

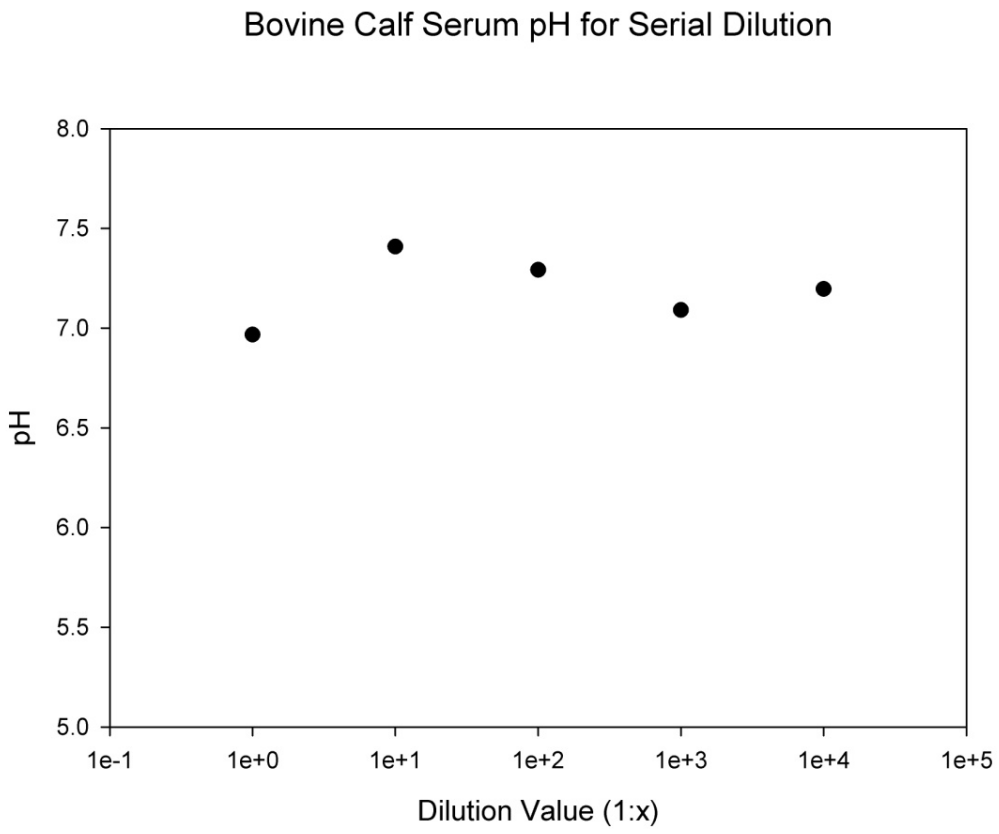

Figure 17 - Serum pH values for serial dilutions

This figure is of a scatterplot of pH measurements of serum for serial dilutions. Raw serum was combined with DI water as described above to produce 5 solutions, each with a tenth of the total concentration of the previous dilution. The y-axis displays the pH values measured for each solution and the x-axis displays the dilution value on a logarithmic scale, e.g. x=100 refers to the 1:100 dilution. From this plot we were convinced that pH values for raw blood serum are relatively independent of the dilution volume.

However, conductivity measurements from these dilutions clearly indicate its dependence on the amount of serum. It is no surprise that blood serum is highly conductive due to its high

concentration of dissolved ions [31]. A scatterplot of conductivity values for the five solutions was created with conductivity on a linear scale and the dilution value on a logarithmic scale. The plot appeared to follow an exponential curve, seen below in Figure 18, indicating that conductivity is highly dependent on the volume of raw serum.

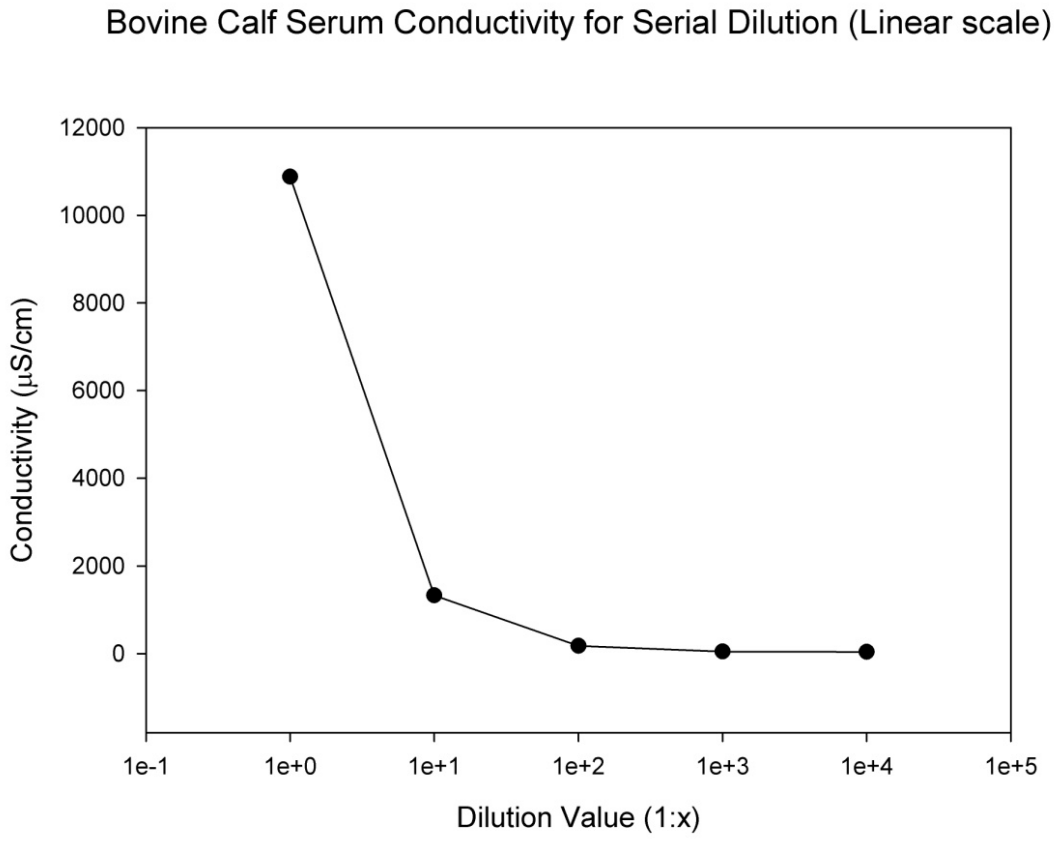

Figure 18 - Serum conductivity values for serial dilutions - linear y-scale

This scatterplot displays conductivity measurements for the 5 serial dilutions. Raw serum was diluted with DI water as described previously. The y-axis displays conductivity values for the solutions, in µS/cm, while the x-axis displays the dilution value on a logarithmic scale. From this plot we determined that solution conductivity for serum follows a curve indicative of exponential decay.

Manipulation of solution conductivity will likely involve the addition of large volumes of buffer to small sample volumes. Due to the volume and concentration dependence of conductivity, future work will be necessary to determine strategies to achieve desired conductivity. Once we

correct for the conductivity of the buffering solution, it appears that only a small amount of serum should be added to the buffer in order to arrive at the correct dilution.

Viscosity data for blood serum was collected for 21 solutions, each with a different volume percent of serum. The total volume of each solution was normalized to 400 microliters by adding DI water and pipetted into the 0.5ml sample cups supplied by Vilastic. After the data was collected, a linear regression analysis was performed to verify the apparent linear dependency of viscosity on the amount of serum in a solution, seen in Figure 19.

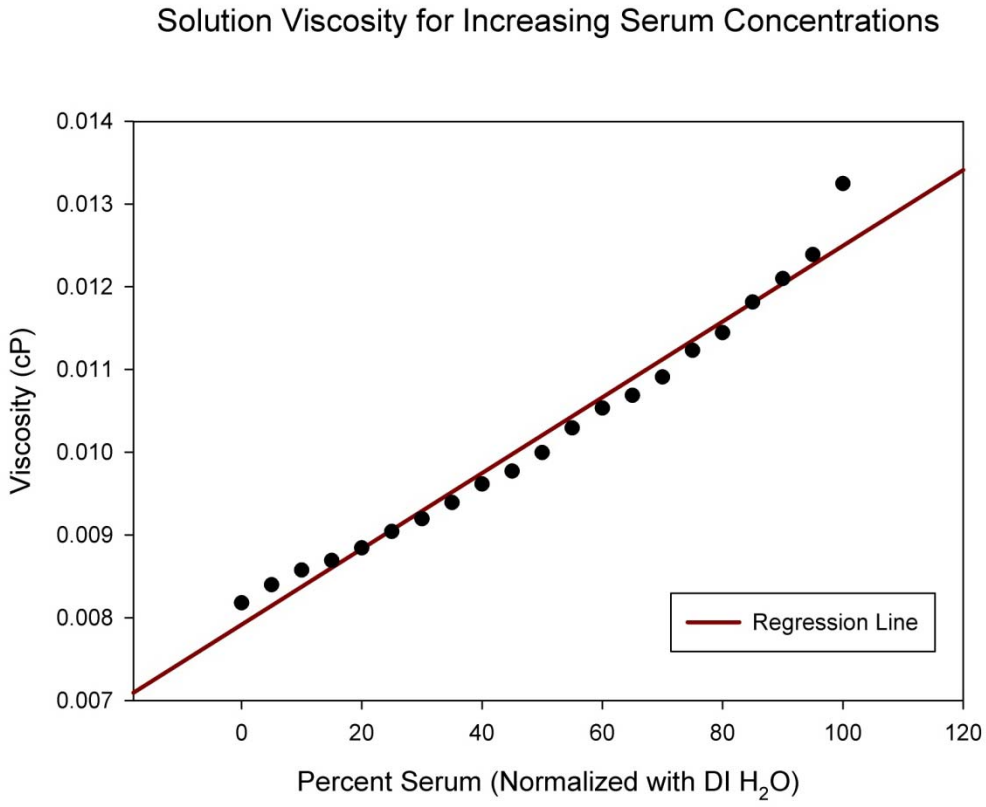

Figure 19 - Scatterplot of serum viscosity data

This figure displays a scatterplot of viscosity values for raw serum over a linear dilution scale. Raw serum was combined with DI water, where 21 solutions were prepared over a range of serum percentages, as indicated on the x-axis. Viscosity was recorded with the Vilastic-3 in cP and displayed on the y-axis. From this plot we fit a linear regression line to emphasize the linear relationship between serum solution viscosity and the amount of serum.

After running our regression analysis, we are convinced that there is a positive association between an increase in the amount of serum in a solution and the solution's viscosity, with all else being constant. Since our target viscosity value was around 1.0cP, it appears that a solution with less than 50% serum will be desirable. Even though DI water was used in the linear dilutions, the viscosities of the specific buffer solutions measured viscosities almost identical to DI water and should therefore not affect the results depicted here. Assuming that equal inlet flow rates of sample and buffer will result in an equal volume of the two in the mixing chamber, we will likely be operating with 50% serum solutions in our chip. Downstream combinations of the two fluids will theoretically obtain a viscosity within our allowable range.

3.1.2 Buffer Analysis

Even though buffer concentrations were already supplied through the literature search [14], a thorough analysis was performed to determine the most optimal combination of the two buffering solutions, in terms of concentrations and volumes. Please note that all of these tests were aimed at determining the optimal conditions to arrive at the target pH, conductivity, and viscosity values and have no indication on how they will function experimentally in an electrokinetic separation chip. For consistency, we will refer to MGA as the operational electrolyte since it is the primary buffer used in solution, and both EACA and GABA as co-ions, which are added to MGA to assist in separating sample fractions. As noted earlier, the identity of the buffers as well as the target parameters are entirely dependent on the sample and the target separation fractions. The buffers and parameters chosen here only apply to serum protein separations into the previously described five major fractions.

As part of the buffer analysis, different concentrations of each buffer were observed separately in terms of pH, conductivity, and osmolality. Since osmolality is a measure of the amount of dissolved solute in a solution as a function of solvent volume, this measurement served as a check

to ensure that increasing the concentration of each buffer likewise increased the osmolality of the solution. Concentrations for each of the three buffers ranged from 0.1M to 0.4M by 0.1M increments. The solutions were prepared in the same way referred to earlier, except that 6ml solutions were obtained so that the conductivity probe could be used in the 10ml graduated cylinder. The order of measurements followed MGA, EACA, and GABA where all of the 0.1M solutions were measured before the subsequent concentrations. After all the data had been collected, it was imported into Minitab®, a statistical software package, for analysis. Since we were concerned with trends in the data, we ran linear regression analyses in order to see if there was an association between one of the parameters and the concentration of buffer.

3.1.2.1 Separate Buffers

Osmolality plots for each of the three buffers showed a linear dependence with increasing concentration, shown below in Figure 20.

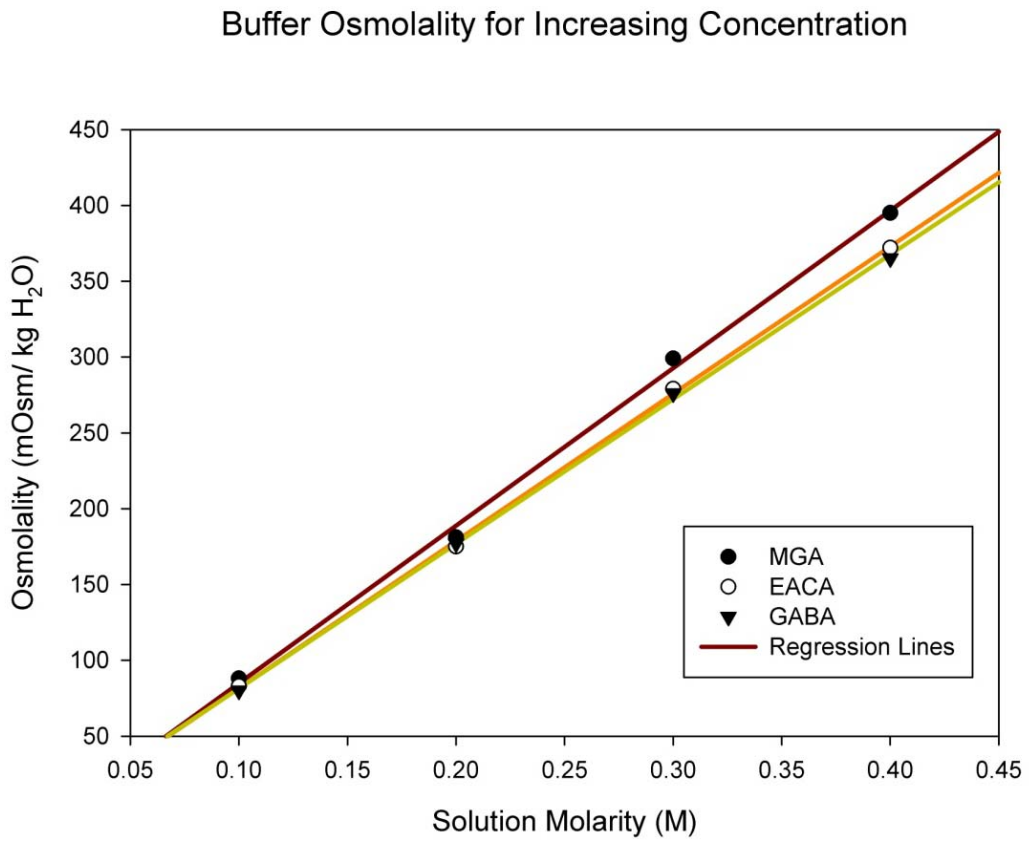

Figure 20 - Scatterplot of osmolality values for increasing buffer concentration

A scatterplot of osmolality values for each of the three buffer solutions at different concentrations is presented above. Concentrations for each of the three buffers were prepared at 01.M, 0.2M, 0.3M, and 0.4M. Regression lines were included to verify the linear relationship between osmolality and solution concentration. From this plot we determined that osmolality had a positive correlation with increases in solution concentration, as was expected due to the higher number of dissolved solutes in solutions with higher concentrations.

This helped confirm our previous notion that concentration of a buffer is directly related to the amount of solute particles present. This also served as a check that the solutions were indeed correctly prepared.

Conductivity of the solutions tended to increase as the concentration of the buffers increased, as seen below in Figure 21.

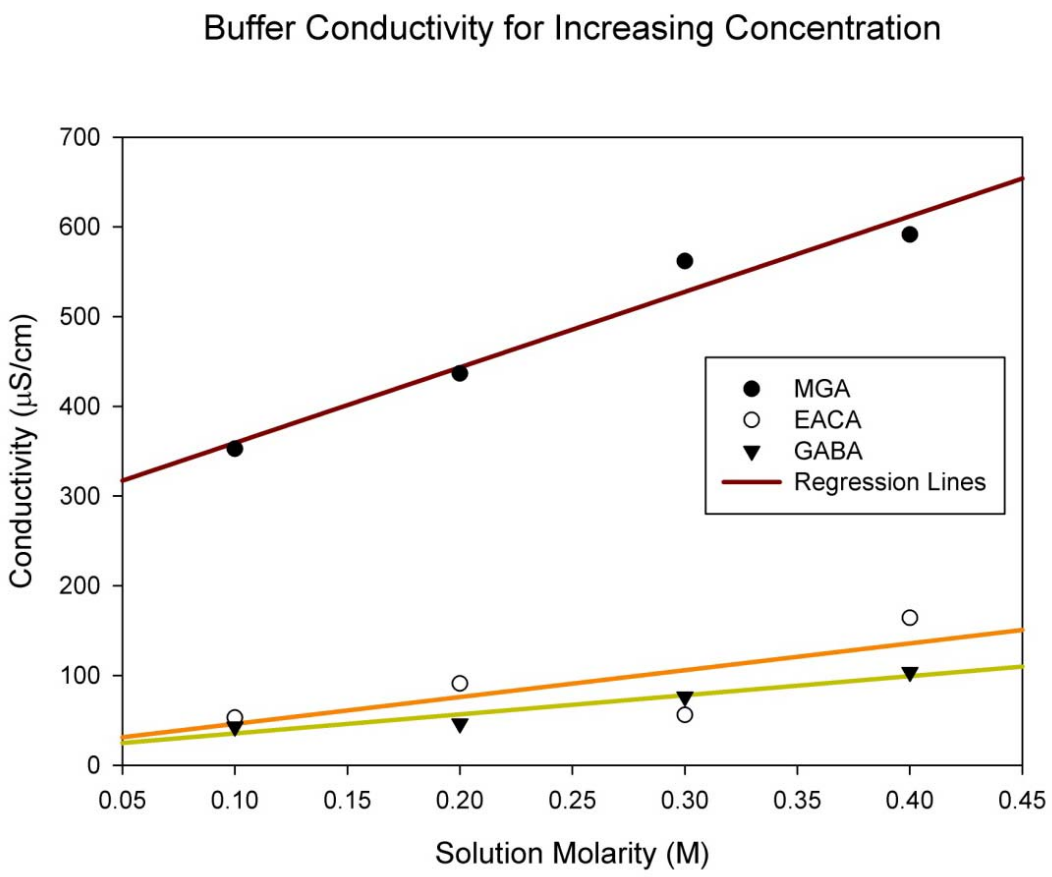

Figure 21 - Scatterplot of conductivity values for increasing buffer concentrations

A scatterplot of conductivity values for each of the three buffer solutions at different concentrations is presented above. Concentrations for each of the three buffers were prepared at 01.M, 0.2M, 0.3M, and 0.4M. Regression lines were included to verify the linear relationship between conductivity and solution concentration. From this plot we determined that conductivity had a positive correlation with increases in solution concentration.

This seems logical since conductivity is dependent on the amount of free ions in solution which should increase as the total solute concentration increases. After visual inspection of our plot and confirmation from our regression analysis, we were convinced that there was a positive association between conductivity and concentration for the three buffers.

There was no noticeable trend in the pH of the solutions for adjusting the concentrations, shown below in Figure 22. Our regression analysis did not provide enough evidence to show a correlation between pH and solution concentration.

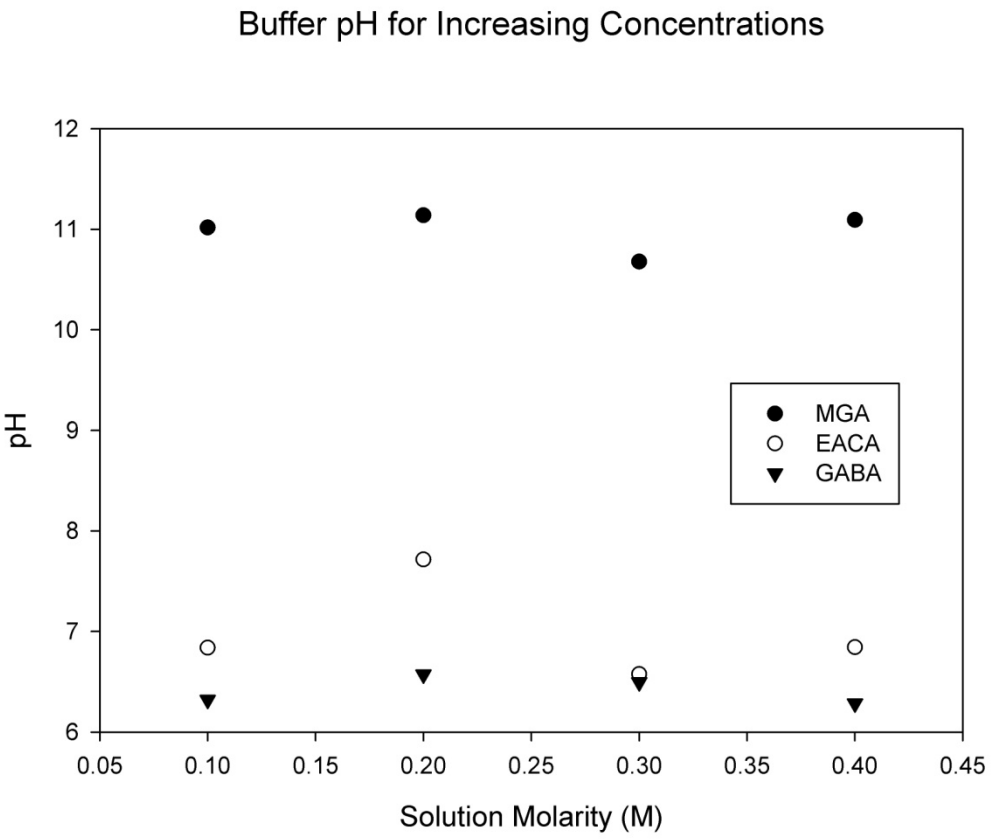

Figure 22 - Scatterplot of pH values for increasing buffer concentration

A scatterplot of pH values for each of the three buffer solutions at different concentrations is presented above. Concentrations for each of the three buffers were prepared at 01.M, 0.2M, 0.3M, and 0.4M. Regression lines were not included in the plot since regression analyses failed to provide enough evidence to indicate any correlation between pH and solution concentration. We therefore determined that solution pH is independent of buffer concentration.

As discussed in the CE buffer section, we are interested in using buffers that have a high pH value but a low conductivity. The high pH leads to higher electroosmotic mobilities and therefore more rapid CE experiments, and the lower conductivity prevents adverse reactions due to joule heating and other issues later on in electrophoretic separations. Therefore, it seems logical to

choose the lowest concentration of buffers that were tested since conductivity is directly associated with the concentration of the buffers and pH has no direct association. It doesn't appear that pH will increase by picking higher concentrations, so it is more pertinent to lower the conductivity of the buffers by selecting buffers of lower concentration. For this reason, and for the reason that 0.1M concentrations were used in Dolnik's research [14], we will be operating with 0.1M solutions of the three buffers MGA, EACA, and GABA.

3.1.2.2 Buffer Mixtures

The next step in our buffer analysis was to assess the optimal volumes of each co-ion, EACA and GABA, combined with the operational electrolyte, MGA. Values for pH and conductivity were recorded and analyzed in Minitab® to determine these optimal volumes.

The first mixture was composed of 0.1M MGA and 0.1 M EACA. Volumes of each solution were varied by 1.0ml such that the total volume equaled 6ml. Values for pH and conductivity were plotted as a function of the concentration of MGA which was corrected to 6ml by the addition of EACA. Our regression analysis revealed a positive association between pH and an increase in the volume of MGA in a 0.1M MGA-0.1M EACA solution. The second mixture contained 0.1M MGA and 0.1M GABA. Solutions were prepared in accordance to the previous mixtures and data analysis followed in suit. Visual inspection confirmed by our regression analysis showed that there was a positive association between pH and an increase in the volume of MGA present in the solution, shown in Figure 23.

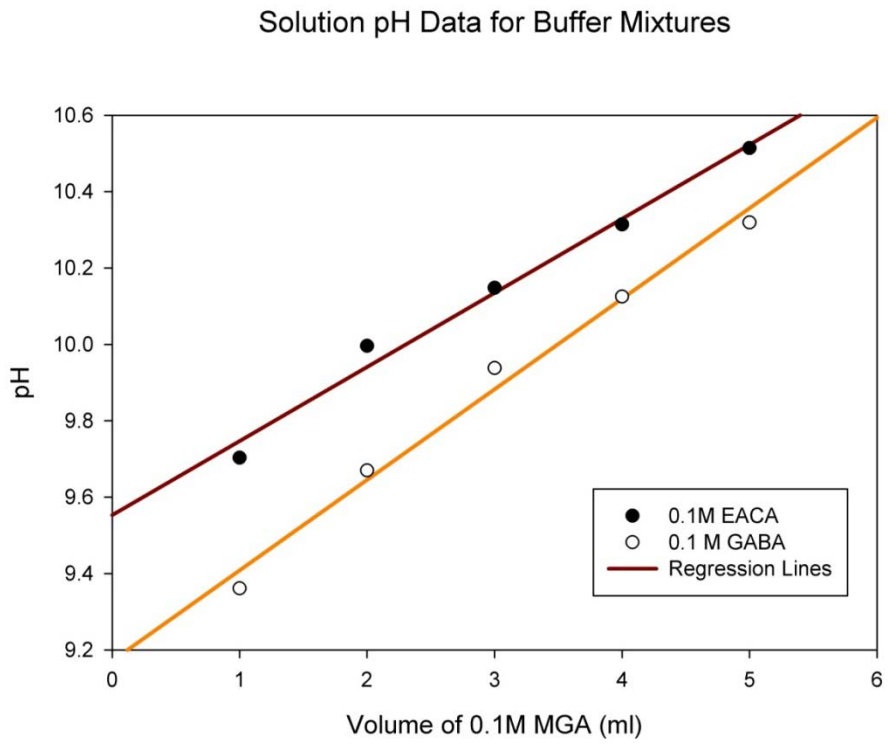

Figure 23 - Scatterplot of buffer mixture pH data

pH values are shown for combinations of MGA with either EACA (filled circle) or GABA (open circle). Five solutions were measured, each with a different volume of 0.1M MGA in a total volume of 6ml, as indicated by the x-axis. Regression lines were included in the plot to verify the linear relationship between MGA volume and pH. From this plot we determined that an increase in the volume of 0.1M MGA corresponded with an accompanying increase in solution pH.

When conductivity values were analyzed for both buffers, we couldn't provide enough evidence to show an association between conductivity and the volume of MGA in the solution, seen in Figure 24.

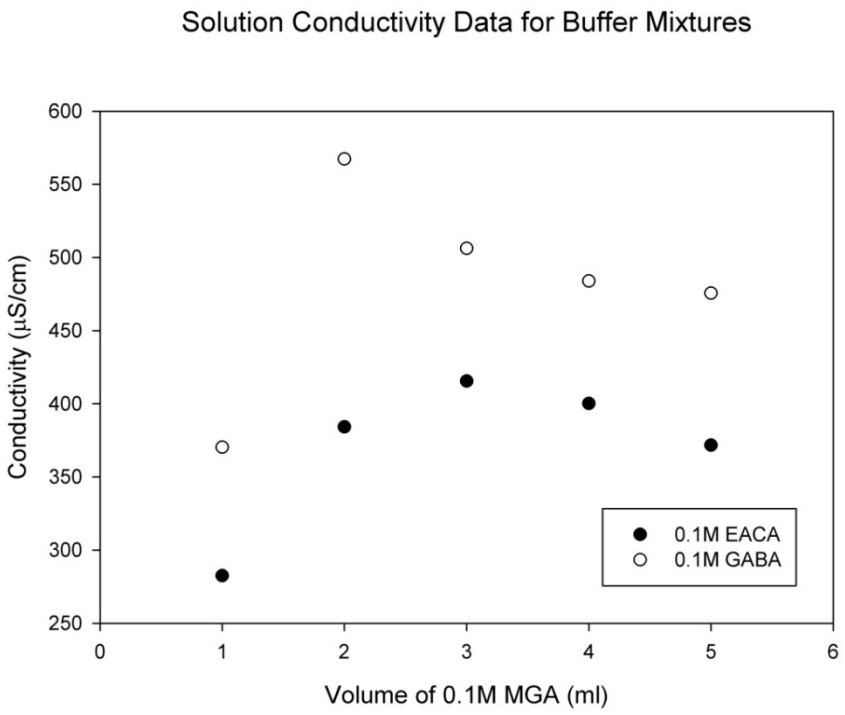

Figure 24 - Scatterplot of buffer mixture conductivity data

Conductivity values are shown for combinations of MGA with either EACA (filled circle) or GABA (open circle). Five solutions were measured, each with a different volume of 0.1M MGA in a total volume of 6ml, as indicated by the x-axis. Regression lines were not included in the plot after regression analyses failed to provide enough evidence to suggest a relationship between solution conductivity and volume of MGA. We determined that solution conductivity is therefore independent on the amount of MGA in solution.

Based on our results for the buffer mixtures we saw a similar dependence of pH on MGA concentration for both types of co-ion. Since we are interested in high pH values it seems logical to select the highest concentration of MGA in each case. Consequently, we also want to ensure that the solution conductivity will not increase beyond acceptable levels. Since there was no apparent relationship between conductivity and the volume of MGA, picking high volumes of MGA should have little or no effect on the conductivity of the solution. Therefore, as a result of the buffer analysis, our two selected buffer solutions include:

0.1M MGA – 0.1M EACA (5:1) v/v

0.1M MGA – 0.1M GABA (5:1) v/v

3.1.3 Serum Pretreatment

After the buffer analysis was complete and after we had a rough idea of some of the attributes of blood serum through dilution measurements, we began to combine the buffers with the blood serum. We adjusted the volumes of the two in order to determine the optimal ratio of blood serum to buffer. Just as in the previous measurements, 6ml solutions were prepared and poured into the 10ml graduated cylinder. However, since the buffer identities had already been determined, stock batches of the two buffers were prepared and used throughout the serum pretreatment. For each buffer, a total volume of 78ml was prepared by combining 65ml 0.1M MGA with 13ml of either 0.1M EACA or 0.1M GABA. All three buffers were prepped individually and combined in a 250ml Erlenmeyer flask. For each measurement, serum was pipetted into a 50ml Erlenmeyer flask and combined with the corresponding volume of MGA. The solution was agitated until well mixed and then poured in the 10ml graduated cylinder where pH and conductivity were measured separately. After the probes were rinsed, 50 microliters of the solution was pulled via pipette and added to a 1.5ml microcentrifuge tube and measured by the osmometer. After values were collected, they were imported into Minitab® for analysis.

Regression data was calculated for each case to determine if there was any effect on solution conductivity or pH related to the amount of serum added. Visual inspection of the plotted values along with our regression analysis confirmed that solution conductivity was linearly dependent on the amount of serum added, as seen in Figure 25.

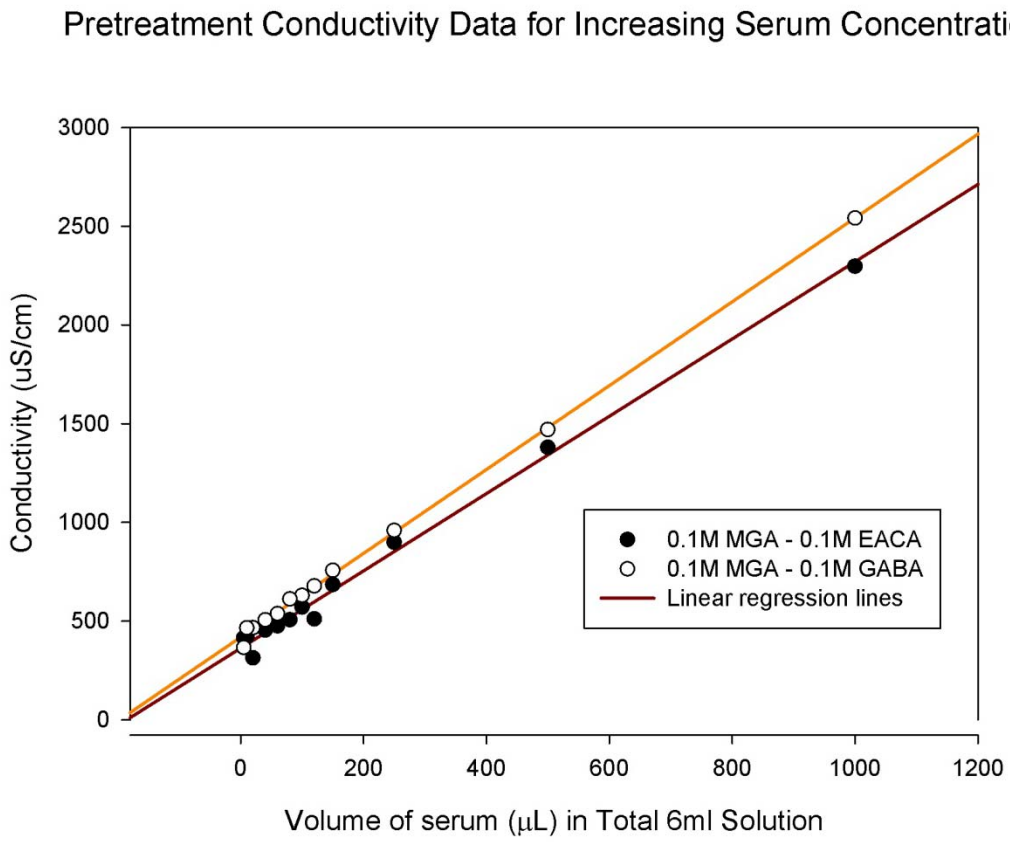

Figure 25 - Scatterplot of pretreatment conductivity data

A scatterplot is displayed for conductivity values over a range of serum volumes added to either 0.1M MGA-0.1M EACA (filled circle) or 0.1M MGA – 0.1M GABA (open circle). The volumes of raw serum ranged from 5µL to 1ml in a total 6ml solution. Regression lines were added to the data to show the linear relationship between solution conductivity and the amount of serum being treated. From this plot, we determined that our optimal range of conductivity values, below 1000µS/cm, would require a volume ratio of at least 1:11, serum to buffer.

However, we did note two unusual observations regarding the values of 6000µL serum and 1000µL serum. The first value was found to have high leverage, high influence, and was also an outlier. The 1000µL serum value was also found to have high leverage and high influence. Since the 6000µL serum value was meant to serve as a serum baseline and did not correspond to our pretreatment regimen, we decided to remove the value from the regression analysis and focus on only the solutions that contained amounts of both serum and buffer. Even though the 1000µL serum value was slightly influential, it remained in our regression analysis as a check on the

extremes of serum volume. These results were very similar between the two buffer treatments, showing a high dependency of solution conductivity on serum volume.

Regression analyses of pH data were also performed for both buffer solution pretreatments. When all serum values were included, we found that the 6000µL serum value was again highly influential. This value actually caused our regression data to appear linear when in fact it was randomly scattered. Both buffer solutions yielded similar occurrences and both regressions were reduced to include only the data where both serum and buffer were present. Based on these results, it appears that volume control will be essential to fully correct for the conductivity of the solution by obtaining a critical ratio of serum to buffer. However, pH appears to be more readily influenced by the buffer treatment.

We understand that solution conductivity is dependent on appropriate volume control and thus cannot be effectively conditioned on our device as it stands. The above linear regression model (Figure 25) indicates that there is a linear relationship between solution conductivity and the amount of serum added to our specific buffers, which could potentially be used to obtain an optimal theoretical ratio of the two solutions for a desired final conductivity.

3.1.4 Serum Titrations

The ability to pre-treat or adjust a certain parameter depends on the response of that parameter to external influences, such as differing volumes of a buffer solution. We determined that conductivity is highly dependent on the concentration and volume of serum and that pH is less dependent on changes in buffer volume after a critical volume has been reached, to allow for the protonation or deprotonation of dissolved species. In order to observe these effects, we performed titrations of raw serum with the addition of our two buffers to measure the changes in pH and conductivity as a function of time-dependent volume added.

We first began with the pH titration of raw serum by adding a continuous stream of our two pretreatment buffers, respectively. We measured pH and conductivity in two separate experiments since the size of the two probes made it unsuitable to test both parameters at once. The selected buffer was loaded into a 10ml syringe (BD) which was connected to a syringe pump. A section of tubing was connected to the end of the syringe and placed over a 10ml beaker to collect the volume of buffer dispensed. Five milliliters of raw serum was added to the 10ml beaker and probed with the pH meter. The syringe pump was set up to dispense buffer at a rate of 1ml/min until 5ml of buffer had been added to the serum, where the volumes of the two would be equal. While the buffer was added to the serum, the beaker was swirled by hand to promote homogenous incorporation of the two fluids. Measurements for pH were collected every 3 seconds by the Accumet and later transferred to SigmaPlot™ for analysis, seen in Figure 26.

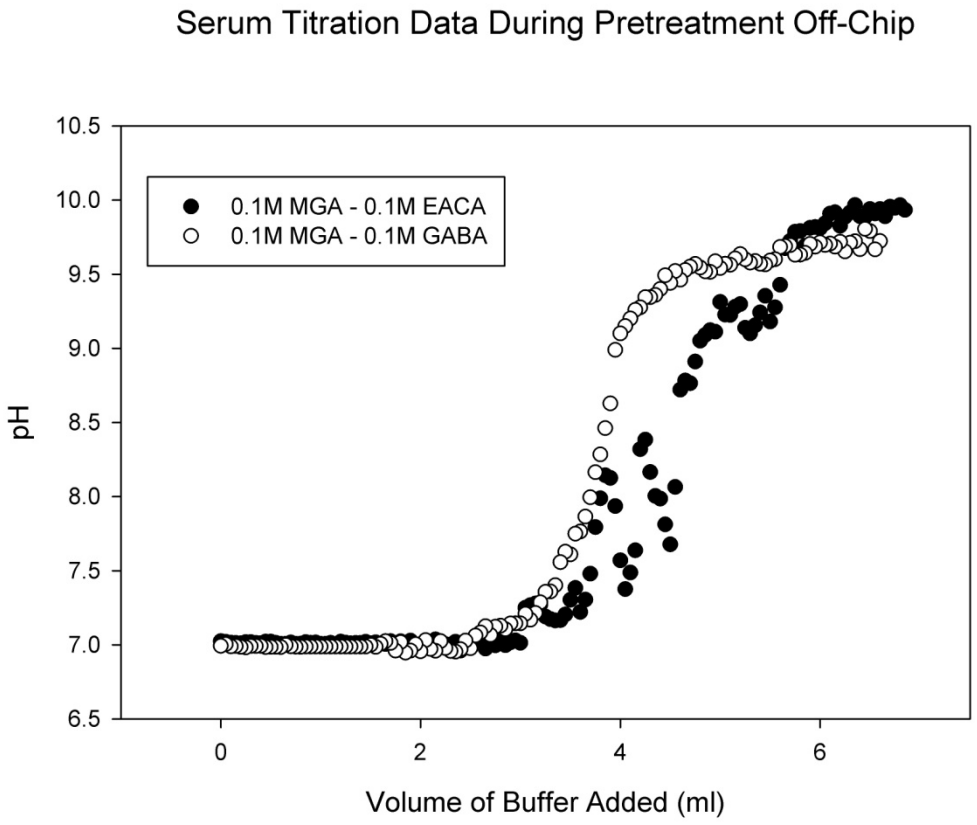

Figure 26 - Serum titration data for pretreatment buffers off-chip

This scatterplot shows a common titration curve of solution pH as a function of the amount of buffer added. Two buffers were used in this experiment: 0.1M MGA – 0.1M EACA, shown as the filled circles, and 0.1M MGA – 0.1M GABA, shown as the open circles. Five milliliters of raw serum was used as the initial solution to which buffer was added at a constant rate. From this plot, we determined that raw serum undergoes a rapid change in pH when the volume of buffer added is between 3 and 5 ml's. This indicates that when an equal volume of buffer is added to serum, the solution pH increases beyond this region and plateaus at a basic pH. Since we are assuming 1:1 volume ratios of serum and buffer in the mixing chamber, we can assume that solution pH will be conditioned on chip.

The conductivity meter required a higher initial volume of serum and therefore was observed for a longer time scale. Seven milliliters of serum were added to a 25 ml graduated cylinder and probed with the conductivity meter. The buffer dispenser was set up as described above for the pH titration with the buffer collected in the graduated cylinder. The cylinder was swirled

throughout the addition of buffer to ensure the mixing of the two fluids. Again, measurements were recorded every three seconds and imported into SigmaPlot™, seen below in Figure 27.

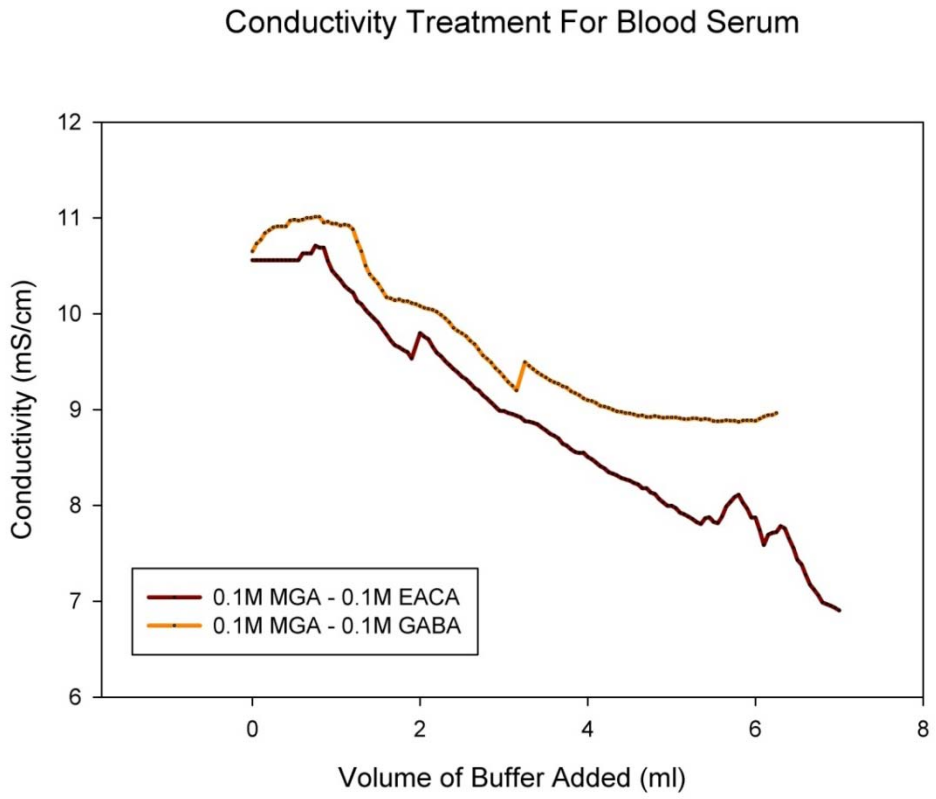

Figure 27 - Conductivity values for serum titration with pretreatment buffers

Experimentally similar to Figure 26, this scatterplot shows solution conductivity values as a function of the amount of buffer added. Two buffers were used in this experiment: 0.1M MGA – 0.1M EACA, shown as the red line, and 0.1M MGA – 0.1M GABA, shown as the orange line. Seven milliliters of raw serum was used as the initial solution to which buffer was added at a constant rate. From this plot, we determined that serum conductivity can be conditioned as a function of the amount of buffer added. However, the amount of buffer required to condition solution conductivity to our acceptable range far surpasses our 1:1 volume ratio assumption. Note also that the units of conductivity in the y-axis are of mS/cm, not µS/cm, further indicating the concentration dependence of conductivity.

3.2 Micro-mixing Results

3.2.1 Stream separation

Separation of green food dye and buffer (DI water) was observed using the aforementioned operating conditions to "prime" the chip for use. A 1:3, inlet : outlet, flow rate ratio was deemed suitable for directing the flow of fluid to the outlet port and bypassing the electrolyte reservoir connecting channels. It was still noted that air was present inside the electrolyte reservoirs. However, the presence of air in these reservoirs might have fortuitously prevented sample and buffer flow to the reservoirs. The connecting channels were still filled with buffer, which was essential before electrodes could be used. After this baseline flow condition had been established, seen in Figures 28 and 29, off-chip electrodes were included into the system.

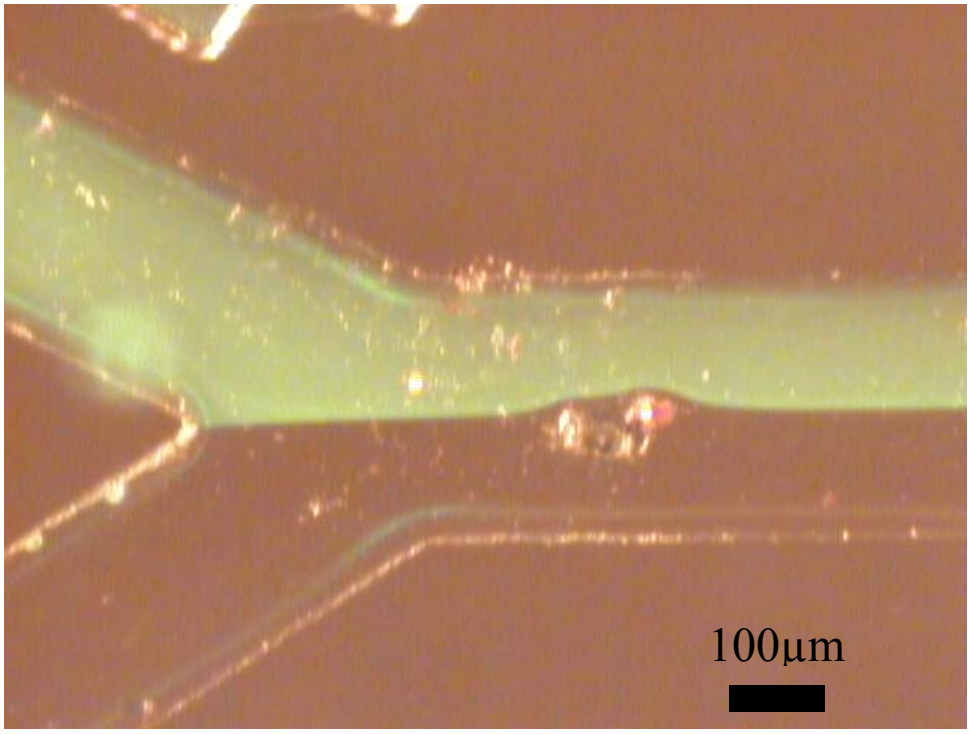

Figure 28 – Sample and buffer partitioning at microchannel union

This image was recorded using the LabSmith™ inverted microscope, where fluid segregation is shown at the inlet channel junction between a sample stream of DI water spiked with fluorescent dye and a buffer stream of DI water. Both sample and buffer fluids were introduced at a rate of 1µL/min while the outlet flow rate was set at 3µL/min.

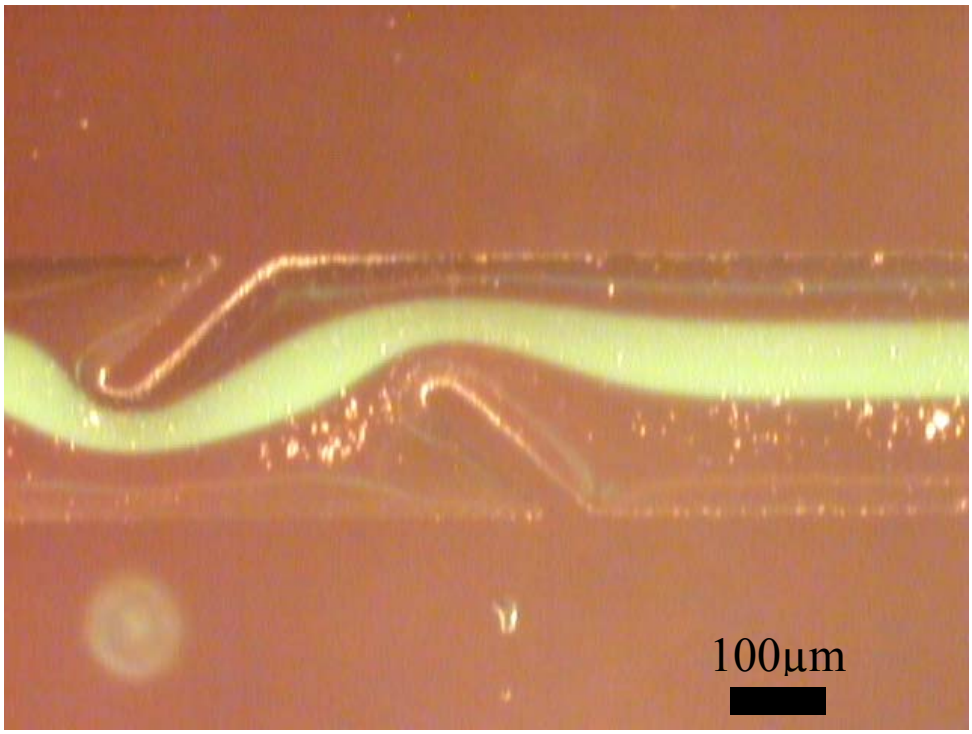

Figure 29 – Sample and buffer partitioning through mixing obstacles in outlet

This image was recorded using the LabSmith™ inverted microscope, where fluid segregation is shown through the exit channel between a sample stream of DI water spiked with fluorescent dye and a buffer stream of DI water. Both sample and buffer fluids were introduced at a rate of 1µL/min while the outlet flow rate was set at 3µL/min. The mixing obstacles divert flow so that the dye propagates over the entire width of the channel; however, the fluid segregation resumes after the fluids pass the last obstacle.

3.2.2 DC continuous testing

We started with a continuous source of DC voltage in order to assess an approximate voltage where micro-mixing would take place and also to observe if electrolysis was present since DC voltage was the default stimulus for the HVS. Green food dye was loaded into the sample syringe and DI water was loaded into the buffer syringe in order to visualize the baseline separation of fluid streams and hopefully their incorporation after the electrical stimulus. Since Oddy and Santiago's [21] experimental design included an AC pulse with an amplitude of 4 kV and a frequency of 5 Hz, it was understood that large voltages would likely be necessary to produce

homogeneous mixing. Therefore, four voltage levels were sourced and observed: 500V, 1000V, 2000V, and 3000V. Each case was sourced for roughly 20-30 seconds while the field of view on the inverted microscope was adjusted to account for any effect the electrical stimulus might have on the fluidic network. However, no effects were noted for any of the different voltage levels anywhere throughout the chip. Instead, the two fluid streams remained distinct and separated. One explanation for this observation was that the conductivity of the fluids might be too low to perturb the experience any influence from the applied field. A saline solution was prepared with a conductivity of 672 μS/cm and replaced the DI water as the active buffer. The same voltage levels were tested once more, though no observations were made of any altered fluid interface in the mixing chamber.

3.2.3 AC testing

Next, we decided to test the effect of AC voltage on the system since Santiago and Oddy's [21] device involved AC voltage as well as our COMSOL™ models. An AC sine wave generator was utilized through the HVS software accompanying the device. The amplitude of the wave was set at 500V, 1000V, and 3000V for subsequent trials. Each test used a frequency of 5 Hz with no voltage offset or delay. The same sample and buffer fluids used in the second DC test were used again to aid in visualizing the baseline fluid segregation. Once the baseline was established using the same flow rates as described above, the AC field was imparted on the system for roughly 10 seconds. Most active micro-mixing chips observed in the literature were capable of mixing the two fluid streams within several milliseconds to a few seconds. We observed longer excitation times only because it was necessary to visualize the effects throughout the entire chip which required time to adjust the field of view on the inverted microscope. Once the 500V sine wave was sourced, no noted effects were visible in the mixing chamber, though activity was noted at

the positive electrode insertion point. Small air bubbles similar to those found in electrolysis were present, though this might have been an artifact of flow conditions with air trapped inside the syringes. The air was forced out through the system by depressing the buffer syringe plunger to eject a few microliters of buffer into the system. Once flow had stabilized and fluid stream segregation was visualized, the amplitude was increased to 1000V and sourced for roughly 10 seconds. Again, no activity was observed in the mixing chamber, though an increase in activity was observed at the positive electrode insertion point. The effects of the 1000V wave were thought to be more related to joule heating in the connecting channel causing air formation rather than the more confined process of electrolysis. Also, electrolysis should not be observed under AC excitation since the polarity of the field constantly changes. Since no effects were observed in the mixing chamber, the voltage was increased to the maximum amplitude of 3000V. The sine wave was sourced for roughly ten seconds followed immediately by air bubble formation and pulsing stemming from the positive electrode and penetrating into the mixing chamber. After the pulse was stopped, air bubble formation ceased, though the connecting channel linking the positive electrode with the mixing chamber appeared to have accumulated PDMS debris, possibly a cause of channel over-heating. Images of this channel damage can be seen in Figures 30 and 31. From this, we determined that the maximum applied voltage for chip functionality must remain under 1000 Volts.

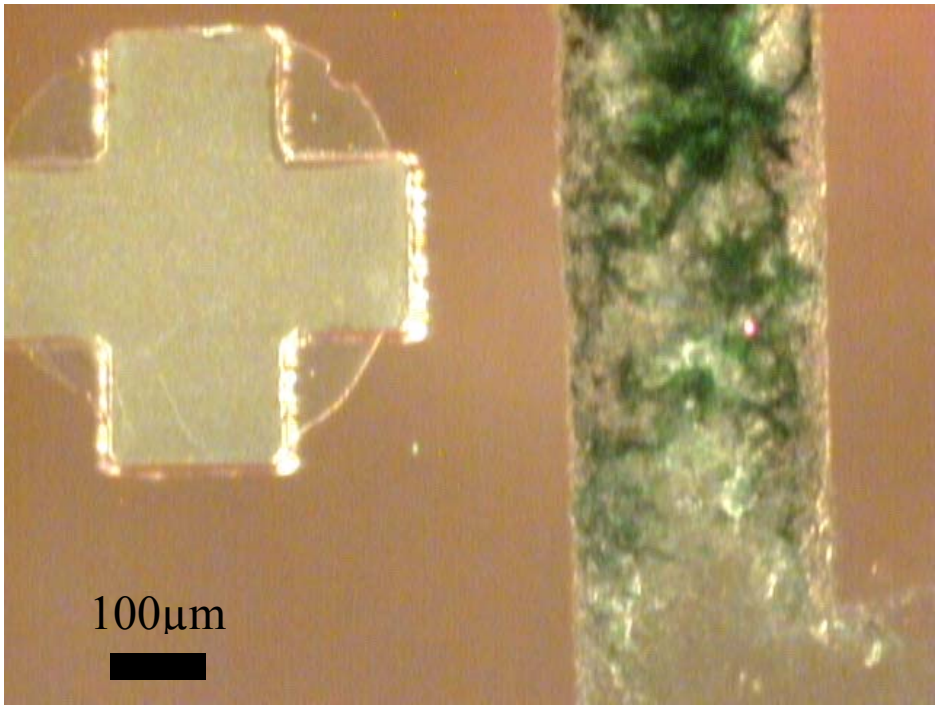

Figure 30 – Inverted microscope image of microchannel damage via high voltage

This figure reveals the extent of electrode damage to the PDMS channel walls after passing the critical voltage. The perpendicular channel shown connects the mixing chamber to the upper electrolyte reservoir. An alignment marker, not part of the fluidic network, is visible to the left of the microchannel. Since these experiments were conducted with green food dye, dye accumulation is seen as well in the microchannel.

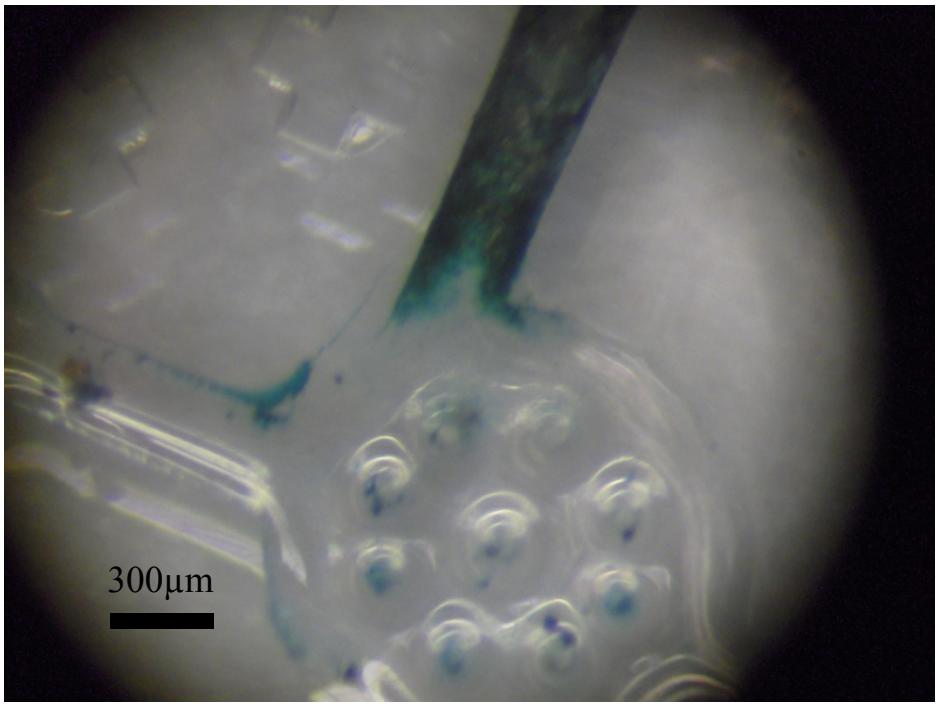

Figure 31 – Light microscope image of microchannel damage via high voltage

A top-down image of the mixing chamber and connecting microchannels further reveals the extent of electrode damage. The entire fluidic network was flushed out with DI water and allowed to air dry before the image was taken. The damaged channel shown connects the mixing chamber with the upper electrolyte reservoir. Dye accumulation is highly defined through the damaged channel but can also be seen along PDMS walls and support posts in the mixing chamber.

The chip was allowed to air dry overnight and then flushed out with acetone, isopropyl alcohol (IPA), and DI water by a hand-held syringe. A syringe was inserted into each of the five ports and administered several microliters into each in order to clear the connecting channel of any debris. Fluid was able to pass through the connecting channel region, meaning that the channel damage had likely been secluded to the walls and did not impede the flow of fluid. It was determined that the chip was still useful for conducting additional electrode tests.

3.2.4 Microbead testing

After the high voltages supplied through AC waves appeared to produce a detrimental heating effect with no observed mixing in the chamber, we reverted back to lower voltages and observed the paths of fluorescent polystyrene microbeads to notice if their streamlines were altered under the influence of an electric field. A solution containing 100µL of 10µm red Fluospheres™ combined with 100µL of DI water was prepared and used for the sample. The beads were easily visualized passing through the mixing chamber, but were too large and dilute to image particle streamlines. Another disadvantage of the large beads is that they tend to accumulate in areas of slow flow and adhere to microchannel walls and to each other, seen in Figure 33. This resulted in several "microbead clots" which began to alter the baseline fluid separation streams. The chip was removed from the connecting syringes and flushed out with DI water in order to dissociate the beads from the walls and restore the baseline flow conditions. A new solution was prepared containing 100µL of 1µm red Fluospheres™ with 100µL DI water and used for the sample. Flow conditions were maintained as before and particle streamline separation was observed, as shown in Figure 32.

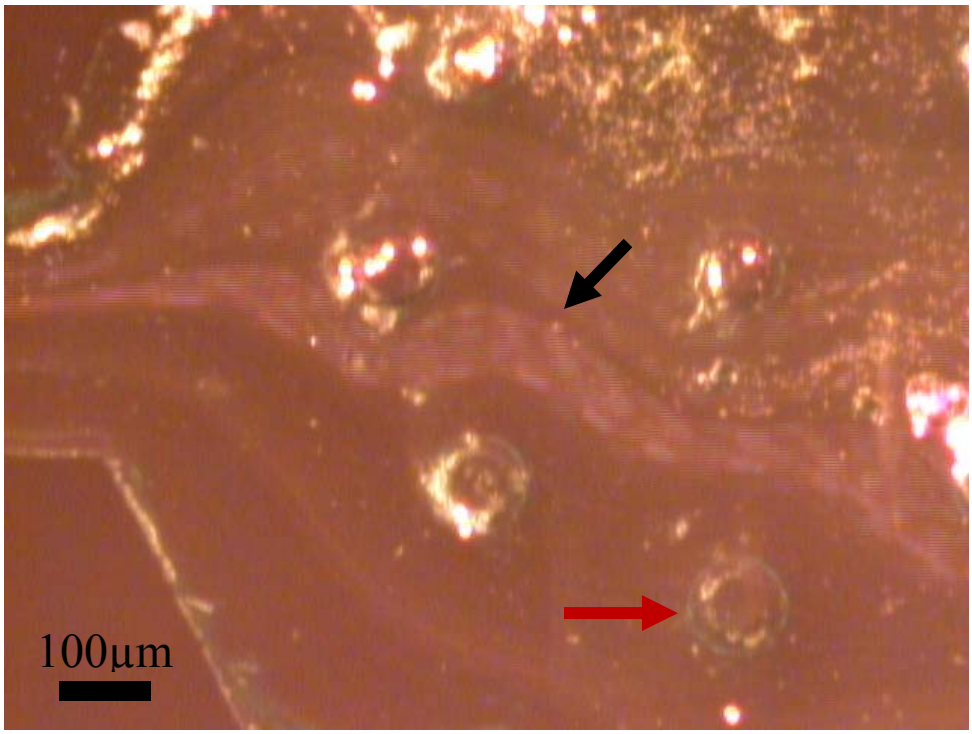

Figure 32 – Particle streamlines of 10 micron fluorescent beads through mixing chamber

The image above, taken with the LabSmith™ inverted microscope, illustrates the 10µm fluorescent bead flow paths through the front half of the mixing chamber, indicated by the black arrow. Support posts can also be viewed in the image, as indicated by the red arrow. Note how the streamlines of the fluorescent beads deflect away from the PDMS posts, due to the posts' hydrophobic surface.

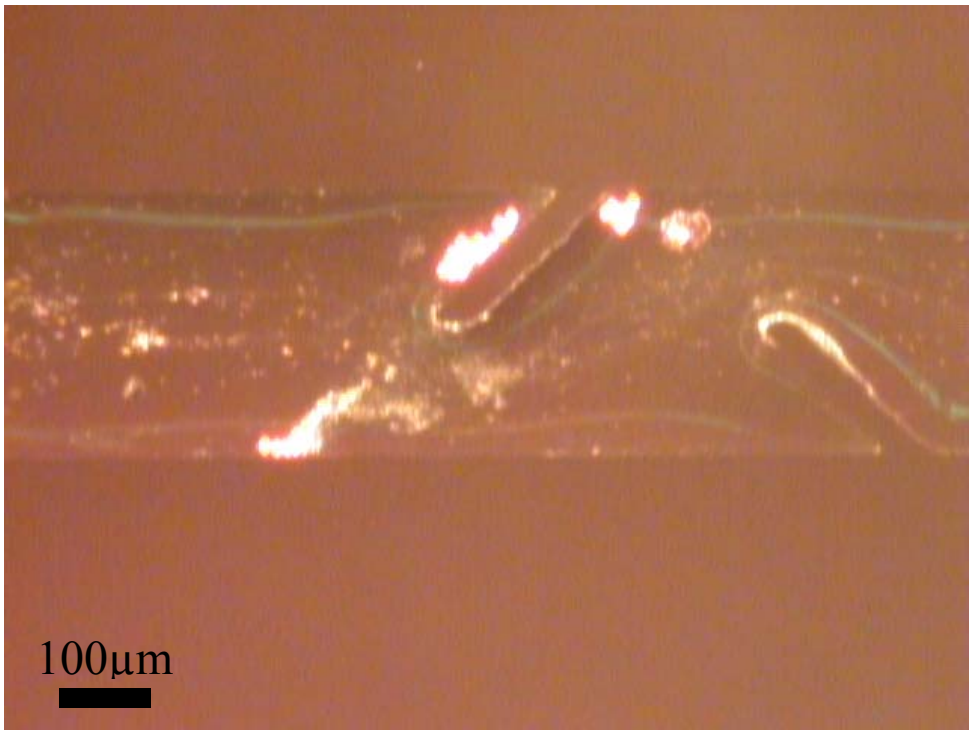

Figure 33 – Fluorescent bead accumulation at surfaces of mixing obstacles and channel walls

The above image, captured with the LabSmith™ inverted microscope, displays accumulations of 10µm fluorescent beads on the contacting surface of the mixing obstacles. The accumulation of the beads is indicative of biofouling issues with protein accumulation on the obstacle surfaces.

AC sine waves were again induced but this time with amplitudes of 1V, 10V, 50V, 100V, and 500V. The frequency for all tested waves was set to 5 Hz. After observing the particle streamlines for each adjusted field, no alterations were noted in the mixing chamber. However, slight fluid/air pulsing was observed at the positive electrode insertion point for voltages of 100V and 500V. DC voltage was again tested in hopes of altering particle streamlines. DC voltages of 200V and 400V were supplied for roughly 10-20 seconds each. Throughout the voltage sourcing, no activity was noted in the mixing chamber, but once the source was stopped, the particle streamlines jumped up a several micrometers and remained in place. The voltage was applied once more, causing the streamlines to fall back to their initially observed position. Again, when the voltage was stopped, the streamlines rose back up. The extent of the jump that the streamlines

exhibited was related to the amount of voltage being sourced. For 200V, the streamlines spanned a smaller lateral distance than when 400V was sourced. When the voltage was switched on and off quickly, the particle trajectories began to cross streamlines, resulting in chaotic mixing. The electrode insertion points did not seem to exhibit any adverse activity while the DC voltages were pulsed or even left sourcing for up to 10 seconds.

Downstream effects of this rudimentary mixing effect were visualized as well. When no voltage was sourced, the fluid streams exhibited their baseline segregation profile, even at the very end of the exit channel. However, once the DC voltage (200V and 400V) had been pulsed repeatedly for several seconds, the fluid streams began to incorporate, causing the microbead paths to span almost the entire width of the exit channel instead of being confined to the upper half. This desired effect was tuned carefully in order to elicit a more pronounced mixing effect.

3.2.5 DC Pulse testing

Now that the DC pulse wave had been determined to be the most effective at arriving at the desired mixing effect, the duty cycle of the pulse was programmed into the voltage sequencer to maximize its precision. Using the complex sequence wizard in the LabSmith™ software, a square wave was created with a 50% duty cycle of 200ms. The amplitude of the wave was varied to observe the corresponding effects.

A new solution was prepared for the sample inlet consisting of 10µL of 0.2µm yellow-green fluorescent carboxylate modified microspheres with 200µL DI water. The solution was vortexed, inverted and tapped onto a square of paraffin wax in order to easily pull the small sample into the loading syringe. This new dye solution was used instead of the 1µm red beads in order to obtain clearer separation and mixing images in the exit chambers since the dye was more continuous than the microbead streamlines. Before the chip was used, it was flushed out with IPA, water and

air which helped to free the fluidic system of residual microbeads. After the syringe pumps were connected to the chip, the outlet pump was activated to pull at a rate of 3μL/min for 5 minutes before the inlets were activated. Using DI water as the buffer and the dye solution as the sample, fluid stream separation was achieved throughout the fluidic system prior to electrode excitation. Once the baseline was established, the electrodes were activated for pulses of about 6 seconds at voltages of 200V, 400V, 600V, and 800V. During these pulses, the inverted microscope was used to record video and still pictures of the mixing chamber, outlet channel, and inlet channel to observe the effects of the electrical stimuli. Dye propagation in the exit channel is visualized in Figure 34.

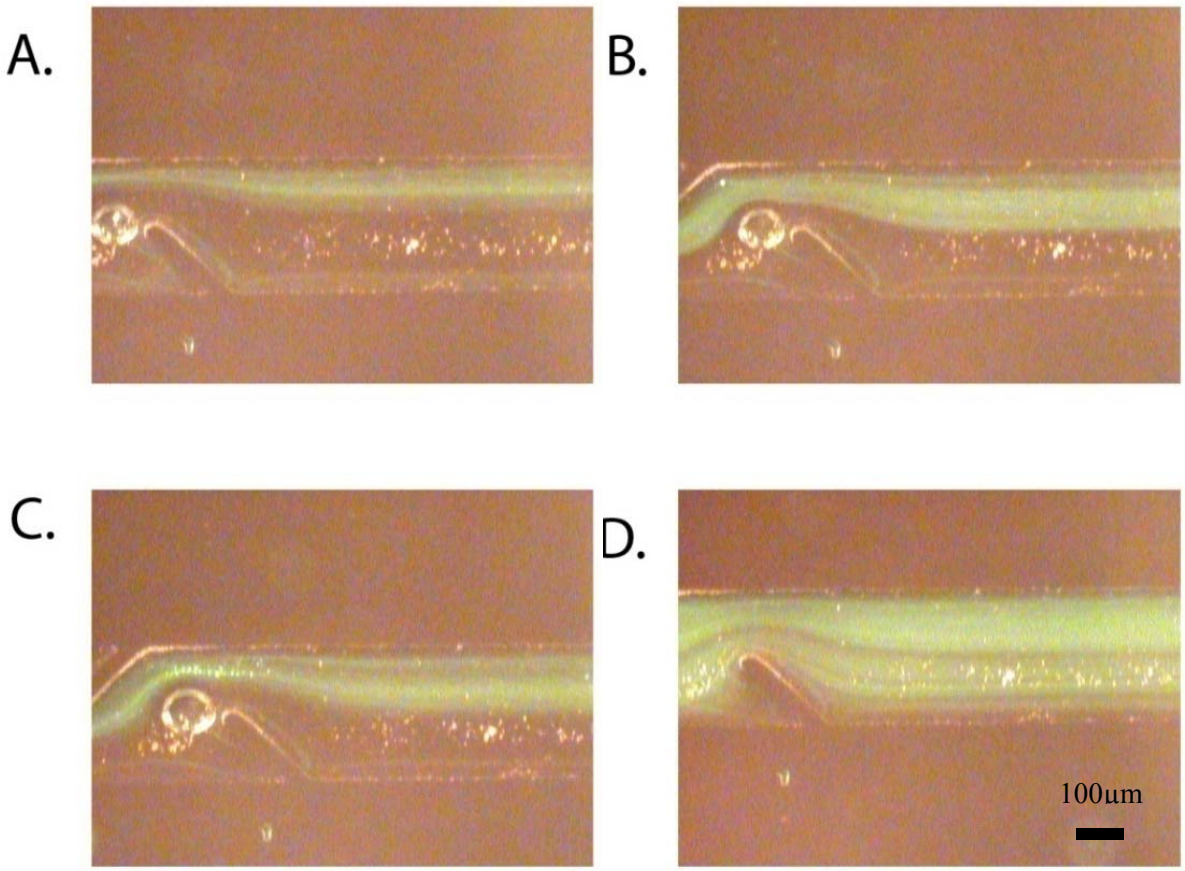

Figure 34 - Dye propagation visualization, 1.5 seconds elapsed

Images A through D display the extent of sample dye propagation distances for four different applied voltages: A) 200V DC, B) 400V DC, C) 600V DC, D) 800V DC. All four cases used otherwise identical operating conditions: inlet flow rates of 1µL/min, outlet flow rates of 3µL/min, 50% duty cycle of 200ms for pulsed DC waves, DI water spiked with 0.2µm yellow-green fluorescent carboxylate modified microspheres as sample, DI water as buffer. Images were recorded at similar outlet positions 1.5 seconds after electric fields were applied. From the images, we determined that an applied voltage of 800V DC was sufficient to ensure homogeneous mixing by observing a fully-propagated sample in the exit channel.

Once video files were collected for the four different voltage amplitudes at the outlet channel, they were sliced into still photos at intervals of 0.5 seconds for 5 seconds from the stimulus. These images were then analyzed using ImageJ [32] by measuring the propagation depth of the fluorescent dye into the exit microchannel. Since the dye spanned about half the width of the microchannel in the baseline condition, an increase in the propagation width would show more

effective mixing until the entire channel width is filled with the fluorescent dye. Since each condition had slightly different values for the baseline width of the dye, all distances were divided by the initial dye propagation depth for each case to yield "corrected" propagation distance values. These values were plotted in SigmaPlot™[33] as a function of time for each of the four voltages, in Figure 35.

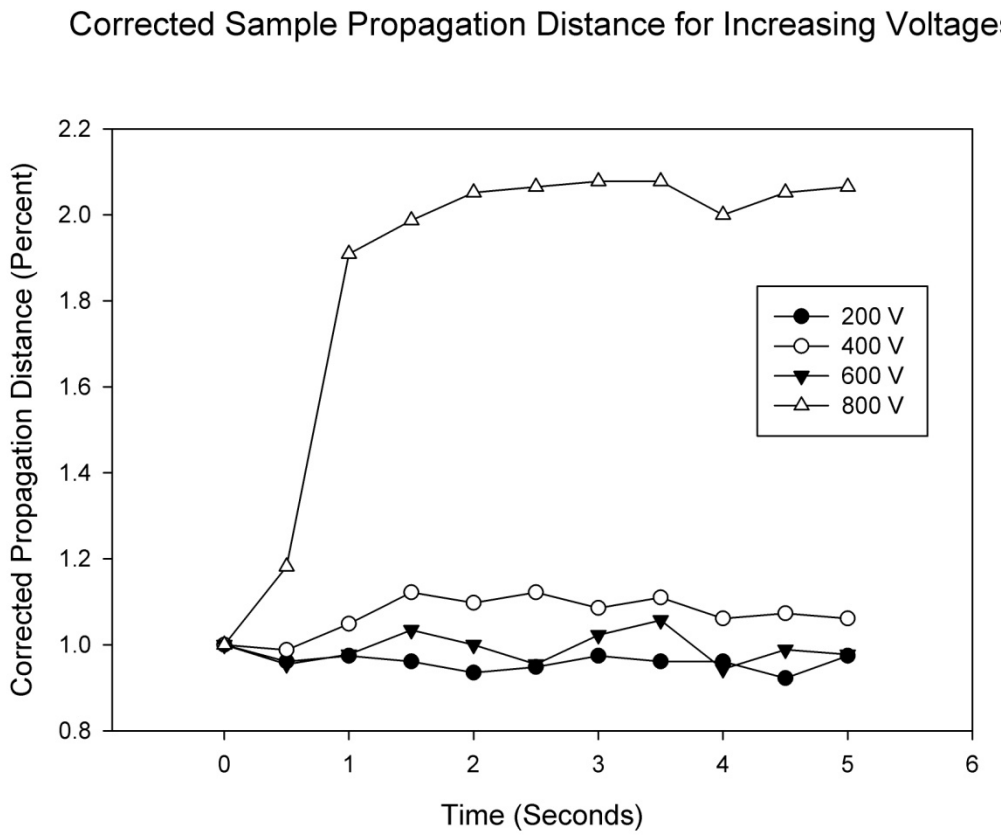

Figure 35 – Dye propagation distances for DC pulse mixing of buffer

Qualitative mixing data from Figure 34 was quantified using ImageJ to measure the dyed sample propagation distances for 11 time points for each of the 4 applied voltages. Each measurement was "normalized" by dividing the length by the initial propagation distance at time zero for each voltage case, since each analysis had slightly different baselines. After plotting these values, it is abundantly clear that applied voltages of 600V DC and below are not capable of achieving homogeneous mixing, while a voltage of 800V DC was shown to achieve homogeneous mixing.

It is important to note that the dye oscillated slightly in the exit channel in response to the oscillating voltage source. Therefore, imaging the channel at predefined intervals may not be an accurate representation of the "maximum propagation distance" for a particular time point, since the dye might be oscillating back to a previous level. When interpreting the results over time, it is more important to observe the trend in channel coverage rather than isolated values at particular time points.

After mixing was observed to be fairly complete with 800V at a 50% duty cycle of 200ms with the dye and DI water, the same conditions were applied to the mixing of BCS and the selected pretreatment buffers.

Bovine calf serum was introduced through the sample inlet port and treated with 0.1M MGA-0.1M EACA from the buffer inlet port. After observations were made with raw serum and the selected buffer, it was determined that the serum/buffer interface was insufficient at being resolved from the inverted microscope. Therefore, we spiked 800 microliters of raw serum with 100 microliters of the same fluorescent beads/dye used in the preliminary mixing analysis experiment. We were unable to determine if the addition of fluorescent dye to the raw serum had any influence on the field-assisted mixing, either by altering solution charge or possibly diluting the raw serum. Once flow had stabilized and yielded a continuous dye separation using the same experimental methods outlined previously, voltages were adjusted in order analyze the appropriate field strength for full dye propagation. Like the initial dye propagation analysis, recorded mixing videos were spliced at discreet time points and analyzed in ImageJ, shown in Figure 36.

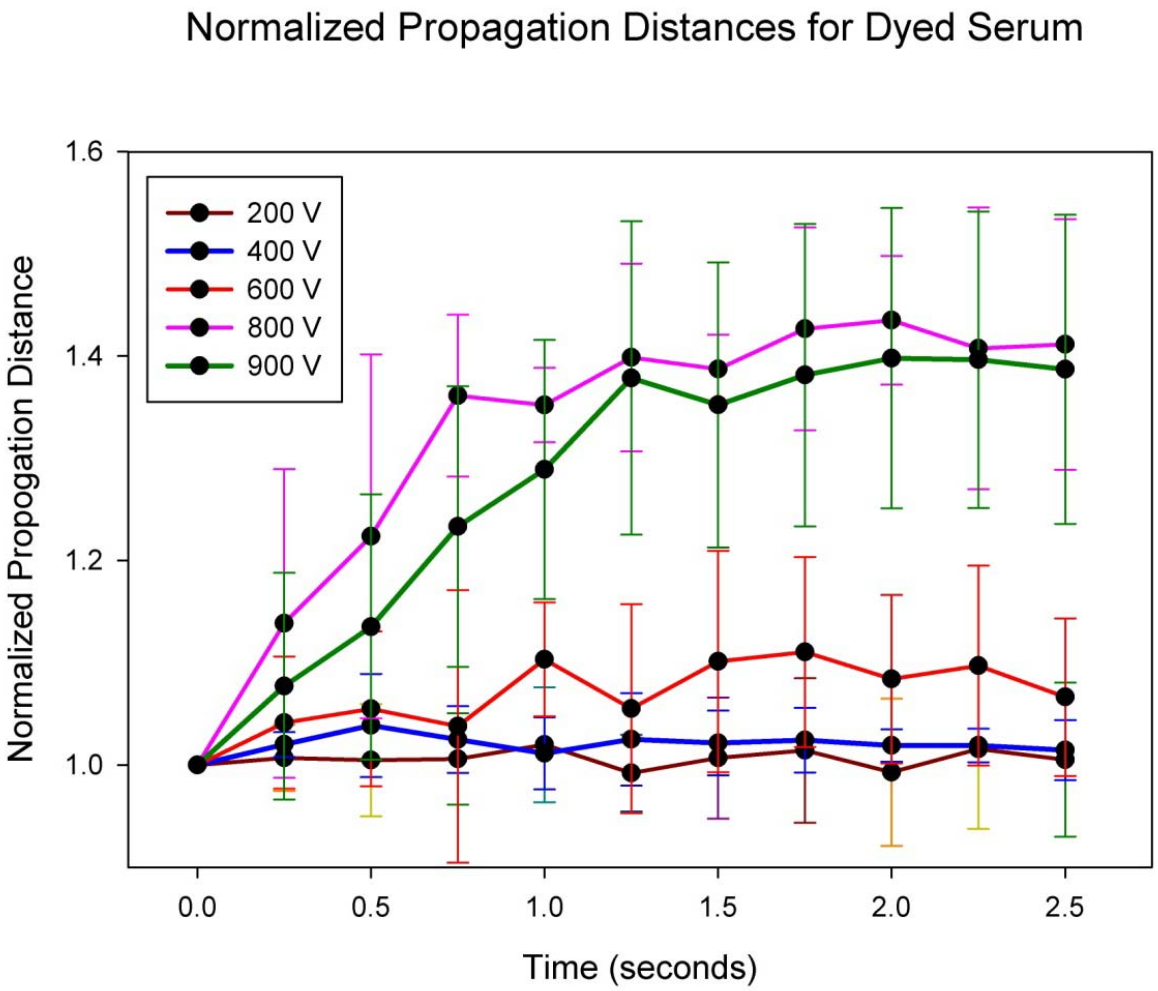

Figure 36 - Normalized dye propagation distances for raw serum micro-mixing

After 5 different applied voltages were recorded with the LabSmith™ inverted microscope, the qualitative mixing data was quantified using ImageJ to measure the dyed serum propagation distances. Each measurement was "normalized" by dividing the length by the initial propagation distance at time zero for each voltage case, since each analysis had slightly different baselines. Six measurements were collected for each time point for the different applied voltages and were used in a variability study. Error bars in the plot indicate the standard deviation of each set of values by the horizontal bars, while the points represent the average values of each set.

Three mixing videos were recorded for each voltage amplitude, each with two separate electric field pulses analyzed for a total of 6 measurements at each time point for the differing voltages. Error bars were added to the plot to display variability within the data set.

4 Conclusions / Discussion

4.1 Pretreatment Conclusions and Validation

A significant element of this pretreatment chip project was the development of an experimentally relevant buffer pretreatment protocol. We relied heavily on previous data in the literature when selecting our buffer solutions in order to gain insight on the relevance of their use in serum fractions. Ultimately, this protocol will require experimental validation of our own integrated downstream sample conditioning chips. However, the buffering solutions used in this project represent the possible capabilities of this pretreatment chip by demonstrating that a raw sample can, in fact, be selectively optimized through the introduction of a buffer solution in a micro-mixing device.

We determined that, in the case of blood serum fractionations, a 5:1 (v/v) ratio of 0.1M MGA to either 0.1M EACA or 0.1M GABA was sufficient to pre-treat a raw sample of bovine calf serum to the optimal pH and conductivity ranges. The optimal ranges were extracted through literature reviews of capillary electrophoresis operating conditions, electrophoretic separation microchips, and overall microchip functionality reviews. Through this search, we obtained the following target range of these three parameters, seen in Table 7.

Table 7 – Initial and target pretreatment parameter ranges

Sample	**pH**	**Conductivity (µS/cm)**	**Viscosity (cP)**
Raw Serum	6.924 – 7.144	10,540 – 10,880	1.21 - 1.32
Target Values	10.26 - 10.62 [14]	< 500 - 1000 [21]	1.0 - 1.1cP [22],[23]

After our initial measurements of pure BCS, it was abundantly clear that there was a large difference between the target and initial parameters, likely implying that a large-scale dilution would be necessary. This large discrepancy could easily be overcome on the bench-scale, as it is frequently performed in most labs. However, on the micro-scale, fine tuning of select parameters, especially when there is a wide range of values, represent continued challenges. Therefore, we not only tested the optimal combinations of the operational electrolyte MGA with co-ion solutions of EACA and GABA, but also the volumetric combinations of BCS with our selected buffers. Results from the serum pretreatment data indicated that a large ratio of serum to buffer volume, roughly 1:60 (v/v), would be necessary to adjust the solution conductivity within its optimal range.

Furthermore, our results from the serum titrations revealed that the two fluid parameters selected for manipulation on this project exhibit different dependencies on the addition of buffer. The results from the pH titration measurements indicate that sufficient addition of our selected buffers result in a completely adjusted pH. The titration curve for serum indicates that in our pH range, serum behaves as a monoprotic acid and reaches a basic "state" after its equivalence point of about pH=8.5 is obtained. Ideally, we can assume that in our mixing chip we are combining equal volumes of serum and buffer since the two inlet geometries are identical and the fluids are injected at the same flow rate. Therefore, we expect that raw serum will combine with an equal amount of buffer on-chip and yield results comparable to the basic plateau region on the titration curve.

Our conductivity results for the serum titrations also indicated a response to the amount of buffer added to raw serum. Even though conductivity appeared to steadily decrease as buffer was added, the range of values was significantly higher than our target range. We showed earlier that multiple serial dilutions with DI water were required to lower the conductivity below 500µS/cm.

After adding equal amounts of buffer to raw serum, we measured a conductivity of around 7-9 mS/cm, which is an order of magnitude larger than our target range. We conclude that the current chip design needs to be modified to adjust serum conductivity to the desired range. Volume control will be a necessary addition to future chips that condition raw serum conductivity. It is possible that different biological solutions may be effectively pretreated on this platform based on their intrinsic parameter values. For instance, we can reason that a sample of saliva would be less conductive than serum and could possibly be pretreated using our device.

After this observation, our focus shifted from conductivity to pH. Our titration data gave us reason to believe that under similar operating conditions on-chip, we could effectively adjust the pH of raw serum to our target range. Validation of the on-chip pretreatment of raw serum proved to be a difficult task. First, the volumes used on-chip are on the order of nanoliters to microliters, which are far less than the necessary milliliter range for our conventional pH probes. Processing the required amount of solution to yield measureable volumes off-chip would require numerous hours of operation, which would be unable to support our claim of rapid pretreatment on-chip. We considered using a micro-pH meter (Orion, Thermo Scientific) used for microtiter plates that could measure the pH of a single droplet of solution. However, our experimental operating conditions would not permit measurement with this method. We required that a third syringe pump be connected to the outlet in order to create a vacuum force which kept the samples from flowing into the electrolyte reservoirs. This meant that if we ran solution through our chip, it would also run through a stretch of tubing connecting to the outlet syringe pump. Over this long distance, the two fluids would likely mix via passive diffusion, and thus provide no analytical significance if the solutions were measured after on-chip pretreatment. Validating conductivity measurements would have also required large volumes of solution and were thus neglected.

The possibility of non-numerical measurements by adding pH indicator dye to our solution was also considered. After reviewing pH ranges of common indicator dyes, we selected a thymolphthalein solution which is clear at pH values below 8 and turns dark blue as it approaches a pH of 11. Off-chip tests with the indicator dye yielded noticeable color changes for serum before and after pretreatment. We also observed that a small volume of the dye could be added to the serum before pretreatment would still undergo a color change as buffer was added. A solution of raw serum combined with a small amount of indicator dye was loaded on our device to try observing the same effects during micro-mixing. Repeated testing verified that the solution was not pronounced enough to visualize any mixing or pH change on-chip. The limitations may be due to the inverted microscope or to the dye itself. Future work could include obtaining a fluorescent pH-sensitive dye to visualize the conditioning of serum pH on-chip. We considered adding the pH-dye to the treated solution after it passed through the chip, but realized this would produce the same insignificant results as measuring pH at the outlet after the solution exited the final length of tubing. This on-chip pretreatment validation remains an issue that will be incorporated into future work on this project. Possible validation measurements could include the incorporation of instrumentation or probes into the device itself. An example of this may be an array of parallel electrodes placed along the outlet channel on the glass substrate which could be used to measure changes in fluidic resistance and convert the measurements to conductivity values. This on-chip validation approach is ideal since ultimately on-chip results are our biggest concern.

Present on-chip pretreatment validation stems from scaling arguments and off-chip pretreatment observations. As stated before, we believe that the pH of raw serum was effectively treated towards our optimal range based on the bench-scale titration data of our selected buffers. Solution conductivity was conditioned on-chip, but did not approach our target range in the same time

scale that pH was conditioned. Future work may also consider an array design where each parameter is conditioned in serial or parallel mixing chambers.

More experimental validation will be necessary in the future to determine the effects of sample pH and conductivity specifically when implemented in an electrophoretic separation chip. Basic theory indicates that solution pH has a major influence on the charged state of the solutes present in a sample, which would refer to proteins and ions in our case. The charged state of these solute analytes is directly correlated with their electrophoretic mobilities, which determines how they will interact with an electric field in an electrophoretic separation chip. Solution conductivity also plays a role in how the bulk solution interacts with the electric field and can influence particle separation resolution, analysis times, and overall chip function. This is apparent when considering the effects of joule heating inside a microsystem. Solutions with higher conductivities demonstrate joule heating effects at lower voltages than solutions with low conductivities. This is a major concern in microfluidic chips where distances between electrodes are on the order of millimeters or even microns yielding high apparent electric field strengths with low applied voltages. However, until the effects of joule heating or the operational effects of solution conductivity are quantified in a microfluidic platform, the importance of solution conductivity remains undetermined. Like conductivity, the effects of solution pH on electrophoretic actions in a microchip should be thoroughly quantified in order to understand the importance of precision tuning. Our application of treating a raw serum sample with a uniform buffer solution is sufficient to demonstrate the capabilities of bulk parameter tuning on-chip.

4.1.1 Future work with pretreatment protocol

Precision tuning of parameters such as pH and conductivity are highly dependent on the volume ratios of serum to the pretreatment buffers. Therefore, precise selection necessitates the future use

of on-chip valving that can refine the volumetric control of each fluid. The downside of volumetric control is that for large ratios of serum to buffer, as was necessary for our conductivity refinement, processing times are greatly increased. An intriguing approach to future volume control combines microfluidic droplet manipulations with micro-mixing. In this case, a raw sample is partitioned into a small droplet that gets combined with a bolus of pretreatment buffer in a mixing chamber and is subsequently portioned into another single droplet. This mode of on-chip serial diluting may prove to be a quick and efficient method for the tuning of robust parameters that require otherwise large volumes of buffer or time-consuming linear dilution operations. The ultimate goal of a pretreatment device would be to treat a raw sample within a few seconds and deliver the fluid directly to the next downstream chip. Research into the exact requirements of a pretreatment buffer might alleviate these concerns if it is determined that solution conductivity only requires slight adjustment, which can be accomplished much faster than a large-scale sample dilution. There are also possibilities of introducing a sample that is already diluted. While this interferes with the "raw sample" principle, this step could possibly be combined with the sample collection process and further improve the functional requirements of the pretreatment chip.

Another area of future work includes the expansion of the pretreatment chip's capabilities to encompass multiple different sample types while correcting for a range of different parameters. This process will necessitate the appropriate selection of sample-specific buffer solutions and carries much added complexity for chip functions. The chip design that we proposed is in no way meant to serve as a universal pretreatment device, but can be modified and adapted to many different situations. Sample solutions, may cover saliva, sweat, or possibly whole blood, for example, which would each require a specific pretreatment protocol and possibly different operational conditions, such as flow rates and voltages.

The buffering solutions used in this project were picked based on prior literature research that encompassed the interactions of buffering molecules and compounds with specific protein fractions. We chose the buffers that obtained the highest resolution electropherograms for serum fractionation, meaning that molecular partitioning occurred in a way that influenced the individual electroosmotic mobilities of each fraction. Adjusting the balance of the solutions, as was done to arrive at a more optimal pH value, could affect the dynamics of this molecular partitioning and may in fact alter the resolution that was recorded. Future work should include studies into the effects of buffer content, and how biomolecular dynamics affects protein fraction resolution. This same information would be essential for the refinement of buffering protocols for various sample types as well.

4.2 Micro-mixing Conclusions

Preliminary mixing analysis with fluorescent dye and water indicated that our micromixer chip was able to effectively combine the two solutions within 1.5 seconds using an 800V 50% duty cycle of 200ms (Figure 39). We determined that 800V was the best amplitude to use for our applied voltage since we wanted to find the lowest possible applied voltage that could elicit homogeneous mixing. Higher voltages run the risk of joule heating, possible cell lysis, and use more energy. As seen in our AC voltage tests (Figures 30, 31), high voltages can even be destructive to the PDMS microchannels.

We first noted the electrokinetic effects of our chip when 0.1µm microbeads were introduced through the sample inlet and a DC voltage of 200V was applied. When the voltage was stopped, the streamlines formed by the fluorescent microbeads shifted up several microns, alerting us to the effects of a pulsed voltage. We believe that the small charge of the microbeads resulted in their ability to be manipulated in the presence of the electric field. All dye solutions that were

used were slightly charged and likely followed the same principles as the microbeads. Future work could include studying the effects of a neutral dye, introduced with a neutral buffer, to see if field-assisted mixing occurs when solutes are not charged. Though this might yield interesting information into the mechanisms behind our mixing action, most biological samples include charged species which will likely perform as our microbeads demonstrate. If the mixing action is dependent on the charge of the particle, our micro-mixer will have operated as a combination of electroosmotic and electrophoretic manipulations. Supposing that our sample stream is more charged than our buffer stream, this charge-dependent mixing effect will actually increase the efficiency of our micro-mixer since we are more interested in the even distribution of analyte than of the two fluid streams. This phenomenon appears to be another factor that separates our design from Santiago and Oddy's [21]. Their micro-mixer attempted to arrive at a homogeneous mixture of two "pure" fluid streams, which required an AC field with high voltages and low conductivity of solution. We found that we could arrive at similar homogeneity using lower voltages, higher solution conductivity, and a very inexpensive means of delivering the electric field instead of depositing any material on the glass substrate. Of course, our chip is also concerned with the combination of the two fluid streams as an opportunity for increased interaction between the two which could yield a "treated" solution. Simply distributing the solute molecules throughout the exit channel may not be sufficient for conditioning the sample.

After initial micro-mixing was performed with dye and water solutions, we tested the effects of mixing raw serum with our specific buffers. Two major differences between these two experiments include the higher viscosity and higher conductivity of the serum solutions compared to the fluorescent dye. We expected these two differences to hinder the field-assisted mixing activity performed on the serum solution. First, since viscosity is an indication of flow impedance, solutions with higher viscosities are not as easily manipulated or stirred as solutions with lower viscosities. Second, we believed that the higher conductivity of serum would actually

lessen the influence of the electric field. Though this may seem counterintuitive, since higher solution conductivities are better conductors of electricity, the high concentration of dissolved ions means that there is an equally high concentration of counter-ions in solution which can potentially null the effects of the active electrodes. The formation of the electric double layer as described earlier occurs under these operating conditions as well since an electric charge is being applied to an electrolyte solution. However, when the ionic concentration of the solution is sufficiently high, the buildup of counter-ions around this charged layer forms a capacitor that can severely reduce the apparent electric field strength in the bulk solution [34]. In order to counteract this capacitance effect, different time scales have been developed that relate to the separation of charge and the formation of the Debeye layer, the term used to describe the distance that the surface charge of an electrode propagates into the bulk fluid. A substantial review of diffuse charge dynamics has been illustrated by Bazant et al [34] and is worth investigation to determine the appropriate time scale for electric field application. Our frequency of 5 Hz seemed to operate reasonably with this charge separation phenomenon and allowed field-assisted mixing to occur. However, lower frequencies may allow for counter-ion charge buildup which would significantly reduce the effects of the electric field. Future work on determining more optimal operating conditions may focus on a mathematical approach by ensuring that the time scale of electric field activation is less than the time scale necessary for capacitance initiation.

We determined from our scatter plot of propagation distances of the dyed serum (Figure 40) that the raw serum behaved similarly to the preliminary dye and water experiments. In fact, we discovered that complete mixing was achieved slightly faster for our serum experiments than the initial dye experiments, though this could be due to the increased number of time steps in the serum analysis which led to greater resolution in our scatter plot. Applied voltages were maintained under 1000V in order to prevent any adverse reactions. These experiments were only performed with one of our buffers, 0.1M MGA-0.1M EACA, since previous data we collected

indicated that the two buffers would behave identically under our experimental conditions on-chip. Just as was seen in the preliminary mixing analysis, an applied 800V with a 50% duty cycle of 200ms was sufficient to induce homogeneous mixing, characterized by a high normalized propagation distance in the exit channel. One interesting occurrence concerned the lower propagation values for an applied 900V than the applied 800V. This phenomenon may be due to the charge shielding effects mentioned above that are possibly field dependent as they are concentration dependent. However, this disparity may just be due to inherent variability with this form of analysis.

There are many possible sources of error in our dye propagation analysis. First, the still images rendered from the mixing videos were meant to be obtained for specific time points, though software limitations occasionally rounded these time points off by a few seconds. This resulted in possible variation amongst different repeated pulses for the same time point. Second, the propagation distances were measured in ImageJ but had to be selected by hand. Images where dye distances in the exit channel were difficult to discern led to variability in distance measurement. These limitations were due to human error and software issues, though one other source of variability was inherent to the mixing phenomenon. While the electrodes were active, we observed that the sample-dye solution experienced a periodic oscillatory motion whereby the charged species within the solution were being electrostatically repelled by the active electrode while the field was on and returned to their resting position when the field was turned off. Altering the frequency of our DC pulse would illustrate this point further since the sample-dye solution would be expected to oscillate faster with increased frequencies and slower with decreased frequencies. Due to this oscillatory motion, some propagation distances may have been recorded as the dye retreated to its original position while others recorded the dye at its peak distance. These sources of variability led to large standard deviations seen in the error bar plot (Figure 36) which may possibly still exist even with larger sample sizes. It is more important to

note, therefore, the trends associated with the average normalized propagation distances rather than the particular values. From our analysis, we have determined that an 800V DC pulse with a 50% duty cycle of 200ms has proven to be sufficient for the homogeneous mixing of raw serum and our selected buffers in less than one second.

4.2.1 Chip Issues

4.2.1.1 Air

Even though the desired action of our chip was observed, we had difficulty with some chip operations. First, air bubbles were a constant occurrence and were difficult to purge without flushing the entire system. This issue might be based on the design of the chip or the chip packaging which could have left small openings for air to enter and escape. Degassing our solutions, though not practical for our sample solution when considering POC applications, might help eliminate dissolved gases in our sample and buffer solutions. Dissolved gases are also highly dependent on the biological sample used, since, for example, serum likely has a higher concentration of dissolved gases than sweat. The air bubbles inside of the chip also influenced large pressure gradients throughout the electrolyte reservoirs and possibly through the mixing chamber itself. The intended function of the electrolyte reservoirs was to house a large volume of an electrolyte solution on-chip that would interface with the mixing chamber in order to achieve electrical connectivity through the system. In reality, these reservoirs possessed too much surface tension to allow for complete surface wetting, and therefore could not be filled without the presence of air. Future designs should either omit or redesign these reservoirs to increase the functionality of the device. It is possible that a redesign of the reservoirs could alleviate air presence concerns by maximizing the volume of liquid in the reservoir. The hydrophilicity of

glass compared to the hydrophobicity of PDMS may explain why on-chip reservoirs did not present any issues in the Santiago and Oddy micromixer[21].

4.2.1.2 Obstacles

We performed a COMSOL™ analysis to determine if the presence of the passive, repeating mixing obstacles in the exit channel were beneficial to the overall degree of mixing. Results from the simulation showed that mixing improved tremendously and was even more effective through purely passive mixing actions than the same chip without the obstacles but with an electric field applied. When dye was run through our chip experimentally with no electric field applied, we failed to observe the same passive mixing actions as our COMSOL™ model. We noticed that regions between the obstacles experienced slightly enhanced dye propagation distances, but did not appear to adjust the segregation of the two fluids through the exit channel. We believe that the COMSOL™ model assumed a much more diffusionally active sample species instead of a more realistic, convection-driven fluid, illustrated in Figure37.

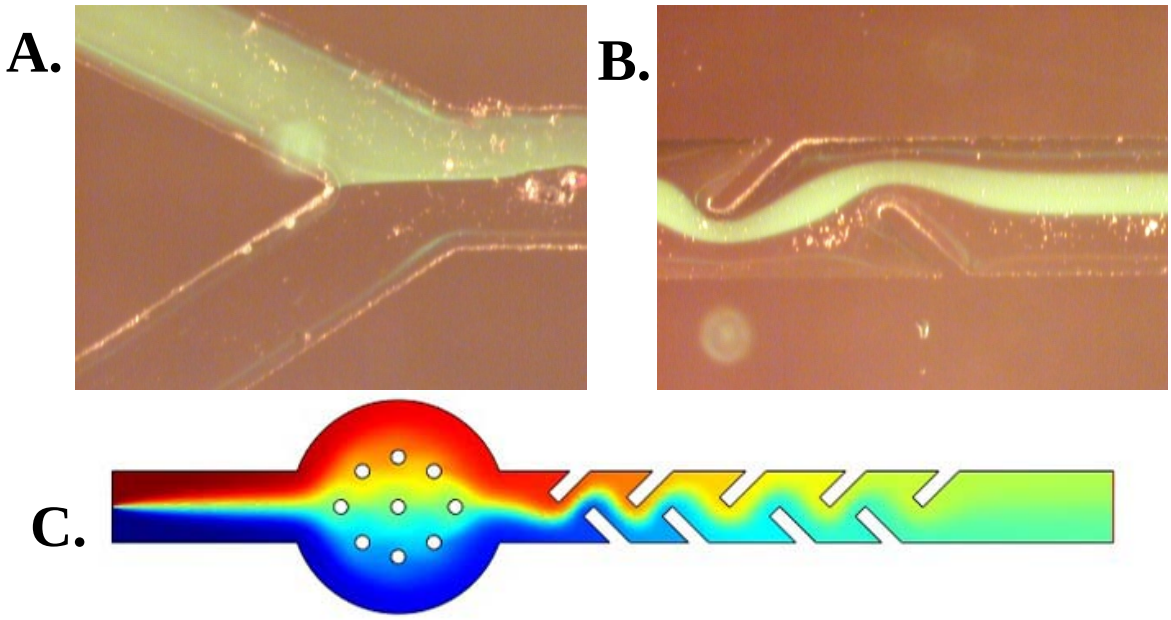

Figure 37 - Comparison of COMSOL™ modeling and experimental conditions

The above images display the disparity between our COMSOL™ modeling results and our experimental results concerning the efficacy of the PDMS mixing obstacles. Images A and B illustrate how our dyed samples did not mix with the buffer solutions when no electric field was applied. Image C, on the other hand, demonstrates how, under similar conditions, our COMSOL™ model predicted that the two fluids would mix via diffusion after passing through the mixing obstacles.

We cannot determine the extent of mixing contributions that the passive obstacles carried since we have no baseline design to compare to. Future work should include an experimental comparison of the two cases which may determine the necessity of the obstacles. One aspect of the obstacles' functionality that COMSOL™ could not test for was the issue of biofouling. When we introduced the 10μm fluorescent beads into the system, we observed significant "clotting" of the spheres onto the surface of the obstacles (Figure 33). The adhesion of the larger beads demonstrates the possibility of protein and small molecule adsorption from raw samples. Disposable, one-time use chips carry little concern for biofouling since they are only in contact

with raw sample for a limited amount of time. However, if our pretreatment chip becomes incorporated into a reusable diagnostic device, biofouling concern might necessitate the removal of the mixing obstacles or the addition of some surface modification to prevent protein adhesion.

4.2.1.3 Packaging

Chip packaging also presented some functional issues through this project. First, we determined that epoxyed connections to the surface of the PDMS were not sufficient at providing a real-world interface since the epoxy did not fully adhere to the hydrophobic PDMS. While the connections did present a suitable option to connect tubing to the ports, they would have needed to be incorporated into a surrounding packaging layer instead of being attached to the PDMS itself. Second, the electrodes that made contact with the fluidic network were inserted manually and created leaks in the PDMS surface by introducing a new fluid path. This method was inexpensive and quick but not necessarily elegant enough to ensure a robust connection and a simple user interface. Like the fluidic tubing adapters, the electrodes could possibly be attached or integrated into a surrounding packaging layer before contacting the PDMS, which could hold them in place and make electrode cable attachment simpler. Future work may include the development of a Plexiglas housing that can encompass the mixing chip and all of its connecting parts while still maintaining the glass substrate to allow inverted microscope imaging.

4.2.2 Future Work - Micromixer

Future work regarding the micromixer will include analysis of the residence time of sample particles in the mixing chamber. Adjusting the flow rates, applied voltage, and the pulse rate should have a large influence on the amount of time that a sample particle will remain in the mixing chamber. The analysis should also include observations into the effects of increased

residence time with parameter tuning. It is possible that increased residence time may correspond with more interactions between sample and buffer and yield a more homogeneous “treatment” solution through the outlet.

Future work might also consider different micro-mixer designs, possibly converting our active micro-mixer into a passive micro-mixer. As discussed earlier, each type of micro-mixer has distinct advantages and disadvantages. One major advantage of passive mixing is that the portability and possibly cost-efficiency of a device is greatly enhanced compared to active micro-mixers which require extra instrumentation to evoke their external stimuli. Other possible designs might include a series or array of mixing chambers to tune different parameters in different regions and possibly add dilution mechanisms. Volume control when adjusting for concentration-dependent parameters such as conductivity will need to be considered in future designs as well.

4.3 Combined Discussion

4.3.1 Combined Future Work

Future work regarding our device as a whole, including the pretreatment protocol and mixing ability, will include protocol validation by use of downstream electrokinetic separation chips. Even though our protocol was based on capillary electrophoresis data, there are several differences present in the micro-separation chips that are used in the Cal Poly Biofluidics lab which may result in different functionality of our sample and buffer. This may help determine a more precise buffer selection for a specific application and possibly adjust experimental configurations as well. The long term goal of this project is to integrate this chip into a portable, point of care diagnostic device in order to condition raw samples and make them more optimized for downstream manipulations. We believe that we have made an important first step towards this end goal by developing an effective micromixer device that can combine raw sample with

specific buffer solutions in a homogeneous mixture in less than one second. Combined with a scaling analysis of how our buffers interact with raw serum off-chip, we determined that solution pH must be treated within this time frame, though solution conductivity required larger volumes of buffer. Even though these two parameters were not able to be directly measured during or after our on-chip pretreatment, we have shown through reasonable scaling assumptions with bench-scale experimentation that both solution viscosity and pH have been rapidly conditioned within our target range on-chip. The results from our off-chip pretreatment of serum yielded a linear correlation between conductivity and the amount of raw serum added to our specific buffers, which could be used to determine the correct ratio of the two solutions for a desired conductivity. Even though volume control will need to be integrated into future models based on our device, we feel that we have shown that a raw sample can be effectively combined with a desired buffer solution on-chip in under one second in order to adjust key parameters of that sample. We have also considered the long term applications of this technology and fabricated our device out of common microfabrication materials to assist in its eventual incorporation with subsequent electrophoretic chips for sample preparation. By encompassing the idea of on-chip sample pretreatment into POC diagnostic devices, future analyses will become more accurate in detecting biomarkers significant to early detection, proper treatment, and global health.

Appendix A: Electrokinetic Separation Theory

A.1 Gel Electrophoresis

One form of electrophoretic separations commonly found in molecular biology and biochemistry is gel electrophoresis, specifically SDS-PAGE (Sodium Dodecyl Sulfide PolyAcrylamide Gel Electrophoresis). In this method, the gel serves as a mechanical filter than has a sieving effect on the solutes that pass through via electrophoretic motion. The SDS component is a detergent that is added to the sample solution that gives almost all proteins the same negative charge [16]. SDS has both polar and nonpolar components that allow it to bind to a variety of proteins. Since all remaining solutes have a similar charge, the electrophoretic separation resolves solutes based on their size, or molecular weight. This process yields relatively quick separations of proteins and nucleic acids that can be further isolated and studied by removing the gel section where the band of interest is located. However, gel electrophoresis is not as efficient at resolving lower molecular weight biomolecules since there is a greater significance of net charge and conformation on the mobilities of small molecules [16]. Many biomarkers of recent interest include low molecular weight biomolecules and even individual ions [35], making gel electrophoresis less practical for microscale manipulations.

A.2 Basic Electrophoretic Separation Theory

In order to understand the necessary requirements for electrophoretic buffering solutions, it is important to grasp some of the underlying principles of operation for common electrophoretic separation techniques. When a charged particle interacts with an applied electric field, it experiences a force due to the field, F_{EF}, which acts in the direction of the applied field. This force is balanced by a viscous force known as Stoke's drag, F_{η}, which resists the particle's motion

based on the interaction between solute and solvent molecules. The equations that govern this principle are listed below:

(3) Columbic Force

$$\bar{F}_{EF} = q\bar{E} \tag{3}$$

In the equation for the Columbic force, F_{EF}, q is the particle surface charge and E is the electric field strength, often represented in units of V/cm.

(4) Viscous Force

$$\bar{F}_{FR} = 6\pi\eta r\bar{v} \tag{4}$$

In the viscous force equation, F_{FR}, η is the buffer viscosity, r is the radius of a spherical molecule, and v is the velocity of the buffer.

(5) Combined Equilibrium Equation

$$\bar{v} = \frac{q\bar{E}}{6\pi\eta r} \tag{5}$$

At equilibrium, equations (3) and (4) can be combined to yield equation (5), where the particle experiences equal Columbic and viscous forces. All variables represent the same properties identified in equations (3) and (4).

(6) Electrophoretic Mobility

$$\mu_E = \frac{\bar{v}}{\bar{E}} = \frac{q}{6\pi\eta r} \tag{6}$$

The electrophoretic mobility is derived by dividing the electrophoretic velocity in equation (5) by the electric field strength, E.

(7) Electroosmotic Velocity

$$\bar{\mu}_{EO} = \left(\frac{\varepsilon_0}{4\pi\eta}\right)\bar{E}\zeta \tag{7}$$

The electroosmotic velocity, μ_{EO} is representative of the resulting buffer velocity under an applied electric field. In this equation, ε_0 is the dielectric constant, a property of the fluid; eta is the fluid viscosity; ζ is the zeta potential, the term used to describe the wall potential; and E is the electric field strength. This equation represents the resulting velocity that the buffer solution experiences as a function of different experimental conditions.

In addition to the forces experienced by the solute particles themselves, there is a bulk movement of the solvent caused by charge buildup at the interface of the capillary and the fluid. This phenomenon is known as electroosmotic flow (EO flow). In CE, EO flow is the driving force behind the fluid flow rather than a pressure gradient, causing the sample solution to elute out at the end of the capillary. When the capillary wall comes in contact with a buffer solution, there is a small diffuse layer of charge that results from the attraction of positively-charged counter-ions to the negatively charged glass walls where they seek to neutralize the surface. Once the electric field is applied, this positively-charged layer is repelled by the positively charged anode, which results in the bulk flow of buffer to the same electrode [17] (refer back to Figure 2). This layer

together with the surface layer is known as the electric double layer where the magnitude of the surface charge is known as the zeta potential, ζ.

Unlike pressure-driven flow that results in a parabolic velocity profile, EO flow results in a flat velocity profile [18]. This is fortuitous in that solute molecules convect at the same rate as the fluid regardless of their orthogonal position. Since the EO flow of the buffer is usually greater than the electrophoretic mobilities of negative solutes, all solutes are convected towards the negative cathode regardless of charge. The benefit of this phenomenon is that all solute molecules can be separated in a single run without having to switch the polarity of the applied electric field. As might be expected, the order of elution from the end of the capillary begins with cations followed by neutral solutes and finally anionic solutes.

A.3 Protein Ionization

The following review has been adapted from Wells, 2003 [36]. Proteins, as well as drugs and endogenous chemicals, contain carboxyl and/or amino groups which are capable of dissociating with hydrogen ions to form different charged "states". Since our focus is primarily on proteins, we will assume the case of a generic amino acid which contains both a carboxyl and amino terminus, shown in Figure 38. When each of these groups is protonated, the resulting compound is in its "acid" state (Figure 38a), whereas the unprotonated state is referred to as its "conjugate base" (Figure 38b).

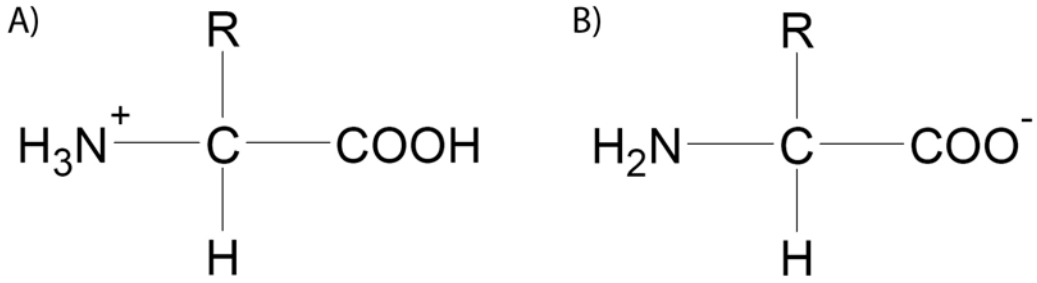

Figure 38 - Protonated (acid) and unprotonated (conjugate base) forms of proteins

Both figures represent the two common states of proteins when introduced to acidic or basic environments. The proteins are represented by their simplified structure where "R" represents the unique side groups that define the 20 amino acids. A) The common protein structure is shown in its protonated or acid state, resulting in an overall positive charge. B) The common protein structure is shown in its unprotonated or basic state, resulting in an overall negative charge. In reality, the side group R has a major influence on the degree of protonation or unprotonation, but is neglected in the above conceptual image.

The strength of an acid or base is determined by the compound's ability to ionize, or release hydrogen ions. This phenomenon is expressed as the dissociation constant, which is the ratio of the dissociation products to the ionized products, shown below.

$$K = \frac{[R{-}COO^-][H^+]}{[R{-}COOH]} \qquad K = \frac{[R{-}NH_2][H^+]}{[R{-}NH_3]} \qquad (8)$$

Like hydrogen ion concentration, the dissociation constant, K, is most commonly expressed in terms of pK, which is the negative natural log of K. Since strong acids tend to dissociate more completely than weak acids, they have lower pK values associated with them. While useful in determining the strength of acids and bases, the pK value can also be related to the solution pH value. When these two indicators are equal, there is a balance between the amounts of protonated and unprotonated species. Therefore, the pH of the solution directly influences the ratio of these two cases, as seen in the Henderson-Hasselbalch equation:

$$\mathbf{pH} = \mathbf{pK_a} + \mathbf{log_{10}}\left(\frac{[\mathbf{conjugate\ base}]}{[\mathbf{acid}]}\right) = \mathbf{pK_a} + \mathbf{log_{10}}\left(\frac{[\mathbf{A-}]}{[\mathbf{HA}]}\right). \quad (9)$$

For example, if the pH of a solution is 2 points higher than the pKa value of a solute, the ratio of unprotonated solutes to protonated solutes will be 100:1. This result seems logical since at higher pH values, fewer hydrogen ions are free in solution, which corresponds with more solutes in their unprotonated state. In terms of proteins, higher pH values will result in more negatively charged groups, as the carboxyl groups obtain a negative charge (R-COOH → R-COO^-) and the amino groups lose their positive charge ($NH_3^+ \rightarrow NH_2$).

A.4 Free flow electrophoresis and Dielectrophoresis

The popularity of CE has also spawned interest into other novel electrophoretic separation techniques. Two of these forms currently researched in our lab include free-flow electrophoresis (FFE) and dielectrophoresis (DEP). While there are inherent differences among these methods, they all operate on a similar phenomenon to achieve electrophoretic separations. The application of an electric field in a fluid stream can create differences in EOMs or a dipolar force which can be selected for in a separation. Since the electrolyte fluid itself is also influenced by the electric field, much attention must be placed on the selection of appropriate buffer solutions that will illicit the desired effects during an electrophoretic separation.

A.5 Free flow electrophoresis (microfluidic)

Free-flow electrophoresis (FFE) is a common separation technique that has been in use since the 1960's and applied to microfluidic since 1994 [37]. Like CE, FFE uses an electric field to aid in the separation of solutes from each other in an electrolytic buffer solution. However, in FFE the electrodes are placed on the walls of the separation chamber instead of at the inlet and outlet;

hence, the applied electric field acts perpendicularly to the direction of fluid flow. Based on differences in electrophoretic mobilities, solutes are phoresed orthogonal to the flow and separate from each other. FFE can continuously separate analytes since sample is introduced by pressure-driven flow and continues to elute into distinct zones based on their mobilities in the electric field. If designed properly, microchip separations can occur within seconds with similar resolutions to bench-scale FFE. When analytes exit the separation chamber, they are collected by different sampling "ports" which correspond to the zones in which the analytes have migrated.

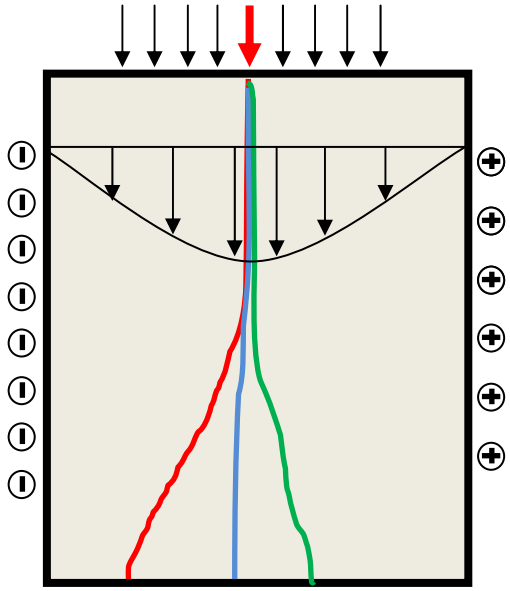

Figure 39 - Conceptual drawing of FFE system

In this conceptual image, the sample is loaded at the location marked by the red arrow and convected towards the bottom of the device via pressure-driven flow. As the different solutes in the sample experience different electrical field strengths based on their size-to-charge ratio, they deflect from the main stream in orthogonal directions and elute at different positions at the end of the device, as shown by the different colored lines. The positive and negative charges displayed on the sides of the device represent the applied electric field. Note that the device is not operated in the vertical position as shown for simplicity but rather is used in the horizontal position.

Like CE, many different modes of FFE exist. The mode most similar to CE and also under development in the Cal Poly Biofluidics lab is free flow zone electrophoresis (FFZE). This

method of FFE uses buffers with a constant pH and conductivity to separate different solutes based on their mobility, which is determined by their size-to-charge ratio. Even though CE is primarily used for analysis of analytes and FFZE is used for analyte separations, there is a direct correlation between the operation of the two [37]. For information concerning the comparison of the underlying theory of both techniques, please refer to Kasicka's paper on this topic [38]. In order to achieve high resolution in FFZE, it is important to operate the device to ensure narrow analyte zones with sharp boundaries. Since the flow is pressure-driven, parabolic velocity profiles can occur in the separation chamber, unlike the plug flow profile seen with electroosmotic flow in CE; however, the parabolic velocity profile can be adjusted by designing the device with separation chamber depths of around 20μm, so that the profile becomes flat. These unequal velocity regions can create intrinsic hydrodynamic broadening of the analyte zones; furthermore, it is important to closely match the conductivities of the sample and carrier buffer since disparities between the two can lead to electromigration dispersion resulting in poor resolution [37]. It is evident that sample conductivity is an important parameter to tune before the sample's introduction into an FFE system.

A.6 Dielectrophoresis (microfluidic)

While free flow electrophoresis exhibits very similar behaviors towards capillary electrophoresis, the dielectrophoresis (DEP) phenomenon is very different in practice. DEP is the phenomenon in which a polarizable particle in a non-uniform electric field experiences induced motion [39]. Since all particles exhibit at least some dielectrophoretic motion in a non-uniform field, DEP can be used on a wide range of analytes regardless of their surface charge. Although there are many different applications of DEP, solute separations are one of its major uses in lab-on-a-chip settings. By employing an electric field that exploits the differences between different solute populations, DEP "filters" can be created to separate particles based on their polarizability [39].

As seen with the previous electrophoretic manipulations, the electrical properties of the buffer solution have a major impact on the desired outcome, namely the strength of the dielectrophoretic force in this application.

Appendix B: Materials Selection – PDMS

Biomedical polymers, such as PDMS (polydimethylsiloxane), have gained widespread use in microfluidic chip fabrication and possess many of the attributes sought after in POC diagnostics. Among these attributes, PDMS is relatively inert, biocompatible, easy to produce and mold, optically transparent, impermeable to water, thermally and electrically insulating, and relatively cheap compared to machining costs associated with glass and polyethylene. PDMS is not a perfect model material for this application, but represents potential success in engineering suitable materials.

B.1 Material Requirements for POC Diagnostics

Diagnostic instruments are currently one of the largest sectors of the global healthcare market, with an estimated $32.2 billion a year impact in 2005 [40]. Not surprising, the United States is the largest market for clinical diagnostics, and therefore has a large impact on the development of such products. However, the potential for POC diagnostic devices extends beyond clinical settings in developed countries and could significantly improve patient diagnoses and treatment in rural, third world settings that can have unique environmental conditions. These new operating conditions give rise to unique design issues and possibly unique materials selection requirements. The materials selection issues are multifaceted. First, the device material must be inexpensive and easy to mass produce. Along the same lines, the material should be disposable, such that the risk for cross-contamination or disease spread is minimized. A chemically inert and resistant material would be advantageous such that the material can perform over a range of solutions without undergoing any adverse effects. Common detection techniques such as fluorescence would likely be performed on or within the material platform, necessitating optical compatibility. Furthermore, when dealing with biological samples, it is also desired that the material be biocompatible in

order to preserve the integrity of the sample. These criteria will have a great effect on the selection of an appropriate platform material for POC diagnostic devices.

B.2 Current use of PDMS

PDMS has been used in numerous applications over several decades. Medical-grade PDMS is a common silicone polymer used in such medical applications as intraocular lenses, joint prostheses, breast implants, and cardiac valves [41]. Due to the distinct elastomeric and dielectric properties of PDMS, a major use of the polymer is in embedding electronic components [42]. Though its use as an implantable silicone or a polymer coating are well documented over several decades, the introduction of PDMS to micro- and nano-technologies in 1995 [42] remains an area of current research. Currently, PDMS is one of the most actively developed polymers for use in prototyping microfluidic and other Micro Electro-Mechanical System (MEMS) devices [43]. Before the polymer breakthrough in microdevices, glass and silicon were the most widely used materials due to their well-developed fabrication and machining techniques. However, these processes can be expensive and time consuming, making these materials unsuitable for disposable diagnostic devices. PDMS devices, on the other hand, can be mass-produced by being cast against a mold and still create features that are less than 0.1 microns [43].

B.3 Polymerization/Fabrication with PDMS

PDMS is usually polymerized through the mixing of a base with a curing or cross-linking agent. The ratio of the two substances used in this process is important in determining the mechanical, chemical, and optical properties of the resulting polymer. For example, the elasticity of PDMS is highly dependent on the amount of curing agent used, since it determines the extent of cross-linking in the polymer. Most often, a ratio of 10:1, base to curing agent, is used in this process

[42, 43]. The silicon hydride groups in the curing agent react with the vinyl groups in the base to create a cross-linked elastomeric solid [43].

One of the most common methods for PDMS fabrication is the production of a mask using photolithography and casting PDMS on the mold in a process known as soft lithography. An example of photolithographic mask production involves the use of SU-8 photoresist, a negative photoresist. First, a drawing of the device geometries is produced using a computer-aided design program and is printed onto a transparency using a high-resolution printer. Next, a silicon wafer is coated with a layer of SU-8 at a desired thickness and baked under specific temperature and time requirements. The transparency is placed over the silicon wafer and exposed to UV light, such that the light does not pass through the areas that were printed. The UV light induces cross-linking in the SU-8 photoresist, which develops the mold. After the residual SU-8 is washed free from the wafer, a functional mold is produced that can be used to replicate the design in PDMS [44]. Soft lithography is a form of non-photolithographic methods for pattern replication. This process involves the curing of PDMS on a previously made mold, which transfers the design to the PDMS. When fabricating larger features (from 20-100μm), this process does not require cleanroom access [45], which can be advantageous. Rapid prototyping of the mold itself can further alleviate production concerns, leading to quick and efficient PDMS device development. After a PDMS device is obtained, it is important to create a seal between the PDMS and another material in order to close the exposed geometries. PDMS can reversibly or irreversibly seal to itself or a wide range of other materials which include glass and polyethylene [45]. The irreversible sealing of PDMS using air-plasma or oxygen-plasma is also much easier to perform than the sealing of glass-glass or glass-silicon which normally require much higher temperatures or voltages [46]. The ability to reversibly bond to another material through Van der Waals interactions at the surface is another advantage of PDMS. Since PDMS is a flexible material, it is

able to conform to minor imperfections in the base material, allowing these interactions to occur. Reversible sealing can occur at room temperature and is normally water-tight, though it cannot withstand high pressures [45].

B.4 Surface Chemistry of PDMS

The surface of PDMS is composed of repeating units of -O-Si-$(CH_3)_2$- groups, resulting in a hydrophobic surface. However, the surface chemistry of PDMS can be modified through the use of air-plasma, the same process seen in the irreversible sealing of PDMS. Exposing PDMS to air- or oxygen-plasma introduces silanol groups (Si-OH) and destroys methyl groups (Si-CH_3), resulting in a hydrophilic surface [46]. When PDMS is irreversibly sealed to glass, this reaction yields Si-O-Si covalent bonds and results in a tight seal that can withstand much greater pressures than reversibly sealed devices [45]. After surface treated, the PDMS must remain in contact with water or a polar organic solvent, otherwise unlinked chains inside the bulk polymer can migrate towards the surface to reduce the surface free energy, reestablishing a hydrophobic surface [45]. The low surface free energy in native, hydrophobic PDMS allows for easy release from the silicon wafer mold without causing damaging [43]. Plasma treating can also tailor the surface chemistry of PDMS by reacting silanes with different functional groups with the exposed silanols on the PDMS surface.

B.5 Solvent compatibility of PDMS

The hydrophobic nature of PDMS makes it suitable for microfluidic applications since water and other common polar liquids are not absorbed and do not penetrate into the PDMS; however, this property limits the usage of organic solvents in PDMS-based microchips. Certain reactions and extractions performed in a POC device could require the use of non-polar buffers or solvents. The three main compatibility issues of solvents with PDMS include the swelling of PDMS in a

solvent, the partitioning of solutes between PDMS and the solvent, and the dissolution of PDMS [47]. Though dissolution of PDMS might seem like the greatest concern, the swelling of PDMS in contact with a solvent has a larger influence on the function of a PDMS-based microchip. Swelling of PDMS can cause adverse effects in the fluidic system by closing off channels or making PDMS valves inoperable. One possibility to adjust the compatibility of PDMS with different organic solvents is to alter the surface chemistry of the PDMS channels.

B.6 Mechanical Properties of PDMS

As mentioned earlier, PDMS is an elastomeric solid. Since PDMS is a polymer, most of its mechanical and physical properties are defined based on the length of the polymer chains and the cross-linking density. Generally, more cross-linking occurs when higher proportions of cross-linking agents are used in preparation of PDMS. However, there is a critical point where all PDMS monomer chains are cross-linked and are unable to further bond. When observing the effects of cell adhesion to differing ratios of prepared PDMS polymers, it was noted that a ratio of 10:3, base to curing agent, was more liquid than a 10:1 ratio since not all of the curing agent was utilized in cross-linked bonds and remained in a liquid state [48]. Higher cross-linking can instead be obtained by curing at higher temperatures or over longer periods of time.

Due to its elastomeric nature, PDMS has a unique shear modulus that can vary between 100 kPa and 3 MPa [30]. This unique flexibility is attributed to its low glass transition temperature of about -125°C which is one of the lowest of any polymer [30]. The shear modulus was determined in one study by fabricating a thick cylinder of PDMS with a height of 1.2mm and a radius of 8mm and placing the cylinder between two circular disks where the bottom disk applied a certain torque and the upper disk measured the torsional force that resulted [30]. The elastic modulus of PDMS was similarly studied by another research group by performing tensile tests of long, thin

bars of the cross-linked polymer. This large length-to-width ratio was used in order to minimize the influence of clamping on the ends. Adjusting the strain rate had a significant influence on the elastic modulus measured, which ranged from 1.54 – 7.5 MPa [42].

B.7 Optical Properties of PDMS

Since most common detection techniques are based on fluorescence or spectroscopic phenomena, a material selected for use in a diagnostic tool should be compatible with the desired detection technology. Since PDMS does not absorb visible light, bulk PDMS is transparent and is compatible with many forms of optical detection. Optical dispersion, or refraction, is dependent not only on material properties but also on microchannel geometries. Therefore, even though PDMS has a fairly low index of refraction ($n_D \approx 1.43$ [42]), design considerations should also account for light scattering. However, some optical instruments reflect or capture light off the bottom substrate of a microchip, which could be composed of a different material. In these cases, the optical properties of PDMS are not of much concern since the light path circumvents any PDMS-related effects.

B.8 Biocompatibility of PDMS

Biocompatibility is a term used to describe how a material interacts with a biological substance and is defined as a materials' ability to perform with an appropriate host response. Normally this term is used to describe implantable biomaterials that have prolonged interactions with a biological system, though it also pertains to short term interactions with biological substances *in vitro*, as described here. Since POC diagnostic devices most commonly contact a biological fluid for a relatively short period of time, in vitro studies can provide very relevant data. In 1990, IUPAC (International Union of Pure and Applied Chemistry) began a pursuit of biological interactions with PDMS and low density polyethylene (LDPE), two materials previously deemed

"primary reference materials". However, Marie-Claire Belanger and colleagues found that biocompatibility results from this study were variable and conflicted in some cases [49]. Still, cross-linked PDMS is arguably the most studied implantable biomaterial considered to be biostable and biocompatible [50].

Most of the biocompatibility issues with PDMS depend also on the specific biological sample tested. For example, if human serum is used instead of whole blood, most of the cell-mediated responses such as pro-inflammatory secretions and thrombogenesis can be neglected.
In vitro hemocompatibility tests have shown that PDMS has relatively lower amounts of platelet adhesion than other common biomaterials such as Dacron™, glass, and polyethylene [51]. Low platelet adhesion is important in fending off a possible clotting cascade or pro-inflammatory secretions. Similarly, a study determined that PDMS experienced two times less protein adsorption than Dacron™ [52], which can initiate similar responses to adsorbed platelets. Proteins adhere within seconds to any material that comes in contact with blood, which inevitably affects any blood-testing POC device. Although PDMS generally displays good hemocompatibility, other studies found that PDMS was less hemocompatible than HDPE [53].

Just as the mechanical and physical properties were influenced by the amount of cross-linking in a PDMS sample, the biocompatibility of PDMS also depends on how the sample was prepared. In a study on the attachment and proliferation of 3T3 fibroblast cells on PDMS, researchers found that different ratios of base to curing agent greatly affected their results since they corresponded to differing amounts of cross-linking [48]. This is likely due to the fact that the stiffness of the PDMS samples influence how cells can attach and grow. However, as noted earlier, differing ratios of base to curing agent produce PDMS samples with different surface properties, since chains that are not cross-linked are mobile and can migrate to the surface. This phenomenon can

be manipulated by different processing conditions of bulk PDMS if cell attachment is either desired or undesired.

B.9 Justification for PDMS Use

In summary, PDMS has several advantages and disadvantages for its use in POC diagnostics. Advantages include the low cost and low time required for fabrication [46], transparency in the UV-visible region of the spectrum, excellent biocompatibility [49], electrical insulation, inertness, low permeability to water, thermal insulation, and low surface free energy which allows reversible sealing with other materials [43]. Some properties of PDMS, such as its elastomeric attributes, can be beneficial or detrimental depending on the application. For example, the elastomeric properties of PDMS allow it to easily conform to different surfaces and release easily from molds [43], but can also lead to shrinking or sagging of features fabricated into the PDMS, causing channel blockage or other deformities [46]. Other disadvantages of PDMS usage include its incompatibility with many organic solvents [47] and the fact that non-specific adsorption of proteins or other molecules may occur with biological samples [46]. However, the popularity and widespread use of PDMS as a platform for microfluidic devices continues despite these few disadvantages. Overall, PDMS has proven to be a unique and advantageous material for use in prototyping microfluidic devices and other micro-technologies.

Works Cited

1. Christopher P. Price, A.S.J., Jocelyn M. Hicks, ed. *Point-of-Care Testing*. 2nd ed. 2004, AACC Press: Washington DC.
2. Curtis D. Chin, V.L., Samuel K. Sia, *Lab-on-a-chip devices for global health: Past studies and future opportunities.* Lab on a Chip, 2007. **7**: p. 41-57.
3. Jan Lichtenberg, N.F.d.R., Elisabeth Verpoorte, *Sample pretreatment on microfabricated devices.* Talanta, 2002. **56**: p. 233-266.
4. Eckard, C.M.a.R., *Sampling and Sample Preparation*, ed. M. Stoppler. 1997: Springer.
5. D. Stevenson, I.D.W., *Sample Preparation for Biomedical and Environmental Analysis*. 1994, New York: Plenum Press.
6. Meiselman, O.K.B.a.H.J., *Blood Rheology and Hemodynamics.* Seiminars in thrombosis and Hemostasis, 2003. **29**(5): p. 435-450.
7. Mitra, S., ed. *Sample Preparation Techniques in Analytical Chemistry*. 2003, Wiley Interscience: Hoboken, New Jersey.
8. Stoeppler, M., ed. *Sampling and Sample Preparation*. 1994, Springer: New York.
9. Beard, A.J.d.M.a.N., *Dealing with 'real' samples: sample pre-treatment in microfluidic systems.* Lab on a Chip, 2003. **3**: p. 11N-19N.
10. Tamiya, M.d.V.a.E., *A rapid sample pretreatment protocol: Improved sensitivity in the detection of a low-abundant serum biomarker for prostate cancer.* Analytical Sciences, 2007. **23**: p. 1443-1446.
11. Sihinobu Sakai, J.-i.O., Haruka Nakamura, Hidenao Toyoda, Toshihiko Toida, Toshio Imanari, and Robert J. Linhardt, *Pretreatment procedure for the microdetermination of chondroitin sulfate in plasma and urine.* Analytical Biochemistry, 2002. **302**: p. 169-174.
12. Fang, Z.-L., *Trends of flow injection sample pretreatment approaching the new millennium.* Analytica Chimica Acta, 1999. **400**: p. 233-247.
13. Anderson, N.L.A.a.N.G., *The Human Plasma Proteome: History, Character, and Diagnostic Prospects.* Molecular And Cellular Proteomics, 2002. **1**: p. 845-867.
14. Dolnik, V., *Capillary zone electrophoresis of serum proteins: study of separation variables.* Journal of Chromatography A., 1995. **709**: p. 99-110.
15. Christa L. Colyer, S.D.M., D. Jed Harrison, *Microchip-based capillary electrophoresis of human serum proteins.* Journal of Chromatography A., 1997. **781**: p. 271-276.
16. Camilleri, P., ed. *Capillary Electrophoresis Theory and Practice*. 1993, CRC Press: Boca Raton, Florida.
17. Paul D. Grossman, J.C.C., ed. *Capillary Electrophoresis Theory and Practice*. 1992, Academic Press, Inc.: San Diego.
18. Baker, D.R., *Capillary Electrophoresis*. 1995, New York: John Wiley & Sons, Inc.
19. Michaelis, L., *Diethylbarbiturate Buffer.* Journal of Biological Chemistry, 1930. **87**(1): p. 33-35.
20. V. Sanz-Nebot, F.B., I. Toro, J. Barbosa, *Electrophoretic behavior of peptides in capillary electrophoresis: Influence of ionic strength and pH in aqueous-organic media.* Journal of Chromatography A., 2001. **921**: p. 69-79.
21. M.H. Oddy, J.G.S., and J.C. Mikkelsen, *Electrokinetic Instability Micromixing.* Analytical Chemistry, 2001. **73**: p. 5822-5832.
22. Bernhard H. Weigl, R.L.B., Natasa Kesler, Christopher J. Morris, *Lab-on-a-chip sample preparation using laminar fluid diffusion interfaces - computational fluid dynamics model results.* Journal of Analytical Chemistry, 2001. **371**: p. 97-105.
23. Anne Varenne, S.D., *Recent strategies to improve resolution in capillary electrophoresis - a review.* Analytica Chimica Acta, 2008. **628**: p. 9-23.

24. Steffen Hardt, F.S., ed. *MIcrofluidic Technologies for Miniaturized Analysis Systems*. 2007, Springer: New York.
25. Todd M. Squires, S.R.Q., *Microfluidics: Fluid physics at the nanoliter scale.* Reviews of Modern Physics, 2005. **77**(3): p. 977-1026.
26. Oliver Geschke, H.K., Pieter Telleman, *Microsystem Engineering of Lab-on-a-chip Devices*. 2008, Weinheim: Wiley-VCH.
27. Chang-Hsien Tai, R.-J.Y., Min-Zhong Huang, Chia-Wei Liu, Chien-Hsiung Tsai, Lung-Ming Fu, *Micromixer utilizing electrokinetic instability-induced shedding effect.* Electrophoresis, 2006. **27**: p. 4982-4990.
28. *AutoCAD 2008 v B.51.0 [Computer Software]*. 2007, Autodesk, Inc.: http://www.autocad.com.
29. *COMSOL Multiphysics v 3.4 [Computer Software]*. 2007: http://www.comsol.com.
30. J. C. Lotters, W.O., P. H. Veltink, P. Bergveld, *The mechanical properties of the rubber elastic polymer polydimethylsiloxane for sensor applications.* Journal of Micromechanical Microengineering, 1997. **7**: p. 145-147.
31. Qi Jin Wan, P.K., Jatisai Tanyanyiwa, Andrea Rainelli, Peter C. Hauser, *Determination of major inorganic ions in blood serum and urine by capillary electrophoresis with contactless conductivity detection.* Analytica Chimica Acta, 2004. **525**(1): p. 11-16.
32. Rasband, W.S., *ImageJ [Computer Program]*. 1997-2009, U.S. National Institutes of Health: Bethesda, Maryland, http://rsb.info.nih.gov/ij/.
33. *SigmaPlot v 11.0 [Computer Software]*. 2008, Systat Software, Inc.: http://www.sigmaplot.com.
34. Martin Z. Bazant, K.T., Armand Ajdari, *Diffuse-charge dynamics in electrochemical systems.* Physical Review E, 2004. **70**(021506).
35. F. Branca, A.B.H., B. Pool-Zobel, H. Verhagen, *Biomarkers in disease and health.* British Journal of Nutrition, 2001. **85**: p. S55-S92.
36. Wells, D.A., *High Throughput Bioanalytical Sample Preparation: Methods and Automation Strategies*. 2003, Amsterdam: Elsevier.
37. Dietrich Kohlheyer, J.C.T.E., Albert van den Berg, Richard B. M. Schasfoort, *Miniaturizing free-flow electrophoresis - a critical review.* Electrophoresis, 2008. **29**: p. 977-993.
38. Vaclav Kasicka, Z.P., Petra Sazelova, Jiri Jiracek, Tomislav Barth, *Theory of the correlation between capillary and free-flow zone electrophoresis and its use for the conversion of analytical capillary separations to continuous free-flow preparative processes* Journal of Chromatography A., 1998. **796**: p. 211-220.
39. Hughes, M.P., *Strategies for dielectrophoretic separation in laboratory-on-a-chip systems.* Electrophoresis, 2002. **23**: p. 2569-2582.
40. Rosen, S., *The worldwide market for in vitro diagnostic tests.* Kalorama Information Market Intelligence Report, April 2006(5th Edition).
41. Pablo Iribarren, S.G.C., Natalia Sodero, and Clelia M. Riera, *Activation of macrophages by silicones: phenotype and production of oxidant metabolites.* BMC Immunology, 2002. **3**(6).
42. Florian Schneider, J.D., Robert Kamberger, Ulrike Wallrabe, *Process and materials properties of polydimethylsiloxane (PDMS) for optical MEMS.* Sensors and Actuators A: Physical, 2009. **151**: p. 95-99.
43. J. Cooper McDonald, G.M.W., *Poly(dimethylsiloxane) as a material for fabricating microfluidic devices.* Accounts of Chemical Research, 2002. **35**(7): p. 491-499.
44. Minteer, S.D., ed. *Microfluidic techniques: reviews and protocols*. 2006, Humana Press: Totowa, New Jersey.

45. J. Cooper McDonald, D.C.D., Janelle R. Anderson, Daniel T. Chiu, Hongkai Wu, Olivier J. A. Schueller, George > Whitesides, *Fabrication of microfluidic systems in poly(dimethylsiloxane).* Electrophoresis, 2000. **21**: p. 27-40.
46. Jessamine M. K. Ng, I.G., Abraham D. Stroock, George M. Whitesides, *Components for integrated poly(dimethylsiloxane) microfluidic systems.* Electrophoresis, 2002. **23**: p. 3461-3473.
47. Jessamine Ng Lee, C.P., George M. Whitesides, *Solvent comaptibility of poly(dimethylsiloxane)-based microfluidic devices.* Analytical Chemistry, 2003. **75**(23): p. 6544-6554.
48. Jessamine Ng Lee, X.J., Declan Ryan, George M. Whitesides, *Compatibility of mammalian cells on surfaces of poly(dimethylsiloxane).* Langmuir, 2004. **20**(26): p. 11684-11691.
49. Marie-Claire Belanger, Y.M., *Hemocompatibility, biocompatibility, inflammatory and in vivo studies of primary reference materials: low-density polyethylene and polydimethylsiloxane: a review.* Journal of Biomedical Materials Research, 2001. **58**: p. 467-477.
50. Suresh K. Jewrajka, G.E., Joseph P. Kennedy, Daniel Ely, Gail Dunphy, Shannon Boehme, Flavius Popescu, *Novel biostable and biocompatible amphiphilic membranes.* Journal of Biomedical Materials Research A, 2007.
51. E M Keough, W.C.M., R Connolly, T Foxall, K Ramberg-Laskaris, J L McCullough, T F O'Donnell Jr., A D Callow, *The interaction of blood components with PDMS (polydimethylsiloxane) and LDPE (low-density polyethylene) in a baboon ex vivo arteriovenous shunt model.* Journal of Biomedical Materials Research, 1985. **19**: p. 577-587.
52. N P Ziats, D.A.P., B P Tierney, O D Ratnoff, J M Anderson, *Adsorption of Hageman factor (factor XII) and other human plasma proteins to biomedical polymers.* Journal of Laboratory Clinical Medicine, 1990. **116**: p. 687-696.
53. K W van der Kamp, W.v.O., *Factor XII fragment and kallikrein generation in plasma during incubation with biomaterials.* Journal of Biomedical Materials Research 1994. **28**: p. 349-352.